

Toric Geometry and String Theory



VINCENT BOUCHARD
Magdalen College
University of Oxford

A thesis submitted for the degree of
Doctor of Philosophy
July 2005

This thesis is dedicated to my parents.

Acknowledgements

First and foremost, I would like to thank Philip Candelas for his invaluable help throughout my four years in Oxford. I also owe special thanks to Bogdan Florea, Marcos Mariño and Harald Skarke for stimulating and enjoyable collaborations on the research topics discussed in this thesis. Thanks also to Lara Anderson, Xenia de la Ossa, Marco Gualtieri, Wen Jiang, Shabnam Kadir, Lionel Mason, David Skinner, Fonger Ypma and many others for interesting mathematical physics discussions.

Many thanks to my parents, who have always supported me in my choices of life and encouraged me to be true and honest with myself. Alexandra, thank you so much for your love and patience; distance relationships are difficult, but you showed me that no matter what the distance is love always exists. Thanks also to my sister Maryse, for your continual support and friendship; and for your invitation to discover Burmese and Malian cultures!

I would like to thank all my friends in Oxford, especially James, Stefano, Silje, Lucy, Kezia, Owen, Rahul; you showed me that better worlds exist, and most importantly that we can start creating them ourselves, right here and right now. Thanks to the OSSTW, OSAN, Oxford and UK Indymedia, ZOMBIE, PGA, OCSET and OARC crews, for the inspiration and the fantastic work to make our communities a better place to live. Thanks also to Maarit, Will and Ralph, for the wonderful Sunday nights spent in your good company. Thanks to all my friends from Québec, particularly David, Sylvie, Hendrick, Félix, Marc; it is amazing that our friendship is still as intense as ever! Finally, I must not forget to thank all the people I have played music with, for all these special moments where collective creation of music engendered unity through diversity...

I must also acknowledge the generous funding of the Rhodes Trust and of the National Science and Engineering Research Council of Canada, without which I could not have pursued my studies in Oxford.

Toric Geometry and String Theory

VINCENT BOUCHARD
Magdalen College
University of Oxford

A thesis submitted for the degree of
Doctor of Philosophy
July 2005

In this thesis we probe various interactions between toric geometry and string theory. First, the notion of a top was introduced by Candelas and Font as a useful tool to investigate string dualities. These objects torically encode the local geometry of a degeneration of an elliptic fibration. We classify all tops and give a prescription for assigning an affine, possibly twisted Kac-Moody algebra to any such top. Tops related to twisted Kac-Moody algebras can be used to construct string compactifications with reduced rank of the gauge group. Secondly, we compute all loop closed and open topological string amplitudes on orientifolds of toric Calabi-Yau threefolds, by using geometric transitions involving SO/Sp Chern-Simons theory, localization on the moduli space of holomorphic maps with involution, and the topological vertex. In particular, we count Klein bottles and projective planes with any number of handles in some Calabi-Yau orientifolds. We determine the BPS structure of the amplitudes, and illustrate our general results in various examples with and without D-branes. We also present an application of our results to the BPS structure of the coloured Kauffman polynomial of knots.

Contents

1	Introduction	1
2	Toric Geometry	9
2.1	Homogeneous Coordinates	10
2.1.1	Toric Divisors	13
2.2	Toric Calabi-Yau Threefolds	13
2.2.1	Definition of a Calabi-Yau Manifold	13
2.2.2	Calabi-Yau Manifolds in Toric Geometry	14
2.3	Toric Diagrams and Symplectic Quotients	17
2.3.1	Toric Manifolds as Symplectic Quotients	17
2.3.2	T^3 Fibration	18
2.3.3	$T^2 \times \mathbb{R}$ Fibration	20
2.4	Examples	22
2.4.1	Resolved Conifold	23
2.4.2	Two dP_2 's Connected by a $\mathbb{C}P^1$	26
2.5	Hypersurfaces in Toric Varieties	27
2.5.1	Reflexive Polytopes	27
2.5.1.1	Lattice Description	28
2.5.1.2	Toric Interpretation	28
2.5.1.3	Calabi-Yau Condition	29
2.5.1.4	Fibration Structure	30
2.5.2	Tops	31
2.5.2.1	Lattice Description	31
2.5.2.2	Toric Interpretation	33
3	The Classification of Tops and String Dualities	34
3.1	Toric Properties and Affine Kac-Moody Algebras	34
3.1.1	Affine Kac-Moody Algebras	35

3.1.2	Higher Dimensional Geometries	38
3.1.3	Elliptic Curve	38
3.2	Classification	39
3.3	Geometrical Interpretation	44
3.3.1	Twisted Algebras: Geometry	44
3.4	String Theory Interpretation	46
3.4.1	Twisted Algebras: String Theory	47
4	Closed Topological Strings on Orientifolds	49
4.1	A-model Topological Strings on an Orientifold	49
4.1.1	Type IIA Superstrings and Topological Strings on an Orientifold	49
4.1.2	Structure of the Topological String Amplitudes	51
4.2	Geometric Transitions	53
4.2.1	Orientifold of the Resolved Conifold and its Geometric Transition	53
4.2.2	Our Main Example	55
4.3	Closed String Amplitudes from Chern-Simons Theory	57
4.3.1	Results from Chern-Simons Theory with Classical Gauge Groups	57
4.3.2	Computation of Open String Amplitudes	63
4.3.3	Duality Map and Closed String Amplitudes	66
4.3.4	The Oriented Contribution	68
4.4	Unoriented Localization	75
4.4.1	Unoriented Localization at 2 Crosscaps and Degree 2 \mathbb{RP}^2 . .	76
4.4.2	Unoriented Localization at 2 Crosscaps and Degree 4 \mathbb{RP}^2 . .	78
4.5	Topological Vertex Computation	82
4.5.1	General Prescription	82
4.5.2	Examples	83
4.5.2.1	Orientifold of the Resolved Conifold	83
4.5.2.2	Local \mathbb{CP}^2 Attached to \mathbb{RP}^2	84
4.5.3	A Theorem Relating the Topological Vertex and SO/Sp Chern-Simons Invariants	85
5	Open Topological Strings on Orientifolds	88
5.1	Open Topological String Amplitudes in Orientifolds	88
5.1.1	BPS Structure of Topological String Amplitudes	88
5.1.2	BPS Structure of Topological Strings on Orientifolds	90
5.2	Examples of Open String Amplitudes	95
5.2.1	The topological vertex on orientifolds	95

5.2.2	The SO/Sp framed unknot	96
5.2.3	\mathbb{CP}^2 Attached to \mathbb{RP}^2	99
5.2.4	SO/Sp Hopf Link Invariant	101
5.2.5	Localization Computations	103
5.2.5.1	The SO/Sp Framed Unknot	105
5.2.5.2	\mathbb{CP}^2 Attached to \mathbb{RP}^2	107
5.2.5.3	SO/Sp Hopf Link Invariant	109
5.3	Application: the BPS Structure of the Coloured Kauffman Polynomial	110
5.3.1	Chern-Simons Invariants and Knot Polynomials	110
5.3.2	BPS Structure: Statement and Examples	111
6	Conclusions and Future Directions	117
A	Useful Formulae	120
A.1	Subsets of Young Tableaux	120
A.2	The Topological Vertex, Chern-Simons Invariants and Schur Functions	121
B	Various Results	124
B.1	Full Classification of Tops	124
B.2	Full Results for the Closed Topological String Amplitudes	131
B.3	BPS Invariants for the Trefoil Knot	132
	Bibliography	134

List of Figures

2.1	The fan Σ of $\mathbb{C}\mathbb{P}^2$	12
2.2	The Γ and $\tilde{\Gamma}$ graphs for $\mathcal{O}(-3) \rightarrow \mathbb{C}\mathbb{P}^2$. The toric diagram Γ is the normal diagram drawn in thick lines. The points $(\nu_i, 1)$ give the fan Σ , where the ν_i are the vertices of $\tilde{\Gamma}$ and are shown in the figure.	17
2.3	Toric diagram Γ of $\mathcal{O}(-3) \rightarrow \mathbb{C}\mathbb{P}^2$ visualized as a three dimensional graph. It encodes the degeneration loci of the T^3 fiber.	20
2.4	Trivalent vertex associated to \mathbb{C}^3 , drawn in the r_α - r_β plan. The vectors represent the generating cycles over the lines.	22
2.5	The Γ and $\tilde{\Gamma}$ graphs for $\mathcal{O}(-1) \oplus \mathcal{O}(-1) \rightarrow \mathbb{C}\mathbb{P}^1$. The toric diagram Γ is the normal diagram drawn in thick lines. The points $(\nu_i, 1)$ give the fan Σ , where the ν_i are the vertices of $\tilde{\Gamma}$ and are shown in the figure.	23
2.6	Toric diagram Γ of $\mathcal{O}(-1) \oplus \mathcal{O}(-1) \rightarrow \mathbb{C}\mathbb{P}^1$ visualized as a three dimensional graph. It encodes the degeneration loci of the T^3 fiber.	24
2.7	Toric diagram of $\mathcal{O}(-1) \oplus \mathcal{O}(-1) \rightarrow \mathbb{C}\mathbb{P}^1$, drawn in the r_α - r_β plan. The vectors represent the generating cycles over the lines. The origin of the second patch U_2 is shifted to $(-t, -t)$	25
2.8	The Γ and $\tilde{\Gamma}$ graphs for the Calabi-Yau threefold X whose compact locus consists of two dP_2 's connected by a $\mathbb{C}\mathbb{P}^1$. The toric diagram Γ is the normal diagram drawn in thick lines.	26
2.9	A top, its dual and the minimal point notation.	32
3.1	Dynkin diagrams of the self-dual untwisted ADE Kac-Moody algebras.	36
3.2	An edge of \diamond^* and the intersection pattern to which it corresponds.	36

3.3	Dynkin diagrams of the duals of untwisted non-simply laced Kac-Moody algebras.	37
3.4	Dynkin diagrams of the duals of twisted Kac-Moody algebras that can be read off from tops.	38
3.5	The 16 two-dimensional reflexive polygons. The polygons $1, 2, \dots, 6$ are respectively dual to the polygons $16, 15, \dots, 11$, and the polygons $7, \dots, 10$ are self-dual.	40
3.6	Possible halves of reflexive polygons.	42
3.7	Three maximal tops (the significance of \bullet vs. \circ will be explained in section 3.3).	43
3.8	A family of tops over squares.	45
3.9	Two families of tops over the dual pair $(4, 13)$	45
4.1	Geometric transition for the orientifold of the conifold. The cross in the figure to the left represents an $\mathbb{R}\mathbb{P}^2$ obtained by quotienting a $\mathbb{C}\mathbb{P}^1$ by the involution I , and the dashed line in the figure on the right represents an \mathbf{S}^3 with SO/Sp gauge group.	54
4.2	The geometry on the closed topological strings side. The orientifolding action acts from left to right, while flopping the $\mathbb{C}\mathbb{P}^1$'s acts top-down. The $\mathbb{R}\mathbb{P}^2$ is represented by a cross at the end of the toric leg.	56
4.3	The geometric transition. The two $\mathbb{C}\mathbb{P}^1$'s and the $\mathbb{R}\mathbb{P}^2$ of the left figure are shrunk to singular points in the middle diagram, and then deformed into three \mathbf{S}^3	57
4.4	The deformed geometry. M_i $i = 1, 2, 3$ are the three spheres and r_{ci} are the Kähler parameters of the cylindrical instantons. The gauge groups of the Chern-Simons theories on the spheres and the framings of the unknots are also indicated.	63
4.5	The geometry in the topological vertex formalism. In brackets next to the representations are the framings in the corresponding propagator.	67
4.6	Toric diagram for local $\mathbb{C}\mathbb{P}^2$ attached to an $\mathbb{R}\mathbb{P}^2$	69
4.7	Two crosscaps and no hyperplane at degree 2 $\mathbb{R}\mathbb{P}^2$	76

4.8	Two crosscaps and one hyperplane at degree 2 \mathbb{RP}^2 . Mirror pairs are $\{(a), (c)\}$ and $\{(b), (d)\}$ respectively.	77
4.9	Two crosscaps and two hyperplanes at degree 2 \mathbb{RP}^2 : type II graphs.	77
4.10	Two crosscaps and three hyperplanes at degree 2 \mathbb{RP}^2 : type II graphs.	78
4.11	Two crosscaps and no hyperplane at degree 4 \mathbb{RP}^2	78
4.12	Two crosscaps and one hyperplane at degree 4 \mathbb{RP}^2 : type III graphs.	79
4.13	Two crosscaps and one hyperplane at degree 4 \mathbb{RP}^2 : type I graphs.	79
4.14	Two crosscaps and two hyperplanes at degree 4 \mathbb{RP}^2 : type I graphs.	80
4.15	Two crosscaps and two hyperplanes at degree 4 \mathbb{RP}^2 : type II graphs.	80
4.16	Two crosscaps and three hyperplanes at degree 4 \mathbb{RP}^2 : type II graphs.	81
4.17	Two crosscaps and three hyperplanes at degree 4 \mathbb{RP}^2 : type II graphs.	81
4.18	Toric diagram for the quotient X/I of a local, toric Calabi-Yau manifold with a single \mathbb{RP}^2	82
5.1	A D-brane in an outer leg of the orientifold of the resolved conifold.	96
5.2	The covering configuration contains two D-branes.	97
5.3	A D-brane in an outer leg of the orientifold of the two \mathbb{CP}^2 's connected by a \mathbb{CP}^1	100
5.4	Two adjacent D-branes in the outer legs of the orientifold of the resolved conifold.	102
5.5	One crosscap, genus 1 and three crosscaps, genus 0 at degree 3 \mathbb{RP}^2 , and winding vector $(0, 1, 0, \dots)$	107
5.6	One crosscap graphs at degree 1 \mathbb{RP}^2 , degree 2 hyperplane and winding vector $(2, 0, \dots)$	108
5.7	Two crosscaps graphs at degree 4 \mathbb{RP}^2 , degree 3 hyperplane and winding vector $(2, 0, \dots)$	109

Chapter 1

Introduction

Whether string theory has a deep rôle to play in our understanding of the universe or not, it has already achieved a great success in the recent decades: building bridges between various areas of mathematics and physics that were previously unrelated. Mathematicians and physicists have always worked together to search the meaning of Nature. But more than ever, both fields have become interlaced, to the extent that it is now difficult to trace a line between what was previously known as mathematics and physics.

Mathematical physics, particularly string theory, has led to fascinating insights, both in mathematics and in physics. The aim of this thesis is to pursue this interaction between mathematics and physics, through the study of toric geometry and string theory.

Recently, toric geometry became an important part of the geometrical study of string theory. Toric varieties provide an elementary way to understand many abstract concepts of algebraic geometry. In a similar fashion, the use of toric varieties in string theory has led to deep insights on the nature of string theory itself, on its various internal dualities and on its numerous relations with other areas of mathematics and physics. Owing to its beauty and simplicity, toric geometry also gives the possibility to compute various non-trivial results in string theory that could not be calculated otherwise.

In this thesis we shall focus on two particular interactions between toric geometry and string theory. On the one hand, we will continue the study of Calabi-Yau hypersurfaces in toric varieties, using Batyrev's reflexive polytopes and their close cousins named 'tops', and investigate their relations with dualities between compactifications of string theory. On the other hand, we will develop a novel approach to closed and

open topological strings on orientifolds of toric Calabi-Yau threefolds, using various mathematical devices; geometric transitions involving SO/Sp Chern-Simons theory, the topological vertex, and unoriented localization techniques.

In chapter 2, we start by summarizing various results in toric geometry relevant for this thesis. The goal of this chapter is not to provide a complete introduction to toric geometry. Toric geometry is a well developed subject, and many thorough accounts already exist in the literature, such as William Fulton's very good *Introduction to Toric Varieties* [1].

Rather, this chapter aims at offering a gentle walk through the concepts of toric geometry that are essential for the rest of this thesis. We tried to formulate a pedagogical synthesis of the required background, starting from the definition of a toric variety and culminating with Batyrev's approach to hypersurfaces in toric varieties. The non-expert reader should be able to find his way through the sometimes abstract concepts of toric geometry, and in that sense it is self-contained. However, many proofs are omitted, and various interesting aspects of toric geometry are not discussed, for the sake of clarity and brevity.

Toric varieties may be approached from various points of view. The "classical" viewpoint makes heavy use of numerous concepts of algebraic geometry. In this approach, toric varieties are built by gluing together affine toric varieties in a certain way associated to a geometrical object called fan. Although this is the most common approach to toric varieties, we will not use it in this chapter. We prefer to follow other avenues that lead to the same results in a somewhat more intuitive way, at least from the point of view of string theory.

A second way to construct toric variety from a fan has been developed by Cox [2]. By associating homogeneous coordinates to the one-dimensional cones of the fan, this approach exploits an interesting similarity between toric varieties and (weighted) projective spaces. It is perhaps the simplest way to get a grip on toric varieties without requiring background knowledge in algebraic geometry. Therefore, we shall follow this path as far as possible.

Thus, we will describe toric varieties using the homogeneous coordinate technology. We will mainly focus on three dimensional toric varieties, in particular toric threefolds, which will be the focus of interest in the remaining chapters. However most of the content of chapter 2 can be generalized to higher dimensional varieties rather straightforwardly.

In string theory, we are often interested in Calabi-Yau manifolds, which are a special kind of Kähler manifolds. Calabi-Yau manifolds are defined in various ways in the literature; we will briefly discuss these definitions and their relations. In this thesis we will say that a manifold is Calabi-Yau if it is Kähler and has vanishing first Chern class. We will not assume that it is compact; in fact, noncompact Calabi-Yau manifolds will play a crucial rôle. One of our objectives is to implement the Calabi-Yau condition in toric geometry. Hence, after having introduced some essential properties of toric threefolds, we will explore various formulations of the Calabi-Yau condition for toric threefolds. In fact, we will show that toric Calabi-Yau threefolds must be noncompact.

Using this property of toric Calabi-Yau threefolds, we will introduce the concept of toric diagrams, which are two-dimensional graphs representing the degeneration loci of the fibers of a toric Calabi-Yau threefold. We will spend some time describing the properties of these graphs, since they play an important rôle in chapters 4 and 5. To this end, we will have to develop another approach to toric varieties, using the symplectic quotient point of view. As most of these notions are not essential for this thesis, we will simply give the reader the necessary background to develop an intuitive understanding of the meaning of toric diagrams.

We then describe two important examples of toric Calabi-Yau threefolds that will be studied in detail in chapters 4 and 5. For the case of the resolved conifold, we provide a complete analysis, using the various approaches referred to above.

Now, it may be disconcerting to learn that compact toric Calabi-Yau threefolds do not exist. We promised that toric geometry leads to fascinating results in string theory, but compact toric Calabi-Yau threefolds do not even exist, while in most realistic compactifications of string theory we need compact manifolds! There is fortunately a beautiful way to circumvent this limitation, due to Batyrev [3]. The fundamental idea is to construct Calabi-Yau manifolds not as toric manifolds, but rather as compact hypersurfaces in compact toric varieties. In this way, the toric variety does not have to be Calabi-Yau nor does the Calabi-Yau manifold need to be toric. Batyrev's approach is to associate reflexive polytopes to Calabi-Yau hypersurfaces in toric varieties. We describe, still using the homogeneous coordinate technique, this construction.

We end this chapter by introducing a similar geometrical object, which we call top. The appearance of tops was first noticed in string duality applications of Batyrev's reflexive polytopes [4]. They were then generalized, and became interesting in their own rights. As they are at the centre of chapter 3, we describe them in detail, both from a lattice and a toric point of view.

In chapter 3 we study our first application of toric geometry to string theory. Toric geometry and Batyrev's construction [3] provide a very useful setup to study dualities between heterotic strings compactified on a Calabi-Yau n -fold and F-theory (or type II) compactified on a Calabi-Yau $(n+1)$ -fold. In [4], Candelas and Font used reflexive polyhedra to study the conjectured duality between the $E_8 \times E_8$ heterotic string compactified on the manifold $K3 \times T^2$ and the IIA string compactified on a Calabi-Yau threefold. It was noticed, and later explained in [5], that the affine Dynkin diagrams of nonabelian gauge groups occurring in type IIA and also in F-theory can be read off from the dual reflexive polyhedron corresponding to the Calabi-Yau manifold used for compactification. The fibration structure of the Calabi-Yau manifold can be directly seen as a nesting structure of the reflexive polyhedron. The elliptic fibration structure of the $K3$ part of the Calabi-Yau divides the three dimensional reflexive polyhedron corresponding to the $K3$ in two parts, a top and a bottom, separated by the two dimensional reflexive polygon of the fiber. The concept of top was then introduced as half of a reflexive polyhedron.

This was just the beginning of the story. The ideas of [4] were studied in detail in many other papers [6, 7, 8, 9, 10, 11, 12]. The Calabi-Yau manifolds analyzed in these papers were $K3$ fibrations with an elliptically fibered $K3$ manifold where the elliptic fibration structure of the $K3$ carries over to the Calabi-Yau manifold. These nested fibration structures can be seen explicitly in the toric diagrams as nestings of the corresponding reflexive polyhedra. The fan for the toric variety describing the base of the elliptic fibration is given by projecting the higher dimensional fan corresponding to the fibered Calabi-Yau manifold along the two dimensions of the reflexive polygon that represents the fiber [13]. Then the way the elliptic fibers degenerate along the curves in the base space can be found, in order to determine the enhanced gauge groups, by considering the preimage of the projection for each toric divisor in the base. The concept of top can now be generalized [11] to the geometrical objects formed by the preimages of the corresponding toric divisors. These objects are three-dimensional lattice polyhedra with one facet containing the origin and the other facets at integral distance one from the origin. This definition implies that the facet containing the origin is a reflexive polygon. Note that this really generalizes the concept initially introduced by Candelas and Font, since the tops defined as half of a reflexive polyhedron have all the properties of the new tops, but the new tops cannot always be completed to reflexive polyhedra. Alternatively the more general definition can be seen as the description of a toric hypersurface that is an elliptic fibration over \mathbb{C} and its degeneration over 0. This geometrical description was briefly explored in chapter 2, where tops were first introduced from a purely geometrical perspective.

In this chapter we classify all the possible tops, using the general definition. In contrast to the case of reflexive polyhedra, there are infinitely many tops, even for each choice of one of the 16 reflexive polygons as the facet containing the origin. We find that there is a precise prescription for assigning an affine Kac-Moody algebra to any top, in a way that involves the lengths of simple roots and the coefficients of the null root. Owing to this fact the classification of tops is related to that of affine Kac-Moody algebras. We also find one parameter families as well as sporadic cases. In addition, for each of the 16 polygons there is also a family depending on $l - 3$ integer parameters where l is the number of lattice points of the polygon; these correspond to the $A_n^{(1)}$ series of affine Kac-Moody algebras in such a way that n is a linear combination of the parameters. Each of the untwisted affine Kac-Moody algebras occurs quite a number of times, and in addition four of the six possible (families of) twisted algebras also occur. The tops featuring the latter are related in a very nice way to string compactifications with reduced rank, i.e. CHL strings [14] and their generalizations and duals.

This chapter is based on [15] which was written in collaboration with Harald Skarke.

In chapter 4 we start investigating our second application of toric geometry to string theory. Geometric or large N transitions relating open and closed topological strings have had a deep impact in the study of topological string theory. Since the original formulation of the duality for local conifold transitions in [16], they have been extended in various directions, leading to the first systematic solution of these models on noncompact, toric Calabi-Yau threefolds through the topological vertex [17] (see [18, 19] for a review).

The study of topological strings on Calabi-Yau orientifolds was initiated in [20], where an orientifold of the geometric transition of [16] relating the deformed and the resolved conifold was studied in detail, and continued in [21] from the mirror B -model point of view. The geometric transition of [16] can be extended to more general toric geometries [22, 23, 24, 25]. Accordingly, in this chapter we propose a generalization of the large N correspondence of [20] to a large class of orientifolds of toric Calabi-Yau threefolds.

We find that the partition function of closed topological strings on the orientifold (including unoriented contributions and oriented contributions from the covering space) is equivalent in the large N limit to the Chern-Simons partition function on the threefold after a geometric transition. The \mathbb{CP}^1 's that were invariant under

the involution, becoming $\mathbb{R}\mathbb{P}^2$'s in the orientifold, give $SO(N)$ — or $Sp(N)$ — Chern-Simons theory on the \mathbf{S}^3 's resulting from the geometric transition. One also has to add instanton contributions localized on the fixed locus of a torus action on the deformed geometry.

This is a highly non-trivial proposal, as more complicated orientifolds involve instanton contributions to the Chern-Simons partition function. Moreover, for more general orientifolds, the geometry of the covering space becomes quite different from the one of the resulting orientifold. It is not obvious at all that both the oriented and unoriented contributions to the closed topological strings partition function are encoded in the Chern-Simons setup. But it turns out to be true in the examples we consider.

We also find that the closed topological string amplitudes on the orientifolds of the type we describe below can be computed with the topological vertex introduced in [17], by using a prescription that takes into account the involution of the target. We explicitly prove that this prescription is equivalent to the large N Chern-Simons dual. This prescription extends the general formalism of the topological vertex to include the case of orientifolds.

To test our result we compute the unoriented contributions on the closed topological strings side using the unoriented localization techniques developed in [26]. This computation does not rely on large N duality at all, consequently providing an independent check of our proposal. In [20] it was found that only unoriented maps with one crosscap contribute to the partition function. However, in the general case, we find that configurations with two crosscaps, that is Klein bottles, do contribute as well.

To make the proposal more concrete we focus on a particular geometry. We consider a noncompact Calabi-Yau threefold X whose compact locus consists of two compact divisors each isomorphic to a del Pezzo surface dP_2 and a rational $(-1, -1)$ curve that intersects both divisors transversely. The divisors do not intersect each other. This geometry was briefly described in chapter 2. We will equip X with a freely acting antiholomorphic involution I and consider an orientifold of the theory obtained by gauging the discrete symmetry σI , where σ is an orientation reversal worldsheet diffeomorphism.

The partition function of the closed topological \mathbf{A} -model with this geometry as target space will sum both over maps from orientable worldsheets to X (with the

Kähler parameters identified by the involution set equal) as well as over non-orientable worldsheets to the orientifolded geometry.

The orientifolded geometry allows a local geometric transition that will be described in detail in section 4.2. This amounts to contracting two $\mathbb{C}\mathbb{P}^1$'s and a $\mathbb{R}\mathbb{P}^2$ and replacing them by three \mathbf{S}^3 's. We conjecture that the dual open string model will consist of a system of Chern-Simons theories supported on the three spheres, with $U(N_1)$ and $U(N_2)$ groups on the spheres corresponding to the contracted $\mathbb{C}\mathbb{P}^1$'s and $SO(N_3)$ - or $Sp(N_3)$ - group on the sphere corresponding to the contracted $\mathbb{R}\mathbb{P}^2$. The new ingredient is that the Chern-Simons theories will be coupled by cylindrical instantons.

This chapter is based on [27] written in collaboration with Bogdan Florea and Marcos Mariño.

In chapter 5 we continue the study of topological string amplitudes on orientifolds of toric Calabi-Yau threefolds initiated in chapter 4. Our main goal is to extend the results of chapter 4 to open topological strings on orientifolds without fixed points. In other words, we consider orientifolds of noncompact Calabi-Yau threefolds with D-branes.

An important property of topological string amplitudes is that they have an integrality structure related to the counting of BPS states, as it was first realized by Gopakumar and Vafa [28] in the case of closed string amplitudes. The integrality structure in the open case was studied in [29, 30]. As a first step in our study of topological string amplitudes on orientifolds without fixed planes we analyze their BPS structure. What we find is that the total orientifold amplitude is the sum of an oriented amplitude (the untwisted sector) and an unoriented amplitude (the twisted sector) with different integrality properties. We explain how to compute the contribution of the twisted sector in the open case. We also spell out in detail the integrality properties of the twisted sector contributions.

This integrality structure provides a strong requirement on open topological string amplitudes, and we check it explicitly on various examples involving orientifolds with D-branes. To compute these open string amplitudes we use the new vertex rule introduced in section 4.5. We also compute the associated Gromov-Witten invariants using independent localization techniques developed in section 4.4 and in [26], and find perfect agreement with the results obtained with the vertex.

One of the most interesting applications of the large N duality between open and closed topological strings consists in the determination of structural properties of knot and link invariants related to the BPS structure of open topological strings. For example, from the results of [29, 30] one can deduce structure theorems for the coloured HOMFLY polynomial of knots and links. The large N duality on orientifolds now involves $SO(N)$ and $Sp(N)$ Chern-Simons theories. Therefore, the BPS structure of the amplitudes should lead to the determination of structural properties of a different type of knot and link invariant: the coloured Kauffman polynomial [31]. Although for arbitrary knots and links we cannot determine in detail the structure of the untwisted sector, we are able to derive general structural results for the coloured Kauffman polynomial. We test again these predictions on various examples involving torus knots.

This chapter is based on [32], written in collaboration with Bogdan Florea and Marcos Mariño.

Finally, in chapter 6 we discuss the results of this thesis. We propose various avenues of research and future directions, and point out some possible extensions of our results to more complicated situations.

Chapter 2

Toric Geometry

In this chapter we explore various aspects of toric geometry relevant for this thesis. For good introductions to toric geometry the reader is referred to [1, 33, 34].

Toric varieties may be approached from various points of view. They can be described using fans and homogeneous coordinates, or viewed as symplectic manifolds, or correspondingly as the Higgs branch of the space of supersymmetric ground states of the gauged linear sigma model (GLSM), or even associated to convex polytopes in integral lattices. Perhaps the simplest approach is the homogeneous coordinate description [2]; therefore we shall proceed as far as possible using this approach.

First, we will introduce toric varieties and rapidly describe how to extract a toric variety from a fan using homogeneous coordinates. We will then examine what the Calabi-Yau condition becomes for toric variety, and deduce that toric Calabi-Yau manifolds must be noncompact. Using this result, we shall introduce toric diagrams, and explain their meaning using the symplectic manifold point of view. We then give a few examples of toric Calabi-Yau threefolds that will be used in chapters 4 and 5.

In the remaining of this chapter we explain how compact Calabi-Yau manifolds may be obtained in toric geometry, namely as hypersurfaces in compact toric manifolds using Batyrev's well known reflexive polytopes [3]. We then introduce the concept of 'top' — which is the object of interest of chapter 3 — and explain its meaning in toric geometry.

To understand toric geometry, we must dive into the abstract world of algebraic geometry. We will assume here a basic knowledge of algebraic geometry; a standard reference is [35].

2.1 Homogeneous Coordinates

An interesting aspect of Cox's approach to toric geometry is that by using the homogeneous coordinate construction, toric varieties look very much like the usual complex (weighted) projective spaces. In fact, from that point of view we can understand toric varieties as an algebraic generalization of complex (weighted) projective spaces.

To start with, let us explain roughly what a toric variety is. Consider \mathbb{C}^m and an action by an algebraic torus $(\mathbb{C}^*)^p$, $p < m$. We identify and then subtract a subset U that is fixed by a continuous subgroup of $(\mathbb{C}^*)^p$, then safely quotient by this action to form

$$\mathcal{M} = (\mathbb{C}^m \setminus U) / (\mathbb{C}^*)^p. \quad (2.1)$$

\mathcal{M} is called a *toric variety*, as it still has an algebraic torus action by the group $(\mathbb{C}^*)^{m-p}$ descending from the natural action of $(\mathbb{C}^*)^m$ on \mathbb{C}^m .

For instance, $\mathbb{C}\mathbb{P}^2$ is a toric variety. Indeed, a standard way of describing $\mathbb{C}\mathbb{P}^2$ is by embedding it into \mathbb{C}^3 :

$$\mathbb{C}\mathbb{P}^2 = (\mathbb{C}^3 \setminus \{0\}) / (\mathbb{C}^*), \quad (2.2)$$

where the quotient is implemented by modding out by the equivalence relation

$$(x, y, z) \sim \lambda(x, y, z), \quad (2.3)$$

where $\lambda \in \mathbb{C}^*$. We see that this description of $\mathbb{C}\mathbb{P}^2$ satisfies the general definition of a toric variety given above.

We now describe how to extract toric varieties from a fan using the homogeneous coordinate approach developed by Cox [2].

Let M and N be a dual pair of lattices, viewed as subsets of vector spaces $M_{\mathbb{R}} = M \otimes_{\mathbb{Z}} \mathbb{R}$ and $N_{\mathbb{R}} = N \otimes_{\mathbb{Z}} \mathbb{R}$. Let $(u, v) \rightarrow \langle u, v \rangle$ denote the pairings $M \times N \rightarrow \mathbb{Z}$ and $M_{\mathbb{R}} \times N_{\mathbb{R}} \rightarrow \mathbb{R}$.

Definition 2.1. A strongly convex rational polyhedral cone $\sigma \in N_{\mathbb{R}}$ is a set

$$s = \{a_1 v_1 + a_2 v_2 + \dots + a_k v_k \mid a_i \geq 0\} \quad (2.4)$$

generated by a finite number of vectors v_1, \dots, v_k in N such that $\sigma \cap (-\sigma) = \{0\}$.

Let us put words on this definition. Suppose the lattice N is n -dimensional, that is $N \cong \mathbb{Z}^n$. A convex rational polyhedral cone is a n or lower dimensional cone in $N_{\mathbb{R}}$, with the origin of the lattice as its apex, such that it is bounded by finitely many hyperplanes ('polyhedra'), its edges are spanned by lattice vectors ('rational') and it contains no complete line ('strongly convex').

A face of a cone σ is either σ itself or the intersection of σ with one of the bounding hyperplanes.

Remark 2.2. *In the remaining of this chapter we will refer to convex rational polyhedral cones simply as cones.*

Definition 2.3. *A collection Σ of cones in $N_{\mathbb{R}}$ is called a fan if each face of a cone in Σ is also a cone in Σ , and the intersection of two cones in Σ is a face of each.*

Now let Σ be a fan in N . Let $\Sigma(1)$ be the set of one dimensional cones (or edges) of Σ . From now on we will focus on three dimensional toric varieties, or correspondingly on three dimensional lattices $M, N \simeq \mathbb{Z}^3$.

Let $v_i, i = 1, \dots, k$ be the vectors generating the one dimensional cones in $\Sigma(1)$, where $k = |\Sigma(1)|$. To each v_i we associate an homogeneous coordinate $w_i \in \mathbb{C}$. From the resulting \mathbb{C}^k we remove the set

$$Z_{\Sigma} = \bigcup_I \{(w_1, \dots, w_k) : w_i = 0 \forall i \in I\}, \quad (2.5)$$

where the union is taken over all sets $I \subseteq \{1, \dots, k\}$ for which $\{v_i : i \in I\}$ does not belong to a cone in Σ . In other words, several w_i are allowed to vanish simultaneously only if there is a cone such that the corresponding v_i all belong to this cone.

Then the toric variety is given by

$$\mathcal{M}_{\Sigma} = \frac{\mathbb{C}^k \setminus Z(\Sigma)}{G} \quad (2.6)$$

where G is $(\mathbb{C}^*)^{k-3}$ times a finite abelian group. For all the toric varieties we consider in this thesis the finite abelian group is trivial, so from now on we will omit it (see [36] for an explanation of this group). The quotient by $(\mathbb{C}^*)^{k-3}$ is implemented by taking equivalence classes with respect to the following equivalence relations among the coordinates w_i :

$$(w_1, \dots, w_k) \sim (\lambda^{Q_a^1} w_1, \dots, \lambda^{Q_a^k} w_k) \quad (2.7)$$

with $\lambda \in \mathbb{C}^*$ and $\sum_{i=1}^k Q_a^i v_i = 0$. Among these relations, $k - 3$ are independent. We choose the Q_a^i such that they are integer and the greatest common divisor of the Q_a^i with fixed a is 1.

Using this construction, it is easy to see that the complex dimension of a toric variety is always equal to the real dimension n of the lattice $N \cong \mathbb{Z}^n$.

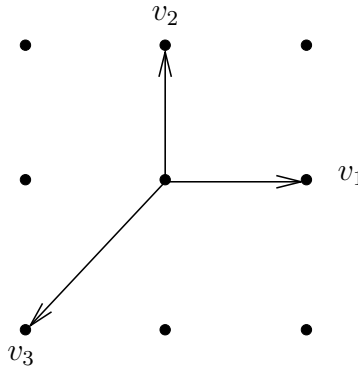


Figure 2.1: The fan Σ of $\mathbb{C}\mathbb{P}^2$.

Example 2.4. Let us come back to the example of $\mathbb{C}\mathbb{P}^2$ (which is two dimensional rather than three dimensional, but easier to visualize as a first example). The fan is given in figure 2.1. There are three one-dimensional cones generated by the vectors $v_1 = (1, 0)$, $v_2 = (0, 1)$ and $v_3 = (-1, -1)$, to which we associate the homogeneous coordinates w_1, w_2 and w_3 of \mathbb{C}^3 . The set Z_Σ is simply $\{0\}$, and thus the toric variety is given by

$$\mathcal{M}_\Sigma = (\mathbb{C}^3 \setminus \{0\}) / (\mathbb{C}^*). \quad (2.8)$$

Moreover, we have that $1(1, 0) + 1(0, 1) + 1(-1, -1) = (0, 0)$, so the \mathbb{C}^* quotient is implemented by the equivalence relation $(w_1, w_2, w_3) \sim \lambda(w_1, w_2, w_3)$. This is the usual description of $\mathbb{C}\mathbb{P}^2$.

In toric geometry it is straightforward to know whether a toric variety is compact or not:

Proposition 2.5. A toric variety \mathcal{M}_Σ is compact if and only if its fan Σ fills $N_{\mathbb{R}}$.

The reader is referred to [1] for a proof of this proposition.

2.1.1 Toric Divisors

In a toric variety there is a natural set of divisors called toric divisors.

Definition 2.6. *Let \mathcal{M}_Σ be a toric variety described by a fan Σ . Associate a homogeneous coordinates w_i to each vector v_i generating the one dimensional cones of Σ . The toric divisors D_i of \mathcal{M}_Σ are the hypersurfaces defined by the equations $w_i = 0$.*

Since we associated a homogeneous coordinates w_i to each one dimensional cones v_i in the fan Σ of \mathcal{M}_Σ , we can think of the vectors v_i as corresponding to the toric divisors defined by $w_i = 0$.

Similarly, higher dimensional cones of Σ correspond to lower dimensional algebraic subvarieties of \mathcal{M}_Σ .

In fact, it can be shown (see [1]), by using methods very similar to those used for complex projective spaces, that the canonical bundle of \mathcal{M}_Σ is given by

$$K_{\mathcal{M}_\Sigma} = \mathcal{O}\left(-\sum_i D_i\right). \quad (2.9)$$

This result will be useful to determine whether a toric variety is Calabi-Yau or not.

2.2 Toric Calabi-Yau Threefolds

First, let us briefly explain what a Calabi-Yau manifold is.

2.2.1 Definition of a Calabi-Yau Manifold

It was in 1954 that Calabi stated his conjecture [37, 38], which was proved by Yau in 1976 [39, 40]. Given a compact Kähler manifold M with $c_1 = 0$, the proof of the conjecture guarantees the existence of a Ricci-flat Kähler metric on M , that is a Kähler metric with zero Ricci form. Such a manifold is called a Calabi-Yau manifold.

However, many different definitions of Calabi-Yau manifolds exist in the literature; let us now list some of the most common definitions.

A Calabi-Yau manifold of real dimension $2m$ is a compact Kähler manifold (M, J, g) :

1. with zero Ricci form,

2. with vanishing first Chern class,
3. with $\text{Hol}(g) = SU(m)$ (or $\text{Hol}(g) \subseteq SU(m)$),
4. with trivial canonical bundle,
5. that admits a globally defined and nowhere vanishing holomorphic m -form.

We will not study in detail these definitions and their interrelations in this thesis; for such an analysis the reader is referred to [41, 42]. Let us simply say that strictly speaking, these definitions are all inequivalent.

An important point common to all these definitions is that the manifold is assumed to be *compact*. However, it is also possible to define *noncompact* (or local) Calabi-Yau manifolds; by local or noncompact Calabi-Yau manifolds we mean open neighbourhoods in compact Calabi-Yau manifolds. These are very useful in many applications in physics, for instance in topological strings [18, 19]. They are also relevant in the study of geometric transitions [43]. In fact, they will play a crucial rôle in the remaining of this thesis, especially in chapters 4 and 5.

In this thesis we will adopt the following definition of Calabi-Yau manifolds.

Definition 2.7. *A Calabi-Yau manifold is a Kähler manifold (M, J, g) with trivial canonical bundle.*

This definition applies for both compact and noncompact Calabi-Yau manifolds. The simplest noncompact Calabi-Yau manifold is obviously \mathbb{C}^m .

2.2.2 Calabi-Yau Manifolds in Toric Geometry

We will now implement the Calabi-Yau condition on toric threefolds.

It is a well known fact (see for instance [35, 41, 42]) that to a divisor $D = \sum_i a_i N_i$ we can associate a line bundle with a meromorphic section such that the meromorphic section has a zero of order a_i along N_i if $a_i > 0$ and a pole of order $-a_i$ along N_i if $a_i < 0$. The N_i are irreducible hypersurfaces, that is hypersurfaces that cannot be written as the union of two hypersurfaces.

In the toric case, the toric divisors D_i defined by $w_i = 0$ are irreducible hypersurfaces. Therefore, using the above correspondence we see that the toric divisor D_i is associated to a line bundle $\mathcal{O}(D_i)$ with a section s that has a zero of order one along

D_i ; thus the section s is simply w_i . Hence we see that each homogeneous coordinate w_i is a section of the line bundle $\mathcal{O}(D_i)$ associated to the toric divisor D_i .

Now, if we consider a monomial $w_1^{a_1} \cdots w_k^{a_k}$; for $a_i > 0$, it has zeroes of order a_i along D_i , while for $a_j < 0$, it has poles of order $-a_j$ along D_j . Therefore it is a section of the line bundle $\mathcal{O}(\sum_i a_i D_i)$.

Let us now consider the case where $a_i = \langle v_i, m \rangle$, $i = 1, \dots, k$ for some $m \in M$. Under the equivalence relations of the toric variety the monomial becomes

$$(\lambda^{Q_1^1} w_1)^{\langle v_1, m \rangle} \cdots (\lambda^{Q_k^k} w_k)^{\langle v_k, m \rangle} = \lambda^{\langle \sum_{i=1}^k Q_a^i v_i, m \rangle} w_1^{\langle v_1, m \rangle} \cdots w_k^{\langle v_k, m \rangle}. \quad (2.10)$$

But since $\sum_{i=1}^k Q_a^i v_i = 0$, this monomial is invariant under the equivalence relations and therefore it is a true meromorphic function on our toric variety. This means that it must be a section of the trivial line bundle, i.e.

$$\sum_{i=1}^k \langle v_i, m \rangle D_i \sim 0 \quad \text{for any } m \in M. \quad (2.11)$$

Conversely, if $\sum_{i=1}^k a_i D_i \sim 0$, then there exists a $m \in M$ such that $a_i = \langle v_i, m \rangle$ for all i .

Now, we know that a Kähler manifold is Calabi-Yau if and only if its canonical class is trivial. We saw in section 2.1.1 that the canonical line bundle of a toric variety \mathcal{M}_Σ is given by $K_{\mathcal{M}_\Sigma} \cong \mathcal{O}(-\sum_{i=1}^k D_i)$. Therefore the canonical bundle is trivial if and only if $\sum_{i=1}^k D_i \sim 0$. Using (2.11), we see that this condition is equivalent to the existence of a $m \in M$ such that $\langle v_i, m \rangle = 1$ for all i , which leads to the following proposition.

Proposition 2.8. *Let \mathcal{M}_Σ be a toric manifold defined by a fan Σ . \mathcal{M}_Σ is Calabi-Yau if and only if the vectors v_i generating the one-dimensional cones of \mathcal{M}_Σ all lie in the same affine hyperplane.*

It is thus very easy to see whether a toric variety is Calabi-Yau or not; in fact, it can be read off directly from the fan Σ of the toric variety.

A consequence of proposition 2.8 is the following:

Corollary 2.9. *A toric Calabi-Yau manifold is noncompact.*

Since the v_i lie in a hyperplane, Σ does not fill $N_{\mathbb{R}}$. Thus proposition 2.5 tells us that \mathcal{M}_{Σ} is noncompact.

This seems like a serious limitation of toric geometry, since in string theory we are often interested in compact Calabi-Yau manifolds. However, we will see in section 2.5 how to construct compact Calabi-Yau manifolds in toric geometry.

The Calabi-Yau condition can be rewritten in yet another equivalent form. In (2.7) we defined the ‘charges’ (the meaning of this name will become clear in section 2.3) Q_a^i satisfying $\sum_{i=1}^k Q_a^i v_i = 0$. Therefore $\sum_{i=1}^k Q_a^i \langle v_i, m \rangle = 0$ for any $m \in M$. In particular, there exists an $m \in M$ such that $\langle v_i, m \rangle = 1$ for all i if and only if $\sum_{i=1}^k Q_a^i = 0$ for all a . But we showed that a toric manifold is Calabi-Yau if and only if there exists an $m \in M$ such that $\langle v_i, m \rangle = 1$ for all i . Therefore, the condition can be restated as follows:

Proposition 2.10. *A toric manifold is Calabi-Yau if and only if the charges Q_a^i satisfy the condition $\sum_{i=1}^k Q_a^i = 0$ for all a .*

This condition is also very simple to verify. We only have to check that the charges Q_a^i given in the toric data describing the manifold add up to zero. Thus, if we are given a fan we simply check that the v_i lie in an affine hyperplane, while if we are given the toric data we simply verify that the charges add up to zero.

To conclude this section we introduce a nice pictorial way of characterizing toric Calabi-Yau threefolds. We showed that for toric Calabi-Yau threefolds the v_i lie in a two dimensional plane P . Therefore, we can draw the two dimensional graph $\tilde{\Gamma}$ given by the intersection of the plane P and the fan Σ . $\tilde{\Gamma}$ determines completely the fan Σ of a toric Calabi-Yau threefold. Given $\tilde{\Gamma}$, we can draw a ‘dual’ graph Γ in the sense that the edges of $\tilde{\Gamma}$ are normals to the edges of Γ and vice-versa. Γ is called the *toric diagram* of a toric Calabi-Yau threefold \mathcal{M}_{Σ} . It represents the degeneration of the fibers of the torus fibration. We will describe in more details toric diagrams in section 2.3.

Conversely, given a toric diagram Γ , it is straightforward to recover the fan Σ of the toric Calabi-Yau threefold. One first draws the dual graph $\tilde{\Gamma}$, and then defines the vectors $v_i = (\nu_i, 1)$ where ν_i are the vertices of $\tilde{\Gamma}$. Because of the symmetries of a three dimensional lattice, the v_i must be the generators of the edges of the fan Σ of the toric Calabi-Yau threefold \mathcal{M}_{Σ} . Linear relations between the vectors v_i give the charges Q_a^i . In other words, the fan Σ is a three dimensional cone over the two dimensional graph $\tilde{\Gamma}$. An example of graphs Γ and $\tilde{\Gamma}$ is given in figure 2.2.

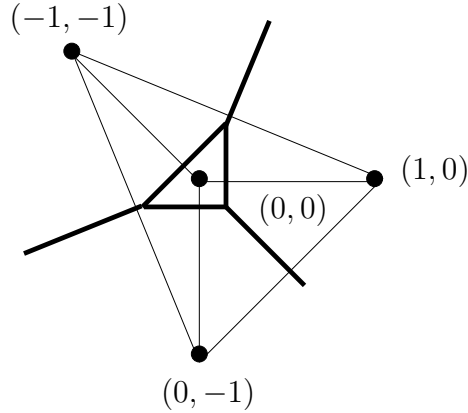


Figure 2.2: The Γ and $\tilde{\Gamma}$ graphs for $\mathcal{O}(-3) \rightarrow \mathbb{C}\mathbb{P}^2$. The toric diagram Γ is the normal diagram drawn in thick lines. The points $(\nu_i, 1)$ give the fan Σ , where the ν_i are the vertices of $\tilde{\Gamma}$ and are shown in the figure.

2.3 Toric Diagrams and Symplectic Quotients

In this section we describe the toric diagrams introduced above. To do so, we need to leave momentarily the homogeneous coordinates approach to toric varieties and see toric manifolds as symplectic quotients, or correspondingly as the Higgs branch of the space of supersymmetric vacua of the GLSM.

2.3.1 Toric Manifolds as Symplectic Quotients

Let z_1, \dots, z_k be the coordinates of \mathbb{C}^k . Let $\mu_a : \mathbb{C}^k \rightarrow \mathbb{C}$, $a = 1, \dots, k-3$ be the $k-3$ moment maps defined by

$$\sum_{i=1}^k Q_a^i |z_i|^2 = \text{Re}(t_a), \quad (2.12)$$

where the t_a are complex numbers. The Q_a^i are the same charges that were introduced in (2.7). Therefore, the Calabi-Yau condition imposes that $\sum_{i=1}^k Q_a^i = 0$ for all a . We also consider the action of the group $G = U(1)^{k-3}$ on the coordinates defined by

$$z_j \rightarrow \exp(iQ_a^j \alpha_a) z_j, \quad a = 1, \dots, k-3. \quad (2.13)$$

It turns out that

$$\mathcal{M} = \frac{\bigcap_{a=1}^{k-3} \mu^{-1}(\text{Re}(t_a))}{G} \quad (2.14)$$

is a toric Calabi-Yau threefold. The $k - 3$ parameters t_a are the complexified Kähler parameters of the Calabi-Yau threefold.

Furthermore, since the charges Q_a^i are the same as in (2.7), it is easy to recover the fan of \mathcal{M} . One only has to find distinct vectors v_i satisfying $\sum_{i=1}^k Q_a^i v_i = 0$; the v_i generate the one dimensional cones of Σ . Moreover, since the Calabi-Yau condition tells us that $\sum_{i=1}^k Q_a^i = 0$, we can choose (because of the symmetries of three dimensional lattices) vectors v_i of the form $v_i = (\nu_i, 1)$. The problem is then reduced to a two-dimensional problem which can easily be solved by inspection. We see that the charges Q_a^i are the important data defining the toric Calabi-Yau manifolds. This is usually called the *toric data* of the manifold.

This description of toric manifolds also arise in gauged linear sigma models. This is a two-dimensional $U(1)^{k-3}$ gauge theory with k chiral superfields Φ_i , whose scalar components are the z_k . The charges of the superfields Φ_i under the gauge group $U(1)^{k-3}$ are denoted by Q_a^i , $a = 1, \dots, k - 3$. This is why the Q_a^i are generally called *charges*. It turns out that – in the Higgs branch – the supersymmetric ground states of the theory are parameterized by the so-called D-term equations modulo gauge equivalence, which are nothing but the moment maps μ_a defined in (2.12). In other words, the Higgs branch of the space of supersymmetric ground states of the GLSM is the toric variety \mathcal{M} defined above.

Now equipped with the description of toric Calabi-Yau threefolds as symplectic quotients, let us come back to the toric diagrams introduced in section 2.2. There, we claimed that these diagrams encode the degeneration of the fibers of the manifold. This can be seen in two different ways: by looking at the threefold as a T^3 fibration or as a $T^2 \times \mathbb{R}$ fibration. We will start with the first approach in section 2.3.2, which is probably simpler. We will explore the second point of view in section 2.3.3, using the topological vertex approach to toric Calabi-Yau threefolds.

2.3.2 T^3 Fibration

We look at the threefolds as T^3 fibrations over three dimensional base manifolds with corners. Locally, we can introduce complex coordinates on the toric manifold: these are the z_i introduced in (2.12). They are not all independent; for a threefold, there are $k - 3$ relations between them given by the moment maps (2.12). Let us rewrite these coordinates as $z_j = |z_j|e^{i\theta_j}$, and introduce a new set of coordinates $\{(p_1, \theta_1), \dots, (p_k, \theta_k)\}$, with $p_i \equiv |z_i|^2$, $i = 1, \dots, k$. The base of the threefold is then parameterized by the coordinates p_i , while the phases θ_i describe the fiber T^3 .

Since $|z_i|^2 \geq 0$, the coordinates p_i satisfy $p_i \geq 0$. Therefore the boundaries of the base are where some of the coordinates p_i vanish. But when $p_j = 0$ the circle $|z_j|e^{i\theta_j}$ degenerates to a single point. Hence, the boundaries of the base correspond to degenerations of the corresponding fiber directions θ_j . Geometrically, this means that the fiber degenerates in the direction given by the unit normal to the boundary.

To draw the toric diagram, we first use the moment maps (2.12) to express the coordinates p_j , $j = 4, \dots, k$ in terms of the three coordinates p_1, p_2, p_3 . Consequently, the boundary equations $p_j = 0$, $j = 4, \dots, k$ become equations in the coordinates p_1, p_2 and p_3 involving the Kähler parameters t_j of (2.12). In fact, each boundary equation gives a plane in the space generated by p_1, p_2 and p_3 . The intersections of these planes are lines; they form the toric diagram of the toric variety, visualized as a three dimensional graph in the space generated by p_1, p_2 and p_3 .

Hence, in this approach the toric diagram is simply the boundary of the three dimensional base parameterized by the p_i . There is a T^3 fiber over the generic point, which degenerates at the boundaries in a way determined by the unit normal. Thus, from this point of view toric diagrams should be visualized as three dimensional diagrams, encoding the degeneration of the T^3 fiber. It is perhaps simpler to understand this approach by working out a specific example.

Example 2.11. *Let us find the toric diagram of $\mathcal{O}(-3) \rightarrow \mathbb{C}\mathbb{P}^2$ from this point of view. This manifold is defined by the moment map $p_1 + p_2 + p_3 - 3p_4 = t$, which we can use to express $p_4 = \frac{1}{3}(p_1 + p_2 + p_3 - t)$. The boundary planes are then given by $p_1 = 0$, $p_2 = 0$, $p_3 = 0$ and $p_1 + p_2 + p_3 = t$. The intersections of these planes give the toric diagram of $\mathcal{O}(-3) \rightarrow \mathbb{C}\mathbb{P}^2$, which is drawn in figure 2.3. We see that it is the same toric diagram as the one shown in figure 2.2, but visualized as a three dimensional graph. Note that from the fourth boundary equation one can see that the Kähler parameter t controls the size of the $\mathbb{C}\mathbb{P}^2$, as it should be.*

This is indeed an easy way to visualize the geometry of the manifold from the toric diagram; another example of this approach will be given in section 2.4. However, it turns out that in many situations it is more enlightening to consider the manifold as a $T^2 \times \mathbb{R}$ fibration, especially from the topological vertex perspective. Let us now describe this alternative viewpoint.

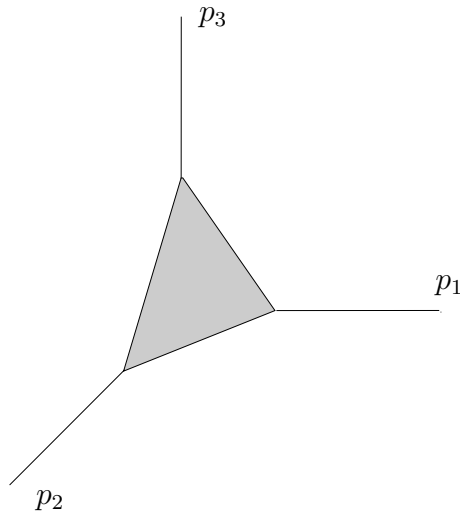


Figure 2.3: Toric diagram Γ of $\mathcal{O}(-3) \rightarrow \mathbb{C}\mathbb{P}^2$ visualized as a three dimensional graph. It encodes the degeneration loci of the T^3 fiber.

2.3.3 $T^2 \times \mathbb{R}$ Fibration

In this language, a toric diagram Γ is a two-dimensional graph which represents the degeneration locus of the $T^2 \times \mathbb{R}$ fibration over the base \mathbb{R}^3 . Over a line in Γ in the direction (q, p) , the cycle $(-q, p)$ of the T^2 fiber degenerates.

To exhibit this structure, we will now follow the topological vertex approach to toric Calabi-Yau threefolds developed by Aganagic, Klemm, Mariño and Vafa in [17]. A good review is given in [18].

The fundamental idea behind this approach is that toric Calabi-Yau threefolds are built by gluing together \mathbb{C}^3 patches. Therefore, the first step is to describe \mathbb{C}^3 (which is the simplest noncompact toric Calabi-Yau threefold) as a $T^2 \times \mathbb{R}$ fibration and exhibit its degeneration locus in a two dimensional graph Γ , which turns out to be a trivalent vertex. Then, more general geometries are constructed by gluing together \mathbb{C}^3 patches, which, in the toric diagram language, corresponds to gluing together trivalent vertices in a way specified by the toric data of the manifold.

Conversely, given a toric Calabi-Yau threefold, we can find a decomposition of the set of all coordinates into triplets that correspond to the decomposition of the threefold into \mathbb{C}^3 patches. The moment maps (2.12) relate the coordinates between the patches, therefore describing how the trivalent vertices corresponding to the \mathbb{C}^3 patches are glued together to form the toric diagram of the manifold.

Let us start by describing \mathbb{C}^3 from this point of view. Here we will only sketch the description; the details are given in [17, 18]. Let $z_i, i = 1, 2, 3$ be complex coordinates on \mathbb{C}^3 . Define the functions

$$\begin{aligned} r_\alpha(z) &= |z_1|^2 - |z_3|^2, \\ r_\beta(z) &= |z_2|^2 - |z_3|^2, \\ r_\gamma(z) &= \text{Im}(z_1 z_2 z_3). \end{aligned} \tag{2.15}$$

It turns out that these functions generate the fiber $T^2 \times \mathbb{R}$. More specifically, \mathbb{R} is generated by r_γ while the T^2 fiber is generated by the circle actions

$$\exp(i\alpha r_\alpha + i\beta r_\beta) : (z_1, z_2, z_3) \rightarrow (e^{i\alpha} z_1, e^{i\beta} z_2, e^{-i(\alpha+\beta)} z_3). \tag{2.16}$$

The cycles generated by r_α and r_β are then respectively referred to as the $(0, 1)$ and $(1, 0)$ cycles.

We now describe the degeneration loci of the fibers. We see from (2.15) and (2.16) that the $(0, 1)$ cycle degenerates when $r_\alpha = 0 = r_\gamma$ and $r_\beta \geq 0$, while the $(1, 0)$ cycle degenerates when $r_\alpha \geq 0 = r_\gamma$ and $r_\beta = 0$. There is also a one-cycle parameterized by $\alpha + \beta$ that degenerates when $r_\alpha - r_\beta = 0 = r_\gamma$ and $r_\alpha \leq 0$.

The toric diagram is a planar graph that encodes the degeneration loci of the fibers. We can set $r_\gamma = 0$ and draw the graph in the plane $r_\alpha - r_\beta$. The graph consists in lines $pr_\alpha + qr_\beta = c$ where c is a constant. Over this line the $(-q, p)$ cycle of the T^2 fiber degenerates (up to the equivalence $(q, p) \sim (-q, -p)$). For \mathbb{C}^3 , the degeneration loci can be represented as a toric diagram with lines defined by the equations $r_\alpha = 0, r_\beta \geq 0$; $r_\beta = 0, r_\alpha \geq 0$ and $r_\alpha - r_\beta = 0, r_\alpha \leq 0$. Over these lines respectively the cycles $(0, 1)$; $(-1, 0) \sim (1, 0)$ and $(1, 1)$ degenerate. This gives the trivalent vertex associated to \mathbb{C}^3 , which is shown in figure 2.4.

For more general geometries, we first find a decomposition of the set of coordinates $z_i, i = 1, \dots, k$ into triplets of coordinates associated to the \mathbb{C}^3 patches. We choose a patch and describe the functions r_α and r_β as above. It turns out that we can use these coordinates as global coordinates for the T^2 fiber in the \mathbb{R}^3 base. As usual, we refer to the cycles r_α and r_β respectively as the $(0, 1)$ and $(1, 0)$ cycles. Using the moment maps (2.12) defining the toric Calabi-Yau threefold, we can find the action of the functions r_α and r_β on the other patches and therefore draw the toric diagram giving the degeneration loci of the T^2 fiber. An explicit example of this approach will be worked out in section 2.4.

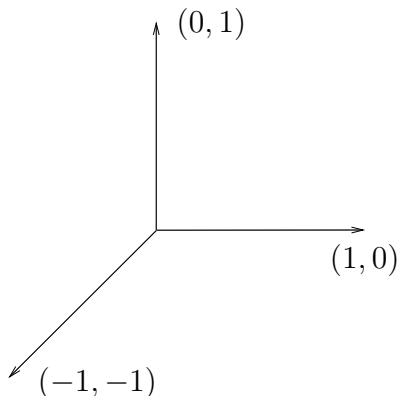


Figure 2.4: Trivalent vertex associated to \mathbb{C}^3 , drawn in the r_α - r_β plan. The vectors represent the generating cycles over the lines.

This decomposition of toric Calabi-Yau threefolds into \mathbb{C}^3 patches leads to a similar decomposition of topological string amplitudes on toric Calabi-Yau threefolds into a basic building block associated to the trivalent vertex of the \mathbb{C}^3 patches, which is called the *topological vertex*. By gluing together these topological vertices one can build topological string amplitudes on any toric Calabi-Yau threefold. This beautiful property of topological amplitudes is the essence of the topological vertex approach developed in [17]. We will not expand further on this subject, although we will use the topological vertex in various occasions in chapters 4 and 5. The interested reader is encouraged to go through the details of the construction in [17].

In the next section we illustrate these different approaches to toric Calabi-Yau threefolds in specific examples.

2.4 Examples

We now describe two examples of toric Calabi-Yau threefolds. The first example is the resolved conifold, namely $\mathcal{O}(-1) \oplus \mathcal{O}(-1) \rightarrow \mathbb{C}\mathbb{P}^1$. In this simple case, we illustrate in detail the different viewpoints explained in the previous sections. The second example is a more complicated geometry. It is a noncompact Calabi-Yau threefold whose compact locus consists of two compact divisors each isomorphic to a del Pezzo surface dP_2 ¹ and a rational $(-1, -1)$ curve that intersects both divisors transversely. We will give the toric data describing the manifold and draw the corresponding toric diagram.

¹A del Pezzo surface dP_n , $n = 0, \dots, 8$ is a complex two-dimensional Fano variety, that is $\mathbb{C}\mathbb{P}^2$ blown up in n points.

2.4.1 Resolved Conifold

The resolved conifold $Y = \mathcal{O}(-1) \oplus \mathcal{O}(-1) \rightarrow \mathbb{CP}^1$ is a noncompact Calabi-Yau threefold which admits a toric description given by the following toric data:

$$\begin{array}{cccc} & z_1 & z_2 & z_3 & z_4 \\ \mathbb{C}^* & 1 & 1 & -1 & -1 \end{array} \quad (2.17)$$

The lines in this table give the charges Q_a^i corresponding to the torus actions on the homogeneous coordinates z_i . We see that $\sum_i Q^i = 1 + 1 - 1 - 1 = 0$; therefore Y is Calabi-Yau. Y is defined as the space obtained from

$$|z_1|^2 + |z_2|^2 - |z_3|^2 - |z_4|^2 = t \quad (2.18)$$

after quotienting by the $U(1)$ action specified by the charges in (2.17).

We now find the fan Σ describing Y . We have the relation $\sum_{i=1}^4 Q^i v_i = v_1 + v_2 - v_3 - v_4 = 0$. We choose distinct vectors $v_i = (\nu_i, 1)$ where the ν_i are two dimensional. A solution is $v_1 = (1, 0, 1)$, $v_2 = (-1, 0, 1)$, $v_3 = (0, 1, 1)$ and $v_4 = (0, -1, 1)$. These four vectors generate the four one dimensional cones of Σ .

The two dimensional graph $\tilde{\Gamma}$ is given by the intersection of the plane $z = 1$ and Σ . The vertices are $(1, 0), (-1, 0), (0, 1)$ and $(0, -1)$. We can also draw the toric diagram, which is the dual graph Γ . They are shown in figure 2.5.

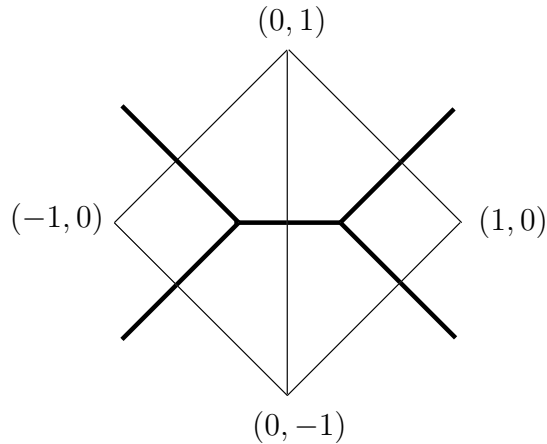


Figure 2.5: The Γ and $\tilde{\Gamma}$ graphs for $\mathcal{O}(-1) \oplus \mathcal{O}(-1) \rightarrow \mathbb{CP}^1$. The toric diagram Γ is the normal diagram drawn in thick lines. The points $(\nu_i, 1)$ give the fan Σ , where the ν_i are the vertices of $\tilde{\Gamma}$ and are shown in the figure.

If we look at the resolved conifold as a T^3 fibration, we have to understand the toric diagram Γ as a three dimensional graph representing the base, where the T^3 fiber

degenerates at the boundaries. The base is parameterized by the four coordinates $p_i \equiv |z_i|^2$ subject to the relation (2.18). We can use (2.18) to eliminate p_4 ,

$$p_4 = p_1 + p_2 - p_3 - t. \quad (2.19)$$

Therefore, since $|z_i|^2 \geq 0$, the boundary equations of the toric base are given by

$$\begin{aligned} p_1 &= 0, \\ p_2 &= 0, \\ p_3 &= 0, \\ p_1 + p_2 - p_3 &= t. \end{aligned} \quad (2.20)$$

The intersections of these planes give the toric diagram of the resolved conifold shown in figure 2.5, but visualized as a three dimensional graph as in figure 2.6. Note that as in example 2.11, by the fourth boundary equation above one can see that the Kähler parameter t controls the size of the $\mathbb{C}\mathbb{P}^1$, as it should be.

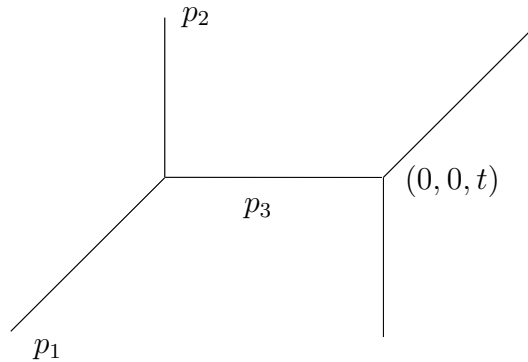


Figure 2.6: Toric diagram Γ of $\mathcal{O}(-1) \oplus \mathcal{O}(-1) \rightarrow \mathbb{C}\mathbb{P}^1$ visualized as a three dimensional graph. It encodes the degeneration loci of the T^3 fiber.

We can also describe the resolved conifold as a $T^2 \times \mathbb{R}$ fibration, using its decomposition into \mathbb{C}^3 patches. We choose the first patch to be defined by $z_1 \neq 0$. Using (2.18) we can express z_1 in terms of the other coordinates, so the patch is parameterized by (z_2, z_3, z_4) . We define the functions

$$\begin{aligned} r_\alpha &= |z_3|^2 - |z_2|^2, \\ r_\beta &= |z_4|^2 - |z_2|^2. \end{aligned} \quad (2.21)$$

This gives the usual trivalent graph of \mathbb{C}^3 .

The other patch is defined by $z_2 \neq 0$, therefore parameterized by (z_1, z_3, z_4) . Using (2.18) we can rewrite the functions (2.21) in terms of the coordinates on this patch:

$$\begin{aligned} r_\alpha &= |z_1|^2 - |z_4|^2 - t, \\ r_\beta &= |z_1|^2 - |z_3|^2 - t. \end{aligned} \quad (2.22)$$

These functions generate the circle action

$$\exp(i\alpha r_\alpha + i\beta r_\beta) : (z_1, z_3, z_4) \rightarrow (e^{i(\alpha+\beta)} z_1, e^{-i\beta} z_3, e^{-i\alpha} z_4). \quad (2.23)$$

In this patch, the $(0, 1)$ cycle degenerates when $r_\alpha \leq -t$ and $r_\beta = -t$. The $(1, 0)$ cycle degenerates when $r_\alpha = -t$ and $r_\beta \leq -t$. The $(1, 1)$ cycle degenerates when $r_\alpha - r_\beta = 0$ and $r_\alpha \geq -t$. Therefore, the graph associated to this patch is identical to the first one, although it is shifted such that its origin is at the point $(-t, -t)$. The two graphs are joined through the common edge given by $r_\alpha - r_\beta = 0$. t gives the ‘length’ of the internal edge, and correspondingly is the Kähler parameter associated to the \mathbb{CP}^1 . This gives the toric diagram of the resolved conifold shown in figure 2.7.

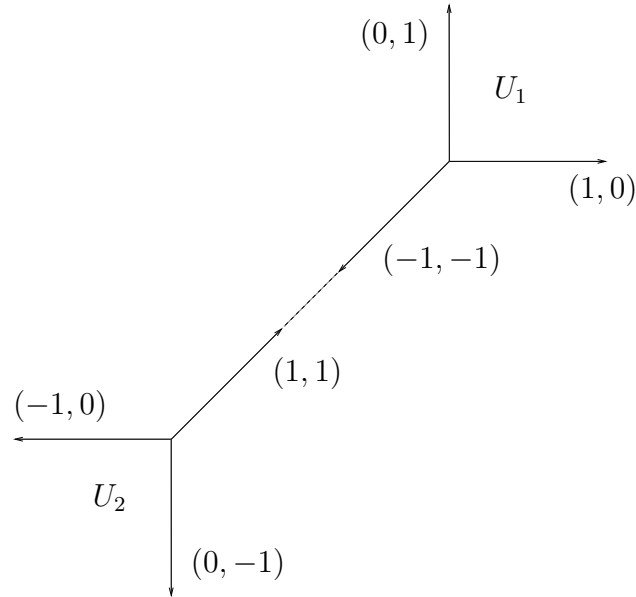


Figure 2.7: Toric diagram of $\mathcal{O}(-1) \oplus \mathcal{O}(-1) \rightarrow \mathbb{CP}^1$, drawn in the r_α - r_β plan. The vectors represent the generating cycles over the lines. The origin of the second patch U_2 is shifted to $(-t, -t)$.

2.4.2 Two dP_2 's Connected by a \mathbb{CP}^1

The next example is a noncompact Calabi-Yau threefold X whose compact locus consists of two compact divisors each isomorphic to a del Pezzo surface dP_2 and a rational $(-1, -1)$ curve that intersects both divisors transversely. The divisors do not intersect each other. This manifold is described by the following toric data:

$$\begin{array}{rcccccccccc}
 & z_1 & z_2 & z_3 & z_4 & z_5 & z_6 & z_7 & z_8 & z_9 & z_{10} \\
 \mathbb{C}^* & -1 & 1 & 1 & -1 & 0 & 0 & 0 & 0 & 0 & 0 \\
 \mathbb{C}^* & 1 & 0 & -1 & -1 & 0 & 1 & 0 & 0 & 0 & 0 \\
 \mathbb{C}^* & 1 & -1 & 0 & -1 & 1 & 0 & 0 & 0 & 0 & 0 \\
 \mathbb{C}^* & 0 & 0 & 0 & 1 & -1 & -1 & 1 & 0 & 0 & 0 \\
 \mathbb{C}^* & 0 & 0 & 0 & 0 & 1 & 0 & -1 & -1 & 0 & 1 \\
 \mathbb{C}^* & 0 & 0 & 0 & 0 & 0 & 1 & -1 & 0 & -1 & 1 \\
 \mathbb{C}^* & 0 & 0 & 0 & 0 & 0 & 0 & -1 & 1 & 1 & -1.
 \end{array} \tag{2.24}$$

We see that the charges in each line add up to zero, hence X is Calabi-Yau. The toric diagram Γ of X and its dual $\tilde{\Gamma}$ are shown in figure 2.8.

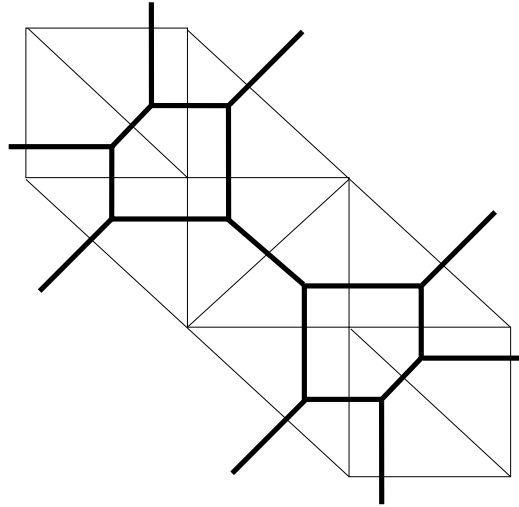


Figure 2.8: The Γ and $\tilde{\Gamma}$ graphs for the Calabi-Yau threefold X whose compact locus consists of two dP_2 's connected by a \mathbb{CP}^1 . The toric diagram Γ is the normal diagram drawn in thick lines.

It is often useful [22] to consider a related Calabi-Yau threefold \tilde{X} obtained from X by flopping the two exceptional curves outside of the compact divisors. This is shown in figure 4.2.

This Calabi-Yau threefold — and a simplified one where some of the Kähler parameters of \tilde{X} are sent to infinity — will be the focus of interest of chapter 4 and 5.

2.5 Hypersurfaces in Toric Varieties

In the remaining of this chapter we explain how compact Calabi-Yau manifolds may be obtained in toric geometry, namely as hypersurfaces in compact toric manifolds using Batyrev's well known reflexive polytopes [3].

2.5.1 Reflexive Polytopes

In section 2.1 we described in details toric Calabi-Yau threefolds. In particular, we showed that toric Calabi-Yau threefolds are noncompact. However, from a string theory perspective, it is often desirable to consider compact Calabi-Yau manifolds. Hence it seems that toric geometry is not a good setup for such geometries.

Fortunately, there is a way to construct compact Calabi-Yau manifolds in toric geometry, namely as compact hypersurfaces in compact toric varieties. Batyrev's reflexive polytopes [3] provide a very useful description of such compact Calabi-Yau manifolds. The toric variety itself is not Calabi-Yau, consequently it can be compact. Reflexivity of the polytopes then ensures that the compact hypersurface, which is not toric itself, is Calabi-Yau.

An elementary introduction to these concepts and their applications to string theory and dualities can be found in [36]. The following is partly based on the first sections of [15].

As in section 2.1, in the following we focus our attention on three-dimensional toric varieties, therefore leading to two-dimensional Calabi-Yau hypersurfaces, i.e. K3 surfaces. It is however straightforward to generalize the concepts to higher dimensional toric varieties.

2.5.1.1 Lattice Description

A polytope in $M_{\mathbb{R}}$ is the convex hull of a finite number of points in $M_{\mathbb{R}}$, and a polyhedron in $M_{\mathbb{R}}$ is the intersection of finitely many half-spaces (given by inequalities $\langle u, v \rangle \geq c$ with some $v \in N_{\mathbb{R}}$ and $c \in \mathbb{R}$) in $M_{\mathbb{R}}$. It is well known that any polytope is a polyhedron and any bounded polyhedron is a polytope. If a polyhedron $S \subset M_{\mathbb{R}}$ contains the origin $\mathbf{0}$, its dual

$$S^* = \{v \in N_{\mathbb{R}} : \langle u, v \rangle \geq -1 \text{ for all } u \in S\}. \quad (2.25)$$

is also a polyhedron containing $\mathbf{0}$, and $(S^*)^* = S$.

A lattice polytope in $M_{\mathbb{R}}$ is a polytope with vertices in M .

Definition 2.12. *A polytope $\Delta \subset M_{\mathbb{R}}$ containing $\mathbf{0}$ is called reflexive if both Δ and Δ^* are lattice polytopes.*

This is equivalent to Δ being a lattice polytope whose bounding equations are of the form $\langle u, v_i \rangle \geq -1$ with $v_i \in N$ (in coordinates, $\sum_j u_j v_{ij} \geq -1$ with integer coefficients v_{ij}). By convexity it is sufficient to consider only those equations corresponding to v_i that are vertices of Δ^* . In this way there is a duality between vertices of Δ^* and facets of Δ ; similarly, there are dualities between p dimensional faces of Δ and $(n - p - 1)$ dimensional faces of Δ^* (in three dimensions: between edges and dual edges).

An interior point u of a reflexive polytope must satisfy $\langle u, v_i \rangle > -1$ for all v_i , so an interior lattice point must satisfy $\langle u, v_i \rangle \geq 0$. Thus if u is an interior lattice point, then nu is also an interior lattice point for any non-negative integer n . For $u \neq \mathbf{0}$ this would be in conflict with the boundedness of Δ , implying that $\mathbf{0}$ is the only interior lattice point.

2.5.1.2 Toric Interpretation

Given a three dimensional pair of reflexive polytopes $\Delta \in M_{\mathbb{R}}$, $\Delta^* \in N_{\mathbb{R}}$, a smooth K3 surface can be constructed in the following manner. Any complete triangulation of the surface of Δ^* defines a fan Σ whose three dimensional cones are just the cones over the regular (i.e., lattice volume one) triangles. To any lattice point $p_i = (\bar{x}_i, \bar{y}_i, \bar{z}_i)$ on the boundary of Δ^* one can assign a homogeneous coordinate $w_i \in \mathbb{C}$, with the rule that several w_i are allowed to vanish simultaneously only if there is a cone such

that the corresponding p_i all belong to this cone. The equivalence relations among the homogeneous coordinates are given by

$$(w_1, \dots, w_n) \sim (\lambda^{Q_a^1} w_1, \dots, \lambda^{Q_a^k} w_k) \text{ for any } \lambda \in \mathbb{C}^* \quad (2.26)$$

with any set of integers Q_a^i such that $\sum Q_a^i p_i = 0$; among these relations, $k - 3$ are independent. This construction gives rise to a smooth compact three dimensional toric variety \mathcal{M}_Σ (smooth because the generators of every cone are also generators of N , compact because the fan fills $N_{\mathbb{R}}$). The loci $w_i = 0$ are the toric divisors D_i .

To any lattice point q_j of M we can assign a monomial $m_j = \prod_i w_i^{(q_j \cdot p_i) + 1}$; the exponents are non-negative as a consequence of reflexivity. The hypersurface defined by the zero-locus of a generic polynomial $P = \sum a_j m_j$ transforms homogeneously under (2.26) and can be shown to define a K3 hypersurface in \mathcal{M}_Σ (actually it defines a family of hypersurfaces depending on the coefficients a_j).

Remark 2.13. *A good way to remember this construction is to notice that the polytope in $\Delta^* \in N_{\mathbb{R}}$ gives the fan of the ambient toric variety, while the polytope in $\Delta \in M_{\mathbb{R}}$ gives the Monomials.*

2.5.1.3 Calabi-Yau Condition

It was shown by Batyrev [3] that the hypersurface defined by the vanishing of a generic polynomial in the class determined by Δ is a smooth Calabi-Yau manifold for $n \leq 4$, where n is the dimension of the lattice M . For $n \leq 3$ the underlying toric variety is smooth; in particular for $n = 3$ the hypersurface describes a smooth K3 surface as explained above. For $n = 4$ it may have point-like singularities, which are however missed by the generic hypersurface describing the Calabi-Yau threefold.

Let us now explain why the hypersurface is a Calabi-Yau manifold. Let a manifold X be defined by the equation $P = 0$ in a toric variety \mathcal{M} . The polynomial P defines a section of a line bundle (other sections are defined by different coefficients a_j). The divisor class of the line bundle can be read off from any monomial in P . Since the origin is always included in the polytopes, P always includes the monomial $\prod_{i=1}^k w_i$, which corresponds to the divisor class $[\sum_{i=1}^k D_i]$. Thus, the polynomial P determines a section of the anticanonical bundle of the toric variety \mathcal{M} .

Roughly speaking, on X the section P maps points of X to 0 in the fibers of the anticanonical bundle of \mathcal{M} , since X is defined as the zero-locus of P . Thus, P serves as a coordinate near X , and in fact the normal bundle N_X of X is simply $K_{\mathcal{M}}^*|_X$,

since P is a section of the anticanonical bundle of \mathcal{M} . Thus, the exact sequence $0 \rightarrow T^{1,0}X \rightarrow T^{1,0}\mathcal{M}|_X \rightarrow N_X \rightarrow 0$ becomes (this result is also known as the adjunction formula 1 — see [35, 44])

$$0 \rightarrow T^{1,0}X \rightarrow T^{1,0}\mathcal{M}|_X \rightarrow K_{\mathcal{M}}^*|_X \rightarrow 0. \quad (2.27)$$

Given any holomorphic vector bundle B over X of rank k and any holomorphic sub-bundle A , one can always form the respective determinant bundles $\det B$ and $\det A$ which satisfy the identity $\det B = \det A \otimes \det(B/A)$. Using the above exact sequence, we can then write

$$\det T^{1,0}\mathcal{M}|_X = \det T^{1,0}X \otimes \det K_{\mathcal{M}}^*|_X. \quad (2.28)$$

Now, using the definition of the anticanonical bundle as the determinant line bundle of the holomorphic tangent bundle and the fact that $\det K_{\mathcal{M}}^* = K_{\mathcal{M}}^*$ since $K_{\mathcal{M}}^*$ is a line bundle, we find

$$K_{\mathcal{M}}^*|_X = K_X^* \otimes K_{\mathcal{M}}^*|_X, \quad (2.29)$$

or equivalently

$$K_X = (K_{\mathcal{M}}^* \otimes K_{\mathcal{M}})|_X, \quad (2.30)$$

that is the canonical bundle K_X of X is trivial. If X is smooth, which is guaranteed by reflexivity for $n \leq 4$, then X is a Calabi-Yau manifold.

2.5.1.4 Fibration Structure

Suppose the intersection of Δ^* with the plane $\bar{z} = 0$ gives a reflexive polygon. We may reinterpret P as a polynomial in the w_i for which $\bar{z}_i = 0$, with coefficients depending on the remaining w_i , i.e. we are dealing with an elliptic curve parameterized by the w_i for which $\bar{z}_i \neq 0$. The map $\mathcal{M}_{\Sigma} \rightarrow \mathbb{C}\mathbb{P}^1$,

$$(w_1, \dots, w_n) \rightarrow W = \prod_{i:\bar{z}_i \neq 0} w_i^{\bar{z}_i} \quad (2.31)$$

is easily checked to be consistent with (2.26) and thus well defined. At any point of the $\mathbb{C}\mathbb{P}^1$ that is neither 0 nor ∞ all the w_i with $\bar{z}_i \neq 0$ are non-vanishing, and (2.26) can be used to set all except one of them to 1. This gives the K3 surface the structure of an elliptic fibration.

2.5.2 Tops

We now describe ‘tops’, the close cousins of Batyrev’s reflexive polytopes.

2.5.2.1 Lattice Description

In [4] Candelas and Font considered reflexive polytopes whose intersections with a plane were themselves reflexive polygons; the fact that this intersection cuts the polytope into two parts (‘top’ and ‘bottom’) gave rise to the notion of a ‘top’ as half of a reflexive polytope in this sense. In [11] this definition was generalized in the following way.

Definition 2.14. *A top $\diamond \subset N_{\mathbb{R}}$ is a lattice polytope such that one of its defining inequalities is of the form $\langle u_0, v \rangle \geq 0$ and all others are of the form $\langle u_i, v \rangle \geq -1$, with $u_i \in M$.*

We consider two tops to be isomorphic if they are related by a $GL(3, \mathbb{Z})$ transformation. This allows us to choose coordinates (x, y, z) for M and $M_{\mathbb{R}}$ such that u_0 has coordinates $(0, 0, 1)$ (we will always make this choice whenever we work with specific coordinates). Then the inequality corresponding to the facet $F_0 := \{v \in \diamond : \langle u_0, v \rangle = 0\}$ is given by $\bar{z} \geq 0$ in terms of dual coordinates $(\bar{x}, \bar{y}, \bar{z})$ for $N_{\mathbb{R}}$. F_0 is bounded by the restrictions of the other inequalities to $\bar{z} = 0$; as these are again of the type $\dots \geq -1$ with integer coefficients, F_0 is a reflexive polygon. Thus the more general definition of a top indeed contains all the cases of [4]. A straightforward adaptation of the above argument about reflexive polytopes shows that a top has no interior lattice points.

The dual $\diamond^* \subset M_{\mathbb{R}}$ of \diamond is the polyhedron defined by the inequalities originating from the vertices of \diamond . The vertices $(\bar{x}_i, \bar{y}_i, 0)$ of F_0 lead to inequalities of the form $x\bar{x}_i + y\bar{y}_i \geq -1$; we will refer to the corresponding facets as *vertical facets*. Thus \diamond^* must be contained in a prism over F_0^* (the dual of F_0 in the two dimensional sense). The remaining vertices of \diamond have $\bar{z} > 0$. The corresponding inequalities can be written as

$$z\bar{z}_i \geq -1 - x\bar{x}_i - y\bar{y}_i \tag{2.32}$$

implying that for every fixed $(x, y) \in F_0^*$ there is a minimal (but no maximal) value $z_{\min}(x, y)$ such that $(x, y, z) \in \diamond^*$ for all $z \geq z_{\min}(x, y)$. In this way we can view \diamond^* as the result of ‘chopping off’ the lower parts of an infinitely extended prism. Alternatively, we may see it as a ‘polytope’ with one vertex $u_{\infty} = +\infty u_0$ at infinity,

as it is the dual of \diamond which may be defined by $\langle u_i, v \rangle \geq -1$ for $i \geq 1$ and $\langle \lambda u_0, v \rangle \geq -1$ for arbitrarily large positive λ . \diamond^* has infinitely many interior lattice points $(0, 0, z)$ with z any non-negative integer.

The projection

$$\pi : \diamond^* \rightarrow F_0^*, \quad (x, y, z) \rightarrow (x, y) \tag{2.33}$$

takes vertices of \diamond^* to lattice points of F_0^* . Conversely, every (finite) vertex of \diamond^* is of the form $(x, y, z_{\min}(x, y))$ where (x, y) is a lattice point of F_0^* . This means that by specifying F_0^* and z_{\min} for each of its lattice points, we have specified \diamond^* completely. The projections of non-vertical facets determine a partition of F_0^* . These facts afford a useful pictorial representation of \diamond^* in terms of a picture of F_0^* where every lattice point is labeled with the corresponding z_{\min} .

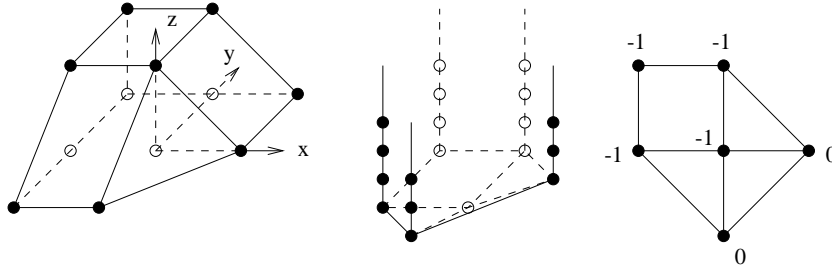


Figure 2.9: A top, its dual and the minimal point notation.

Example 2.15. Suppose \diamond is the convex hull of $(-1, -1, 0)$, $(-1, 1, 0)$, $(1, 1, 0)$, $(1, 0, 0)$, $(0, -1, 0)$, $(0, 0, 1)$, $(-1, 0, 1)$, $(-1, 1, 1)$ and $(0, 1, 1)$, as shown in the first part of figure 2.9. \diamond has 7 facets corresponding to the inequalities

$$\begin{aligned} F_0 : z \geq 0, \quad F_1 : z \leq 1, \quad F_2 : x \geq -1, \quad F_3 : y \leq 1, \\ F_4 : x + z \leq 1, \quad F_5 : x - y + z \leq 1, \quad F_6 : z - y \leq 1, \end{aligned}$$

implying that \diamond is indeed a top and that \diamond^* has the vertices $(0, 0, -1)$, $(1, 0, 0)$, $(0, -1, 0)$, $(-1, 0, -1)$, $(-1, 1, -1)$, $(0, 1, -1)$, in addition to the ‘vertex at infinity’ $(0, 0, \infty)$. Thus F_0^* is the convex hull of $(1, 0)$, $(0, -1)$, $(-1, 0)$, $(-1, 1)$, $(0, 1)$ with z_{\min} as shown in the third diagram of figure 2.9.

2.5.2.2 Toric Interpretation

In section 2.5.1.2 we showed that three dimensional reflexive polytopes describe families of compact K3 surfaces in compact three dimensional toric varieties. Let us now find the toric interpretation of tops.

Let \diamond be a top defined in $N_{\mathbb{R}}$, and let $\diamond^* \subset M_{\mathbb{R}}$ be its dual (notice that we lost the symmetry that was present in the case of reflexive polytopes, since the dual of a top is not a top). A complete triangulation of the surface of \diamond defines a fan Σ , to which we associate a three dimensional toric variety \mathcal{M}_{Σ} . As before, we can also assign a monomial $m_j = \prod_i w_i^{\langle q_j, p_i \rangle + 1}$ to any lattice point q_j of M , and define a generic polynomial $P = \sum_j a_j m_j$. The equation $P = 0$ defines a surface \mathcal{S} in \mathcal{M}_{Σ} .

Although the description is very similar to the K3 case, there are many important differences. Since the fan associated to a top does not fill $N_{\mathbb{R}}$, according to proposition 2.5 the toric variety is noncompact. The surface \mathcal{S} defined by $P = 0$ is elliptically fibered as before, but it is now also noncompact. In fact, since there are no negative exponents in (2.31), the base space of the fibration is now \mathbb{C} instead of $\mathbb{C}P^1$.

In those cases where the top is half of a reflexive polytope, it encodes the geometry of the K3 away from the preimage of the point ∞ . In addition we have an interpretation of a top in the case of an elliptically fibered higher dimensional Calabi-Yau hypersurface in a toric variety. Here the polygon encoding the elliptic fiber is again an intersection of a reflexive polytope with a plane. The base space of the fibration is determined by projecting the fan along the two dimensions spanned by the polygon [13]. Rays in this projected fan determine divisors in the base along which the fiber can degenerate; the inverse image of such a ray is again a top whose structure determines the generic type of degeneration over the intersection of a disc with the divisor. This may lead to tops with far more points than in a three dimensional reflexive polytope [11].

These tops and their associated toric descriptions possess very interesting mathematical properties. They also enter beautifully in the analysis of dualities between compactifications of string theory. In chapter 3 we investigate in detail the geometrical properties of tops and provide a complete classification of these objects, which leads to interesting results in string theory.

Chapter 3

The Classification of Tops and String Dualities

In this chapter we study in detail the geometrical object introduced in section 2.5.2, namely tops. We start by continuing the investigation of the toric properties of tops that was started in section 2.5.2. This leads us to claim that not only tops but also elliptic fibration structures in general should be related to untwisted or twisted affine Kac-Moody algebras. Using Kodaira's classification of degenerations of elliptic fibrations [45], we find a simple way to assign an affine Kac-Moody algebra to a top.

Then in section 3.2 we classify all the possible tops. We present here our classification scheme; the results are shown in appendix B.1. Finally, we discuss our results with particular emphasis on the cases related to twisted algebras, first in terms of geometry (twisted algebras occur only for fibrations that allow orbifold actions) and then in terms of dualities between M-theory, F-theory or type II strings and heterotic strings or CHL type strings.

3.1 Toric Properties and Affine Kac-Moody Algebras

In section 2.5.2 we introduced tops and described some of their fundamental properties. In this section we will pursue further the analysis of their toric properties, which leads to a beautiful correspondence between tops and affine Kac-Moody algebras.

3.1.1 Affine Kac-Moody Algebras

Let us first recall some properties of tops introduced in section 2.5.2. Let \diamond be a top defined in $N_{\mathbb{R}}$, and let $\diamond^* \subset M_{\mathbb{R}}$ be its dual. A complete triangulation of the surface of \diamond defines a fan Σ , to which we associate a noncompact three dimensional toric variety \mathcal{M}_{Σ} . We assign a monomial $m_j = \prod_i w_i^{(q_j, p_i)+1}$ to any lattice point q_j of M , and define a generic polynomial $P = \sum_j a_j m_j$. The equation $P = 0$ defines a noncompact surface \mathcal{S} in \mathcal{M}_{Σ} .

The elliptic fibration structure of \mathcal{S} is exhibited as follows. The intersection of \diamond with the plane $\bar{z} = 0$ gives a reflexive polygon (the 16 reflexive polygons are shown in figure 3.5). We may reinterpret P as a polynomial in the w_i for which $\bar{z}_i = 0$, with coefficients depending on the remaining w_i , i.e. we are dealing with an elliptic curve parameterized by the w_i for which $\bar{z}_i \neq 0$. The map $\mathcal{M}_{\Sigma} \rightarrow \mathbb{C}$,

$$(w_1, \dots, w_n) \rightarrow W = \prod_{i: \bar{z}_i \neq 0} w_i^{\bar{z}_i} \quad (3.1)$$

is consistent with the equivalence relation (2.26), hence well defined. Notice that in (3.1) there are no negative exponents, which is why it is a map to \mathbb{C} rather than \mathbb{CP}^1 as in (2.31). This gives the surface \mathcal{S} the structure of an elliptic fibration over \mathbb{C} .

All of the interesting geometry happens at $W = 0$. Let us start with a top that has only a single vertex p_n at $\bar{z} = 1$ and all other lattice points at $\bar{z} = 0$. This leads to a hypersurface determined by a polynomial in w_1, \dots, w_{n-1} with coefficients that are power series in $W = w_n$ that start with a constant; each of these power series corresponds to a vertical edge in \diamond^* . In the generic case nothing special happens and we get a smooth elliptic curve at $W = 0$. If we restrict some of the W dependent coefficients to start at higher powers of W , this may lead to singularities. Now the non-vanishing coefficients correspond only to a subset \diamond'^* of \diamond^* , and we can resolve the singularity by passing from \diamond to \diamond' , which corresponds to a blow up.

An arbitrary top \diamond always contains at least one lattice point at $\bar{z} = 1$. This can be seen by observing that a complete triangulation of the fan leads to a triangulation of \diamond in terms of tetrahedra of volume one; such a tetrahedron with base at $\bar{z} = 0$ must then have its apex at $\bar{z} = 1$. Thus every top can be interpreted as the smooth resolution of the singularity at $W = 0$ of an elliptic fibration. Such singularities and their resolutions were classified by Kodaira [45], resulting in the following picture (see also [46]). Under certain assumptions fulfilled in the present case, the inverse image of $W = 0$ must consist either of a single (possibly singular) curve or of a collection of smooth rational curves C_i such that the intersections of these curves

obey $C_i \cdot C_j = -M_{ij}$ where M is the Cartan matrix of an untwisted Kac-Moody algebra of ADE type (these are precisely the self-dual affine Kac-Moody algebras); the multiplicities of the C_i are the coefficients of the null vector of the algebra. In other words, the intersection patterns and multiplicities are represented by the Dynkin diagrams with labels, as shown in figure 3.1.

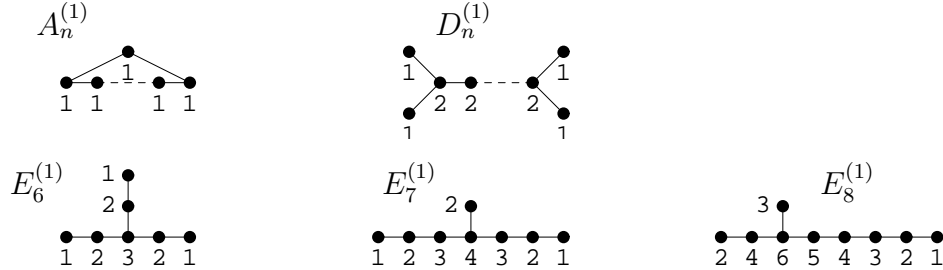


Figure 3.1: Dynkin diagrams of the self-dual untwisted ADE Kac-Moody algebras.

Every toric divisor $D_i = \{w_i = 0\} \subset \mathcal{M}_\Sigma$ may give rise via $D_i \cdot \mathcal{S} = \sum_j C_{ij}$ to one or more curves C_{ij} in \mathcal{S} . This type of intersection theory was worked out in detail for three dimensional reflexive polytopes in [5], with the following results which also hold in the context of tops for the compact divisors with $\bar{z} > 0$.

A lattice point interior to a facet of \diamond determines a divisor D_i that does not intersect \mathcal{S} . A vertex gives rise to a single curve (rational for any vertex at $\bar{z} > 0$ in a non-trivial top). A point interior to an edge corresponds to l rational curves, where l is the length of the dual edge. Each of the rational curves involved has self intersection -2 . Mutual intersections occur only among neighbours along edges; in that case $D_i \cdot D_j \cdot \mathcal{S} = l$. For example, an edge of length 3 dual to an edge of length 2 gives rise to an intersection pattern as indicated in figure 3.2.

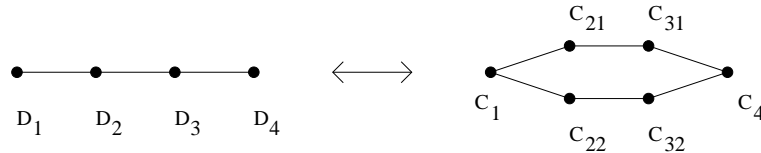


Figure 3.2: An edge of \diamond^* and the intersection pattern to which it corresponds.

Here D_1 and D_4 come from vertices v_1, v_4 of \diamond and D_2 and D_3 from points interior to the edge $\overline{v_1 v_4}$. D_2 and D_3 each give rise to two curves (C_{21}, C_{22} and C_{31}, C_{32} ,

respectively) in such a way that any two curves have mutual intersection one if they are joined by an edge in the second part of figure 3.2.

We can use this information to predict the structure of the edge diagram of the part of \diamond with $\bar{z} \geq 1$. If all the dual edges have length 1, it must have the structure of the Dynkin diagram of an affine ADE algebra. From (3.1) it is clear that the multiplicity of a curve $C_i = D_i \cdot \mathcal{S}$ in $W = 0$ is just \bar{z}_i , i.e. the Dynkin labels encode the heights \bar{z} of the lattice points. If some of the dual edges have lengths > 1 , the edge diagram must be the result of partially collapsing an ADE diagram, as in reading figure 3.2 from right to left. Each of the curves C_{ij} originating from the same D_i must have multiplicity \bar{z}_i in $W = 0$. There are two possibilities. If both vertices are at $\bar{z} > 0$, the uncollapsed diagram contains a closed loop and the only possibility is the A -series.

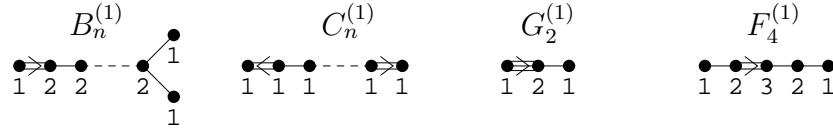


Figure 3.3: Dynkin diagrams of the duals of untwisted non-simply laced Kac-Moody algebras.

The collapsed diagram must then look like the second one in figure 3.3, where we use multiple lines and arrows to indicate that we pass from a point giving rise to more than one curve to a vertex associated with a single curve. The other possibility for an edge whose dual has length > 1 is that one of its vertices is at $\bar{z} = 0$. Then we have to identify two or more ends of one of the D or E Dynkin diagrams. Direct inspection shows that this is possible only for those ends whose last point has a label of 1. These are precisely the ‘extension points’ if the ADE diagram is read as the extended Dynkin diagram of an ADE Lie algebra. If the folding procedure leaves at least one of these points invariant, we may view this as folding an ordinary Dynkin diagram, taking us from a self-dual simply laced algebra to the dual of a non-simply laced one. In this way we get B_n from D_{n+1} , C_n from A_{2n-1} , G_2 from D_4 (by a triple folding), and F_4 from E_6 .

If all of the points with Dynkin label 1 are involved in the folding procedure, we pass from an untwisted Kac-Moody algebra to a twisted one. We find the possibilities $E_7^{(1)} \rightarrow E_6^{(2)}$, $D_{n+3}^{(1)} \rightarrow D_{n+1}^{(2)}$ (two foldings), $D_4^{(1)} \rightarrow A_2^{(2)}$ (quadruple folding) and $E_6^{(1)} \rightarrow D_4^{(3)}$ (triple folding); the resulting diagrams are shown in figure 3.4. Our

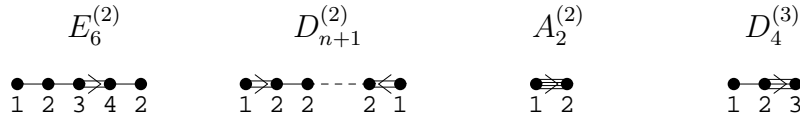


Figure 3.4: Dynkin diagrams of the duals of twisted Kac-Moody algebras that can be read off from tops.

notation is the one used, for example, in [47]. Two further twisted algebras $A_{2r-1}^{(2)}$ and $A_{2r}^{(2)}$ that come from foldings of D diagrams that leave only the central point invariant cannot occur in the context of tops.

3.1.2 Higher Dimensional Geometries

In applications to string theory we are often interested in higher dimensional geometries such that locally there is a product structure involving a neighbourhood of a degeneration of an elliptic fibration. For example, the total space may be a higher dimensional elliptically fibered Calabi-Yau space or a $K3$ bundle over \mathbf{S}^1 . Then it may happen that there is a closed loop such that over every neighbourhood in the loop we have one of Kodaira's degenerations, but upon going around the loop the exceptional curves get permuted. Using the fact that the permuted curves intersect if and only if the original curves intersect and otherwise the same arguments as before (in particular, matching of multiplicities), we see that a folding of an affine ADE diagram can be assigned in any such case, independently of whether we have a description in terms of a top.

3.1.3 Elliptic Curve

Before proceeding to the classification of tops, let us also discuss the toric interpretation of the vertices of a top \diamond in the plane $\bar{z} = 0$. These are just the vertices of the polygon F_0 . In terms of the geometry of the elliptic curve determined by F_0 every such vertex v gives rise to l divisors (i.e., points) in the elliptic curve where l is the length of the edge of F_0^* dual to v . In the context of \diamond there are l sections of the fibration for generic values of the coefficients. If \diamond is part of a three or higher dimensional reflexive polytope, v determines a divisor D in the corresponding Calabi-Yau hypersurface that may be reducible or irreducible. In the latter case this divisor projects to an l -fold cover of the base space of the fibration. In the case of a three dimensional

reflexive polytope, D consists of l curves in the corresponding K3 if v is interior to an edge and is irreducible if v is a vertex of the three dimensional polytope.

3.2 Classification

The classification of reflexive polygons is well known [48, 49]. As we make extensive use of it, the resulting 16 polygons are shown in figure 3.5. More recently, a general algorithm for classifying reflexive polytopes was developed [50, 51, 52] and successfully applied to the three [53] and four dimensional [54] cases.

The main idea of the algorithm of [50, 51, 52] is to look for a set of maximal polytopes that contain all others; these are dual to minimal polytopes that do not contain any other reflexive polytopes. In the present case of classifying tops, we lose the symmetry between the objects we are trying to classify and their duals. Given that the duals are infinite, we will obviously look for maximal objects among the duals and minimal objects among the tops themselves. As every dual \diamond^* of a top must be contained in a prism over one of the 16 polygons of figure 3.5, it is natural to treat these prisms as the maximal polyhedra.

We have already drastically reduced the $GL(3, \mathbb{Z})$ group of isomorphisms between tops by demanding that F_0 lie in the plane $\bar{z} = 0$. A further reduction comes from making a specific choice of coordinates for F_0 . The remaining freedom is in the subgroup G of $GL(3, \mathbb{Z})$ that fixes F_0 (not necessarily pointwise). The elements of G that fix every point of F_0 form a normal subgroup $G_0 \simeq \mathbb{Z}^2$ of G ; elements of G_0 act via

$$(\bar{x}, \bar{y}, \bar{z}) \rightarrow (\bar{x} + a\bar{z}, \bar{y} + b\bar{z}, \bar{z}), \quad (x, y, z) \rightarrow (x, y, z - ax - by) \quad \text{with } a, b \in \mathbb{Z}. \quad (3.2)$$

The quotient G/G_0 can be identified with the subgroup of $GL(2, \mathbb{Z})$ that fixes F_0 ; as it must take vertices to vertices and keep the order (up to reversion), G/G_0 must be a subgroup of the dihedral group of order $2n$ of the n -gon F_0 . The freedom in G can then be eliminated by using (3.2) to fix z_{\min} for two lattice points at the boundary of F_0^* and dealing with the remaining G/G_0 freedom by direct inspection.

The boundary point $b_0 := (0, 0, z_0) \in \diamond^*$ below $\mathbf{0}$ (with $z_0 := z_{\min}(0, 0)$) is invariant under the transformation (3.2). It must belong to one or more facets of the type (2.32), so $1/z_0$ must be a negative integer. Conversely, for every point $p = (\bar{x}, \bar{y}, \bar{z}) \in \diamond$, \bar{z} is invariant under (3.2), and $\langle p, b_0 \rangle \geq -1$ implies $\bar{z} \leq -1/z_0$. The vertices of \diamond at $\bar{z} = -1/z_0$ are dual to the facets of \diamond^* that contain b_0 .

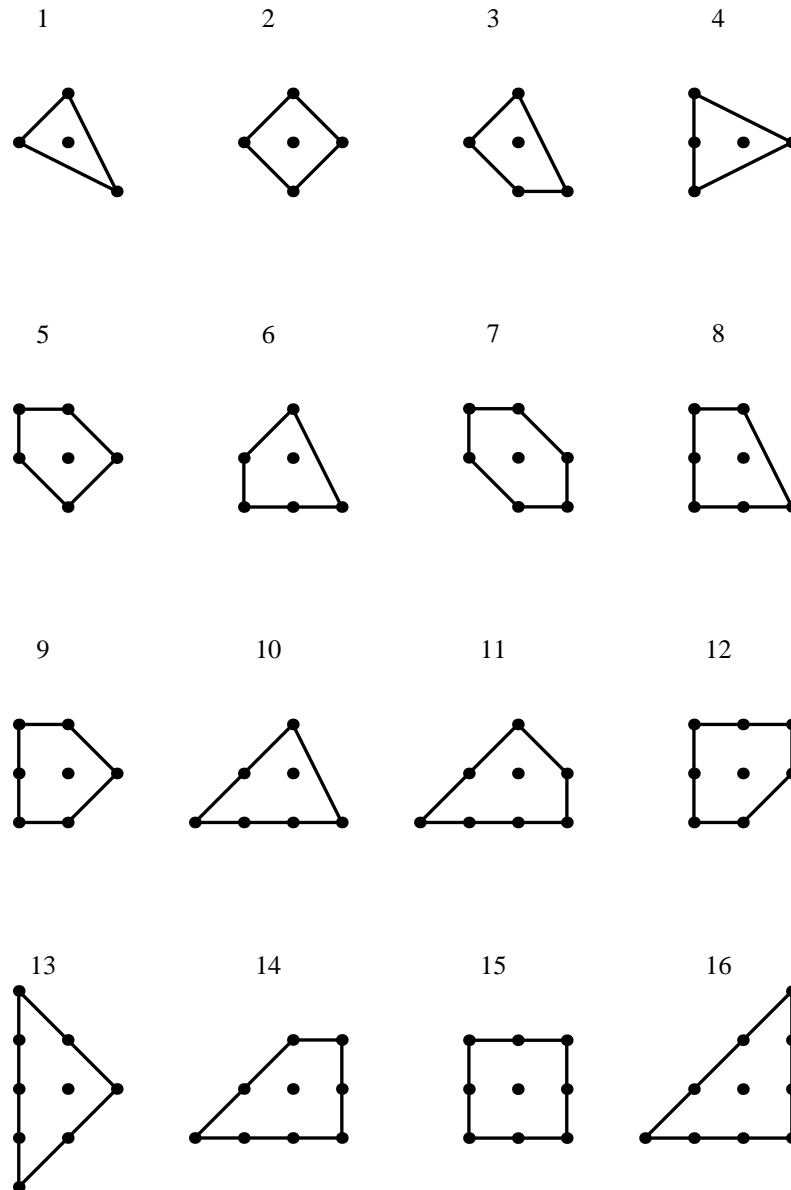


Figure 3.5: The 16 two-dimensional reflexive polygons. The polygons 1, 2, \dots , 6 are respectively dual to the polygons 16, 15, \dots , 11, and the polygons 7, \dots , 10 are self-dual.

Lemma 3.1. *If $b_0 = (0, 0, -1)$, then every non-vertical facet of \diamond^* contains b_0 .*

$b_0 = (0, 0, -1)$ implies that \diamond is bounded by $\bar{z} \leq 1$, so any vertex of \diamond must have either $\bar{z} = 0$, corresponding to a vertical facet of \diamond^* , or $\bar{z} = 1$, corresponding to a facet that contains $b_0 = (0, 0, -1)$.

We are now in a position to enumerate the cases relevant to the classification.

Case 0: \diamond^* has a single non-vertical facet dual to a vertex of \diamond at $\bar{z} = 1$.

We can use (3.2) to have this vertex at $(0, 0, 1)$ and thus $z_{\min} = -1$ everywhere. This trivial case exists for every choice of F_0 .

Case 1: b_0 is a vertex of \diamond^* .

This implies $b_0 = (0, 0, -1)$, dual to a facet F_1 of \diamond corresponding to $\bar{z} \leq 1$. According to lemma 3.1, the structure of \diamond^* is determined by a partition of F_0^* in the style of cutting a cake. Equations of non-vertical facets take the form (2.32) with $\bar{z} = 1$, implying that $z_{\min}(x, y)$ is integer whenever x and y are integer. We have seen an example in figure 2.9; this example should also serve as a useful background for the following discussion.

Consider three consecutive lattice points p_{i-1}, p_i, p_{i+1} along the boundary of F_0^* . It is easily checked that they fulfill $p_{i-1} + p_{i+1} = (2 - l_i) p_i$ where l_i is the length (in lattice units) of the edge of F_0 dual to p_i (with $l_i = 0$ if p_i is not a vertex). The facets of \diamond^* whose projections contain the triangles $b_0 p_{i-1} p_i$ and $b_0 p_i p_{i+1}$, respectively, are dual to vertices $v_{i-1}, v_i \in F_1$, with $v_{i-1} = v_i$ if p_{i-1}, p_i, p_{i+1} belong to the projection of a single non-vertical facet. One can calculate that v_{i-1}, v_i have lattice distance

$$z_{\min}(p_{i-1}) + (l_i - 2)z_{\min}(p_i) + z_{\min}(p_{i+1}) + l_i; \quad (3.3)$$

non-negativity of this expression is just the local convexity condition. The circumference in lattice units of the polygon F_1 is the sum $\sum_i l_i(z_{\min}(p_i) + 1)$ of these expressions.

All possible cases can be enumerated by choosing an integer z_{\min} for every lattice point at the boundary of F_0^* , subject to consistency with convexity, i.e. non-negativity of (3.3) at each lattice point of F_0^* ; to ensure that b_0 is a vertex, we also need that at least three of these expressions are positive. The freedom in (3.2) can be eliminated, for example, by putting two adjacent boundary points at $z = -1$.

Case 2: b_0 lies on a line connecting two lattice points p_1, p_2 of \diamond^* .

Then $b_0 = (p_1 + p_2)/2$, so $2z_0$ must be integer, i.e. $z_0 \in \{-1, -1/2\}$. The projection

of $\overline{p_1 p_2}$ divides F_0^* into two halves. By inspection of figure 3.5 we see that either half must look, up to automorphisms of the two dimensional lattice, like one of the possibilities shown in figure 3.6 (without loss of generality, we assume that $\overline{p_1 p_2}$ is at $x = 0$).

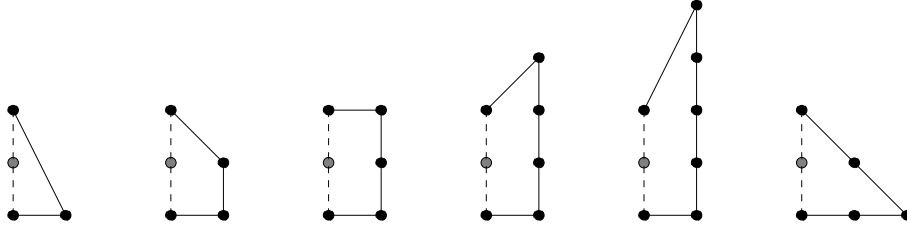


Figure 3.6: Possible halves of reflexive polygons.

a) $z_0 = -1$: Because of lemma 3.1 there are no more than two non-vertical facets corresponding to the two halves with $x \leq 0$ and $x \geq 0$. We can use (3.2) to put either of them, but not both, at $z = -1$. If we choose, say, $z = -1$ for the facet at $x \geq 0$, then the facet at $x \leq 0$ must be the transform of a facet at $z = -1$ by (3.2) with $b = 0$; convexity implies $a \geq 0$. This gives a one parameter family that starts with the case of a single facet at $z = -1$ (case 0). For $a \geq 1$, \diamond has precisely two vertices at $\bar{z} = 1$ whose distance is a .

b) $z_0 = -1/2$: There are one or two vertices of \diamond at $\bar{z} = 2$, dual to the facet(s) containing b_0 . All other vertices of \diamond must be at $\bar{z} = 0$ or 1. We can again treat the halves separately and find that after using up the freedom given by (3.2) there are only finitely many cases for each diagram of figure 3.6, corresponding to partitions such that the facet containing b_0 is dual to a vertex at $\bar{z} = 2$ and all other facets correspond to $\bar{z} = 1$. Here the freedom of applying (3.2) to one of the halves leads to families such that the edge at $\bar{z} = 2$ has length $2a$ or $2a + 1$.

Case 3: Neither of the above.

Then b_0 must be interior to a facet of \diamond^* in such a way that cases 0 and 2 do not apply. In particular, after triangulating this facet b_0 must be interior to one of the triangles $v_1 v_2 v_3$. Applying π , we see that $(0, 0)$ is interior to $\Delta \subseteq F_0^*$ where Δ is the triangle with vertices $\pi(v_i)$. Every two dimensional lattice polytope whose only interior lattice point is the origin is reflexive, so Δ must be one of the triangles occurring in figure 3.5

(numbers 1, 4, 10, 13, 16). The linear relations among the vertices of these triangles imply

$$v_1 + v_2 + v_3 = 3b_0 \quad \text{for the triangles 1, 16,} \quad (3.4)$$

$$v_1 + v_2 + 2v_3 = 4b_0 \quad \text{for the triangles 4, 13,} \quad (3.5)$$

$$v_1 + 2v_2 + 3v_3 = 6b_0 \quad \text{for triangle 10,} \quad (3.6)$$

so $-1/z_0$ must divide one of the numbers 3, 4, 6. We can dismiss the following possibilities.

$z_0 = -1$ implies case 0 by the lemma,

$z_0 = -1/2$ is possible for triangles 4, 10, 13, but easily seen to correspond to case 2,

$z_0 = -1/3$ for triangles 10 or 16 can be reduced to triangle 1,

$z_0 = -1/4$ for triangle 13 can be reduced to triangle 4.

This leaves us with

- a) $z_0 = -1/3$ for triangle 1,
- b) $z_0 = -1/4$ for triangle 4,
- c) $z_0 = -1/6$ for triangle 10.

In each of these cases $\pi(v_2)$ and $\pi(v_3)$ generate the two dimensional lattice, so we can use (3.2) to put v_2 and v_3 at $z = 0$ which forces v_1 to be at $z = -1$. Let us denote by P the prism over Δ cut off at the $v_1v_2v_3$ -plane. Then $P \subseteq \diamond^*$ implies $\diamond \subseteq P^*$, but P^* is a top with a finite number of lattice points. In other words, every top containing points at $\bar{z} > 2$ is contained in one of the three tops shown in figure 3.7. This implies that once a choice of F_0^* as one of the 16 polygons and (if possible) of $\Delta \subseteq F_0^*$ has been made, there is only a finite number of consistent possibilities of assigning z_{\min} to the remaining lattice points in F_0^* .

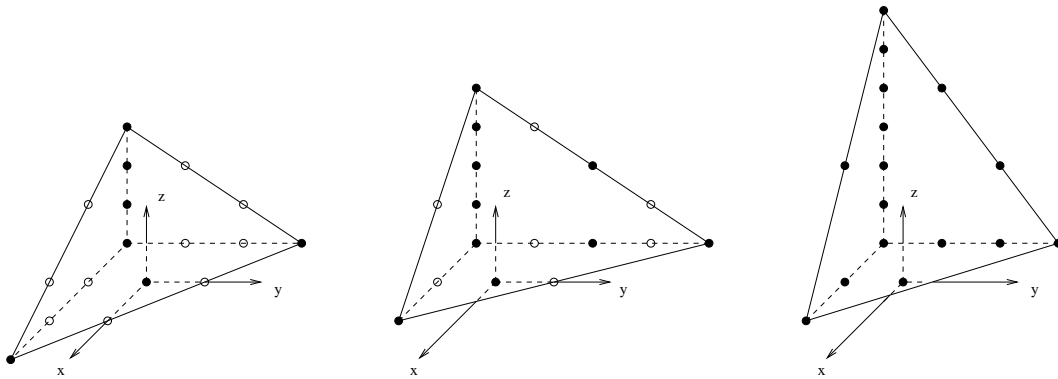


Figure 3.7: Three maximal tops (the significance of ● vs. ○ will be explained in section 3.3).

The classification of all possible tops is then straightforward. All that has to be done is to examine each of the 16 polygons of figure 3.5 with respect to all possibilities of applying one of the cases 0, 1, 2, 3, taking care to avoid overcounting wherever there are non-trivial automorphisms of F_0^* . A complete list is given in appendix B.1.

3.3 Geometrical Interpretation

The results of the classification of course confirm the predictions made in section 3.1 on the structure of the edge diagram of a top at $\bar{z} \geq 1$. By combining the arguments of the previous sections it is clear that case 1 of our classification corresponds to $A_n^{(1)}$ algebras, with

$$n + 1 = \sum_i l_i(z_{\min}(p_i) + 1) \quad (3.7)$$

in the notation used around (3.3). Case 2a leads to $C_n^{(1)}$ diagrams where n is just the parameter a used there, and case 2b to $D_n^{(1)}$ and its folded versions where $n - 4$ is the length of the edge at $\bar{z} = 2$, i.e. $2a$ or $2a + 1$. Cases 3a,b,c correspond to $E_6^{(1)}$, $E_7^{(1)}$, $E_8^{(1)}$ and their folded versions, respectively.

3.3.1 Twisted Algebras: Geometry

There is, however, a great difference between the occurrences of untwisted and twisted Kac-Moody algebras as edge diagrams. While each of the untwisted algebras occurs quite a number of times and five of the reflexive polygons (F_0^* one of 10, 11, 13, 14, 16 of figure 3.5) feature every possible untwisted algebra, twisted algebras are quite rare. Each of the diagrams of $E_6^{(2)}$, $A_2^{(2)}$ and $D_4^{(3)}$ occurs only once, and the members of the $D^{(2)}$ series occur twice.

There are only three pairs (F_0, F_0^*) leading to diagrams of twisted algebras, namely (1, 16), (2, 15) and (4, 13). These reflexive pairs of polygons are quite special in several ways. They are the only dual pairs where F_0^* has no edge of length one; this implies that no vertex of F_0 corresponds to a single section. Moreover each of these polygons is reflexive on two distinct lattices, in such a way that the dual is the same polygon on the other lattice. More precisely, polygon 1 is the same as polygon 16 on a sublattice of index 3, and polygons 2 and 4 are the same as their respective duals on sublattices of index 2. We find that whenever twisted algebras occur, the corresponding tops can be understood as coming from a restriction to a sublattice, suitably extended in the third dimension.

Consider again the first top in figure 3.7. On the full lattice (with points both of the type \circ and \bullet) the edge diagram is an $E_6^{(1)}$ Dynkin diagram, but if we consider the sublattice of index 3 determined only by points shown as \bullet , we find the diagram of $D_4^{(3)}$. This is the only twisted algebra coming from the pair (1, 16).

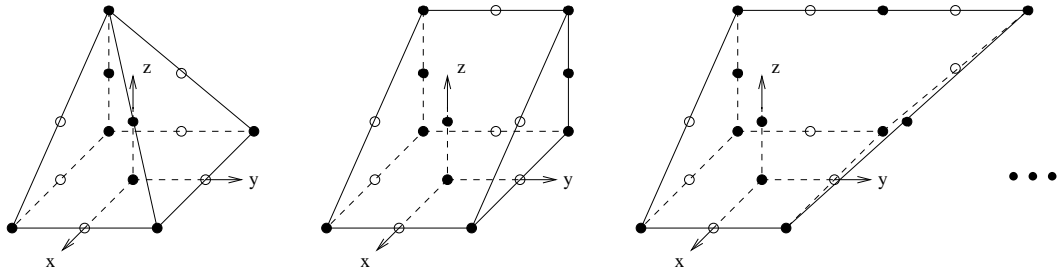


Figure 3.8: A family of tops over squares.

The pair (2, 15) of reflexive squares gives rise to a family of $D^{(2)}$ algebras as shown in figure 3.8. Note, however, that the twisted diagrams $D_{i+3}^{(2)}$ with $i = 0, 1, 2, \dots$ come from sublattice versions of tops corresponding to $D_{2i+4}^{(1)}$, i.e. not the diagrams whose foldings produce the twisted ones.

The situation is most intricate for the pair (4, 13) of reflexive triangles. In the second picture of figure 3.7, passing to the index 2 sublattice indicated by \bullet means that we get an $E_6^{(2)}$ diagram from an $E_7^{(1)}$ diagram. Now consider the tops shown in

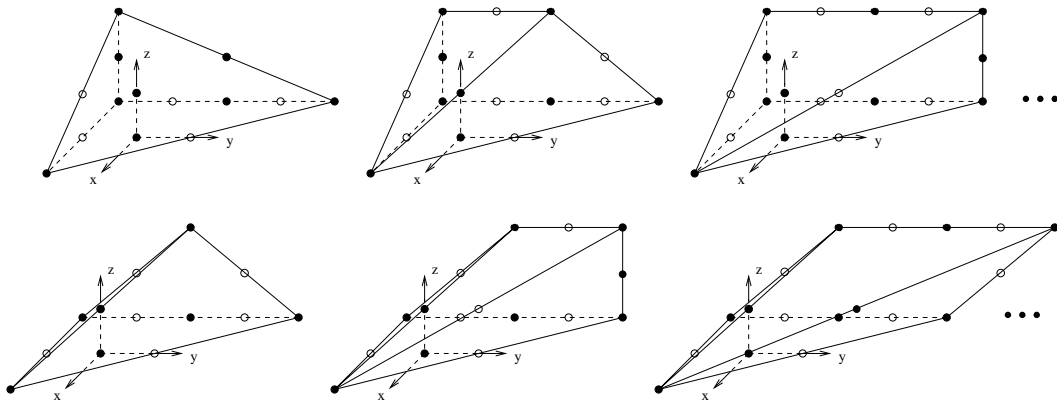


Figure 3.9: Two families of tops over the dual pair (4, 13).

figure 3.9. In the finer lattice including the points \circ , each member of the first family shown in the upper row is isomorphic to the member of the second family directly below; the transformation is (3.2) with $a = 0, b = 1$, resulting in tilting the top along the y direction. The corresponding algebras are $B_3^{(1)}$ and $D_{2i+4}^{(1)}$ with $i \in \{1, 2, \dots\}$.

In the coarser \bullet lattice, however, this isomorphism is lost as it would correspond to half integer parameters in (3.2). The first row gives a family of twisted diagrams $D_{i+3}^{(2)}$ with $i \in \{0, 1, 2, \dots\}$, as in the case of the square. The second row gives another $D_{i+3}^{(2)}$ family for $i \geq 1$ with a special case for $i = 0$ where we have an $A_2^{(2)}$ diagram. As an additional subtlety, the tops for odd i are nevertheless isomorphic, namely by an isomorphism that acts on F_0 by swapping the two vertices of the long edge. For this reason we have listed these tops in table B.4 in the appendix as two families of type $D_{2i+3}^{(2)}$ and one family of type $D_{2i+4}^{(2)}$.

The fact that the tops giving rise to twisted algebras all correspond to pairs of lattices has the following interpretation. Passing from a coarser lattice N to a finer lattice N' in a way that is compatible with the structure of the fan means passing from a toric variety to a quotient of this variety by a finite abelian group isomorphic to N'/N . In the present cases this group is just \mathbb{Z}_3 or \mathbb{Z}_2 . So the varieties corresponding to diagrams related to twisted algebras allow group actions in such a way that taking the quotient would take us to the variety defined by the finer lattice.

3.4 String Theory Interpretation

Finally let us discuss the relation between tops and string theory. The simplest case is that of taking an elliptic K3 surface whose toric polytope consists of two tops. Blowing down all divisors except two at $\bar{z} = \pm 1$ will result in the occurrence of two ADE singularities (at $W = 0/\infty$) corresponding to the unfolded diagram. Compactifying M-theory on such a space leads to a theory where the generic abelian gauge group is enhanced in such a way that the corresponding ADE groups arise. The same groups also arise in compactifications of type IIA and F-theory without background fields.

If a top is part of a diagram describing an elliptically fibered Calabi-Yau threefold or fourfold, the generic local geometry is a product of a neighbourhood U in \mathbb{C} or \mathbb{C}^2 with the two dimensional geometry featuring the ADE pattern; every exceptional rational curve gives rise to a divisor $U \times \mathbb{CP}^1$. Globally several of these divisors may correspond to a single irreducible divisor (this is the non-split case of [55]). Clearly this can happen only if the different \mathbb{CP}^1 's all come from the same lattice point in the toric diagram. In this case there are special loci in the base space over which some or all of the \mathbb{CP}^1 's coincide. Monodromy around these loci will interchange the \mathbb{CP}^1 's. Upon compactifications of the same theories as above this results in non simply laced gauge groups [56], again of the type determined by the toric diagram.

These constructions are conjectured to be dual to compactifications of heterotic strings; in particular the K3 compactifications are dual to toroidal heterotic compactifications with maximal rank of the gauge group. However, the heterotic moduli space also contains components of reduced rank of the gauge theory [14, 57]. These require non-standard IIA and F-theory compactifications as duals. In the IIA case these are compactifications on orbifolds in the presence of a non-trivial RR background [58]; this has an M-theory lift where the orbifolding also acts by a shift on the S^1 in the eleventh dimension. In terms of F-theory a non-generic monodromy group together with non-trivial $B_{\mu\nu}$ flux in the underlying IIB theory is required [59]; F-theory duals were also considered in [60, 61]. We will now see how these requirements are met by the tops that give rise to twisted Kac-Moody algebras; that these algebras should play a role on the heterotic side was predicted in [62].

3.4.1 Twisted Algebras: String Theory

Consider once more the second diagram of figure 3.7. To be specific let us assume that it is part of the reflexive polytope that is obtained by adding the ‘bottom’ that is the reflection of the top through the xy -plane (this reflexive polytope was also considered in [61], but our discussion will be different). Passing from the space determined by the \bullet diagram to its \mathbb{Z}_2 orbifold means that we get singularities that may be resolved by blowing up along the divisors indicated by \circ . In a standard IIA compactification passing to the orbifold means that one loses as many non-algebraic cycles as there are \circ cycles and the rank of the gauge group remains 24. In the compactification with RR background the \circ cycles do not contribute and we end up with reduced rank. By counting with the right multiplicities (one for every \circ point in an edge except $(0, 1, 0)$ which has multiplicity two) we get a rank reduction of eight as it should be [14, 63]. The same reflexive polytope allows for a second fibration structure with the fiber determined by the polygon at $x + y = 0$. Now the orbifolding acts by changing the trivial top at $x + y > 0$ to the $B_3^{(1)}$ top and the $C_6^{(1)}$ top at $x + y < 0$ to the $D_{10}^{(1)}$ top. This is the toric description of the involution discussed in section 2 of [59].

In a similar manner the diagrams of figures 3.8 and 3.9 can be used to construct theories with rank reduction of eight. Taking the first top in figure 3.7 together with its mirror image, we get a K3 with orbifold group \mathbb{Z}_3 . According to [63] this should lead to a rank reduction of 12; with the same counting as before this is indeed confirmed.

The gauge groups that we get are again non simply laced with a mechanism very similar to the one we encountered before. In the M-theory picture we compactify on $(K3 \times S^1)/G$ which is a smooth non-trivial bundle over S^1 with fiber the original $K3$. So locally over a neighborhood in S^1 we get all the \mathbb{CP}^1 's of the untwisted diagram but upon going around the S^1 they are permuted. For obtaining gauge groups we blow down the toric divisors corresponding to all points of a top except for one at $\bar{z} = 1$. The collapsed cycles belong to ordinary ADE Dynkin diagrams (the heights play no role here) that are folded by the permutations. In this way $E_6^{(2)}$, $D_{n+1}^{(2)}$, $A_2^{(2)}$ and $D_4^{(3)}$ give rise to the groups F_4 , B_n , A_1 and G_2 , respectively.

Tops from the families of figures 3.8 and 3.9 that do not fit into three dimensional reflexive polytopes should play a role in theories dual to non-toroidal compactifications of CHL strings [64].

Chapter 4

Closed Topological Strings on Orientifolds

In this chapter we study closed topological strings on orientifolds of toric Calabi-Yau threefolds. We compute all loop topological string amplitudes, using geometric transitions involving SO/Sp Chern-Simons theory, localization on the moduli space of holomorphic maps with involution, and the topological vertex.

We start by summarizing general results for **A**-model topological strings on an orientifold. Then we describe in some details the geometric transition on which we will focus in this chapter. The geometry was presented in section 2.4. In section 4.3 we compute explicitly the Chern-Simons amplitude obtained after the geometric transition. Then we present the unoriented localization computation, and show that it gives exactly the same contributions for the one and two crosscaps instanton configurations. We then propose our prescription based on the topological vertex in section 4.5, proving its equivalence to the Chern-Simons computation.

4.1 **A**-model Topological Strings on an Orientifold

4.1.1 Type IIA Superstrings and Topological Strings on an Orientifold

It is a well known fact that, when type IIA theory is compactified on a Calabi-Yau manifold X , the resulting four dimensional theory is $\mathcal{N} = 2$ supergravity with $h^{1,1}(X)$ vector multiplets t_i . The $\mathcal{N} = 2$ prepotential that governs the effective action of the

vector multiplets, $F_0(t_i)$, can be computed by the genus zero free energy of the **A**-model topological strings with the Calabi-Yau as target space (see [33] for a review of topological strings and related issues). Higher genus free energies $F_g(t_i)$ of the topological string theory also play a rôle in the four dimensional supergravity theory, and compute higher curvature couplings involving the graviphoton [65, 66].

One way to break $\mathcal{N} = 2$ supersymmetry down to $\mathcal{N} = 1$ is to consider an orientifold of the theory. The orientifold is defined by combining an involution symmetry I on the Calabi-Yau X with a diffeomorphism σ on the worldsheet Σ . In the context of type IIA superstrings, the orientifold is only well defined if the involution is anti-holomorphic. Furthermore, the worldsheet diffeomorphism has to be orientation reversal [21, 26, 67]. The resulting theory in four dimensions has $\mathcal{N} = 1$ supersymmetry, and $h_-^{1,1}(X)$ out of the $h^{1,1}(X)$ $\mathcal{N} = 2$ vector multiplets become $\mathcal{N} = 1$ chiral multiplets in four dimensions, where $h_-^{1,1}(X)$ is the number of harmonic $(1, 1)$ forms on X which have -1 eigenvalue under I (see [67] for a description of the spectrum of massless modes in four dimensions).

These considerations hold in the context of **A**-model topological strings as well: **A**-model topological strings possess a worldsheet orientation reversal symmetry when accompanied with an anti-holomorphic involution of the target space [21]. It is thus possible to consider **A**-model topological strings on an orientifold defined as above. The twisted sector of the topological string amplitude on the orientifold includes amplitudes for unoriented Riemann surfaces¹. Recall that a closed, non-orientable Riemann surface is characterized by its genus g and by the number of crosscaps c , which can be one or two (crosscaps can be traded for handles when the number of crosscaps is higher than two). For example, the surface with $g = 0$ and $c = 1$ is the real projective plane $\mathbb{R}P^2$, while the surface with $g = 0$ and $c = 2$ is the Klein bottle. It was shown in [21] that the superpotential of the $h_-^{1,1}(X)$ chiral multiplets is given by the $\mathbb{R}P^2$ amplitude of the topological string theory. As far as we know, the topological amplitudes involving more handles or crosscaps do not have an interpretation in the $\mathcal{N} = 1$ supergravity theory.

Generally speaking, one could consider type IIA superstrings on a noncompact orientifold, with D-branes and orientifold planes [21]. In this chapter we only consider type IIA superstrings without D-branes or orientifold planes. This means that the anti-holomorphic involution must have no fixed points. Moreover, as the parent

¹The attentive reader may have noticed that this nomenclature is slightly strange, as by definition a Riemann surface must be orientable. But as is conventional in the string theory literature, an *unoriented (or non-orientable) Riemann surface* means a non-orientable surface which results from the action of an orientation reversal diffeomorphism on a Riemann surface.

theory has no D-branes, to compute the superpotential we only need to consider **A**-model closed topological strings. Open topological string amplitudes corresponding to orientifolds with D-branes shall be considered in chapter 5.

4.1.2 Structure of the Topological String Amplitudes

Roughly speaking, the free energy of **A**-model closed topological strings counts the number of holomorphic maps from the worldsheet to the target space, weighted by a factor of e^{-A} where A is the area of the embedded curve. In the context of orientifolds, the partition function of topological strings sums over holomorphic maps in two different sectors: the “untwisted” and the “twisted” sectors. The former consists of usual holomorphic maps from orientable worldsheets to the covering space, i.e. the noncompact Calabi-Yau threefold without the involution. The latter consists of equivariant maps $f : \Sigma \rightarrow X$ satisfying the equivariance condition

$$f \circ \sigma = I \circ f, \quad (4.1)$$

where I is the anti-holomorphic involution acting on X , and $\sigma : \Sigma \rightarrow \Sigma$ is the orientation reversal diffeomorphism of the Riemann surface which is needed in order to construct the orientifold action. Notice that, if Σ has genus zero, the action of σ is given by $z \rightarrow -1/\bar{z}$. The relevant maps in the twisted sector are then the maps which are compatible with the orientation reversal diffeomorphism on the worldsheet and the anti-holomorphic involution on the target space, and descend to holomorphic maps from non-orientable worldsheets to the orientifold.

The structure of the total free energy of the **A**-model is then

$$\mathcal{F}(X/I, g_s) = \mathcal{F}(X/I, g_s)_{\text{untwisted}} + \mathcal{F}(X/I, g_s)_{\text{unor}}, \quad (4.2)$$

where g_s is the string coupling constant. In this equation, $\mathcal{F}(X/I, g_s)_{\text{untwisted}}$ is the contribution of the untwisted sector, and $\mathcal{F}(X/I, g_s)_{\text{unor}}$ is the contribution of the twisted sector.

One of the most important results of topological string theory is the fact that topological string amplitudes have an integrality, or BPS structure, which expresses them in terms of numbers of BPS states.

In the case of closed topological strings on Calabi-Yau threefolds, the BPS structure was obtained by Gopakumar and Vafa in [28]. Let us denote by $F_g(t)$ the topological string free energy at genus g , where t denotes the set of Kähler parameters of the Calabi-Yau threefold X , and let

$$\mathcal{F}(t, g_s) = \sum_{g=0}^{\infty} g_s^{2g-2} F_g(t) \quad (4.3)$$

be the total free energy. Then, one has the following structure result:

$$\mathcal{F}(t, g_s) = \sum_{d=1}^{\infty} \sum_{g=0}^{\infty} \sum_{\beta} \frac{1}{d} \frac{n_Q^g}{(q^{\frac{d}{2}} - q^{-\frac{d}{2}})^{2-2g}} e^{-dQ \cdot t}. \quad (4.4)$$

where $q = e^{ig_s}$, the sum over Q is over two-homology classes in X , and n_Q^g (the so-called Gopakumar-Vafa invariants) are *integers*. The factor $(q^{\frac{d}{2}} - q^{-\frac{d}{2}})^{2g}$ comes from computing a signed trace over the space of differential forms on a Riemann surface of genus g , while the factor $(q^{\frac{d}{2}} - q^{-\frac{d}{2}})^{-2}$ comes from a Schwinger computation [28].

We thus find that the untwisted sector has the following structure:

$$\mathcal{F}(X/I, g_s)_{\text{untwisted}} = \frac{1}{2} \mathcal{F}(X, g_s) = \frac{1}{2} \sum_{d=1}^{\infty} \sum_{g=0}^{\infty} \sum_Q \frac{1}{d} \frac{n_Q^g}{(q^{\frac{d}{2}} - q^{-\frac{d}{2}})^{2-2g}} e^{-dQ \cdot t}. \quad (4.5)$$

Here, $\mathcal{F}(X, g_s)$ is the free energy of the covering X of X/I , after suitably identifying the Kähler classes in the way prescribed by the involution I , and we have written it in terms of Gopakumar-Vafa invariants n_Q^g [28].

The unoriented contribution in (4.2) comes from holomorphic maps from closed non-orientable Riemann surfaces to the orientifold X/I . The Euler characteristic of a closed Riemann surface of genus g and c crosscaps is $\chi = -2g + 2 - c$ where c is the number of crosscaps. We then have

$$\mathcal{F}(X/I, g_s)_{\text{unor}} = \mathcal{F}(X/I, g_s)_{\text{unor}}^{c=1} + \mathcal{F}(X/I, g_s)_{\text{unor}}^{c=2}, \quad (4.6)$$

which corresponds to the contributions of one and two crosscaps. Following the arguments in [28] we expect the structure

$$\begin{aligned} \mathcal{F}(X/I, g_s)_{\text{unor}}^{c=1} &= \pm \sum_{d \text{ odd}} \sum_{g=0}^{\infty} \sum_Q n_Q^{g,c=1} \frac{1}{d} (q^{\frac{d}{2}} - q^{-\frac{d}{2}})^{2g-1} e^{-dQ \cdot t}, \\ \mathcal{F}(X/I, g_s)_{\text{unor}}^{c=2} &= \sum_{d \text{ odd}} \sum_{g=0}^{\infty} \sum_Q n_Q^{g,c=2} \frac{1}{d} (q^{\frac{d}{2}} - q^{-\frac{d}{2}})^{2g} e^{-dQ \cdot t}, \end{aligned} \quad (4.7)$$

where $n_Q^{g,c}$ are integers. The \pm sign in the $c = 1$ free energy is due to the following: the target space anti-holomorphic involution does not fully specify the unoriented part of the free energy on the orientifold, since we have to make a choice for the sign of the crosscaps. Depending on this choice, we will have the two different signs for $c = 1$. This corresponds to the choice of SO or Sp group in the gauge theory dual. This remaining choice is also easily understood on the mirror symmetric side [21]. For the conifold, the **B**-model mirror symmetric description involves two orientifold 5-planes. The two choices of signs for crosscap states correspond on the mirror symmetric side to the two following choices for the charges of the $O5$ -planes: $+-$ and $-+$ [21]. A similar story holds for more complicated orientifolds. Notice as well that the sum over multicoverings d in (4.7) is only over *odd* integers. In the case of $c = 1$ this follows from an elementary geometric argument, since there are no even multicoverings (see [20, 21]). For $c = 2$ there is no such a simple argument, but our explicit computations both in Chern-Simons theory and in localization of unoriented instantons indicate that only odd multicoverings contribute.

4.2 Geometric Transitions

4.2.1 Orientifold of the Resolved Conifold and its Geometric Transition

In [20] it was proposed that in the large N limit, closed topological strings on the orientifold of the conifold are dual to $SO(N)/Sp(N)$ Chern-Simons theory on \mathbf{S}^3 , where the choice of gauge group is related to the choice of sign for the crosscaps. Since this is the starting point for our discussion, let us review in some detail the results of [20].

We start with a theory of topological open strings on the deformed conifold defined by $w_1 w_4 - w_2 w_3 = \mu$. The conifold contains an \mathbf{S}^3 , and if we wrap $2N$ branes on the three-sphere, the spacetime description of the open topological string theory is Chern-Simons theory on \mathbf{S}^3 with gauge group $U(2N)$ and at level k (the level is related to the open string coupling constant). We now consider the following involution of the geometry

$$I : (w_1, w_2, w_3, w_4) \rightarrow (\bar{w}_4, -\bar{w}_3, -\bar{w}_2, \bar{w}_1) \quad (4.8)$$

that leaves the \mathbf{S}^3 invariant. The string field theory for the resulting open strings is now Chern-Simons theory with gauge group $SO(N)$ or $Sp(N)$, depending on the

choice of orientifold action on the gauge group. The total free energy of the Chern-Simons theory with gauge group SO/Sp can be written as

$$\mathcal{F} = -\log S_{00}^{SO(N)/Sp(N)} = \frac{1}{2} \sum_{d=1}^{\infty} \frac{1}{d} \frac{e^{-dt}}{(q^{\frac{d}{2}} - q^{-\frac{d}{2}})^2} \mp \sum_{d \text{ odd}} \frac{1}{d} \frac{e^{-dt/2}}{q^{\frac{d}{2}} - q^{-\frac{d}{2}}}, \quad (4.9)$$

where the \mp sign corresponds to SO/Sp , respectively. In (4.9), $q = e^{ig_s}$, with

$$g_s = \frac{2\pi}{k + y}, \quad (4.10)$$

and y is the dual Coxeter of the gauge group, which is $N - 2$ for $SO(N)$ and $N + 1$ for $Sp(N)$. The parameter t in (4.9) is the 't Hooft parameter, given by

$$t = (N \mp 1)g_s, \quad (4.11)$$

for SO/Sp , respectively.

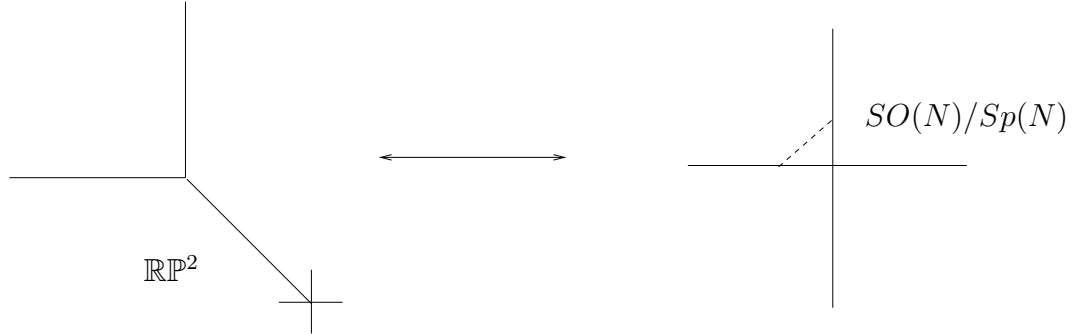


Figure 4.1: Geometric transition for the orientifold of the conifold. The cross in the figure to the left represents an \mathbb{RP}^2 obtained by quotienting a \mathbb{CP}^1 by the involution I , and the dashed line in the figure on the right represents an \mathbf{S}^3 with SO/Sp gauge group.

In the usual geometric transition of [16], the dual to the deformed conifold is the resolved conifold $Y = \mathcal{O}(-1) \oplus \mathcal{O}(-1) \rightarrow \mathbb{CP}^1$. This Calabi-Yau threefold was described in detail in section 2.4.

The involution (4.8) of the deformed conifold maps to the anti-holomorphic involution of Y defined by:

$$I : (z_1, z_2, z_3, z_4) \rightarrow (\bar{z}_2, -\bar{z}_1, \bar{z}_4, -\bar{z}_3). \quad (4.12)$$

It is easy to see that Y/I contains a single \mathbb{RP}^2 obtained from the quotient of the \mathbb{CP}^1 of Y by I . We will represent the quotient of the resolved conifold by that involution in terms of the toric diagram depicted in figure 4.1.

The free energy of the SO/Sp Chern-Simons theory gives the total free energy of closed strings propagating on Y/I . The first term in (4.9) gives the oriented contribution, while the second term gives the unoriented contribution, and they have the structure explained in (4.5) and (4.6). Notice that in the case of the unoriented contribution we have

$$n_{Q=1/2}^{g=0,c=1} = \mp 1 \quad (4.13)$$

depending on the choice of sign for the crosscaps, and all the remaining Gopakumar-Vafa invariants vanish. In particular, the contribution of Riemann surfaces with two crosscaps is zero. As we will see, in more general cases there are two crosscaps contributions. The above prediction of the large N transition for the free energy was checked in [21] against mirror symmetry, and in [26] against localization computations for unoriented Gromov-Witten theory.

4.2.2 Our Main Example

In this paper we want to generalize the open/closed string duality studied in [20] to more general orientifolds. We will mainly focus on the noncompact Calabi-Yau manifold X described in section 2.4.

The compact locus consists of two divisors that are each isomorphic to a del Pezzo surface dP_2 and a rational $(-1, -1)$ curve that intersects both divisors transversely. Note that the two compact divisors do not intersect. We consider a real torus action on X given by:

$$e^{i\phi} \cdot (z_1, z_2, \dots, z_{10}) \rightarrow (e^{i\lambda_1\phi} z_1, e^{i\lambda_2\phi} z_2, \dots, e^{i\lambda_{10}\phi} z_{10}). \quad (4.14)$$

We now define the anti-holomorphic involution as follows:

$$I : (z_1, z_2, z_3, z_4, z_5, z_6, z_7, z_8, z_9, z_{10}) \rightarrow (\bar{z}_{10}, \bar{z}_8, \bar{z}_9, \bar{z}_7, -\bar{z}_6, \bar{z}_5, -\bar{z}_4, \bar{z}_2, \bar{z}_3, \bar{z}_1). \quad (4.15)$$

The subtorus of (4.14) that is compatible with the involution is defined by the following constraints on the weights

$$\lambda_1 + \lambda_{10} = 0, \quad \lambda_2 + \lambda_8 = 0, \quad \lambda_3 + \lambda_9 = 0, \quad \lambda_4 + \lambda_7 = 0, \quad \lambda_5 + \lambda_6 = 0. \quad (4.16)$$

Imposing these constraints does not enlarge the set of invariant curves.

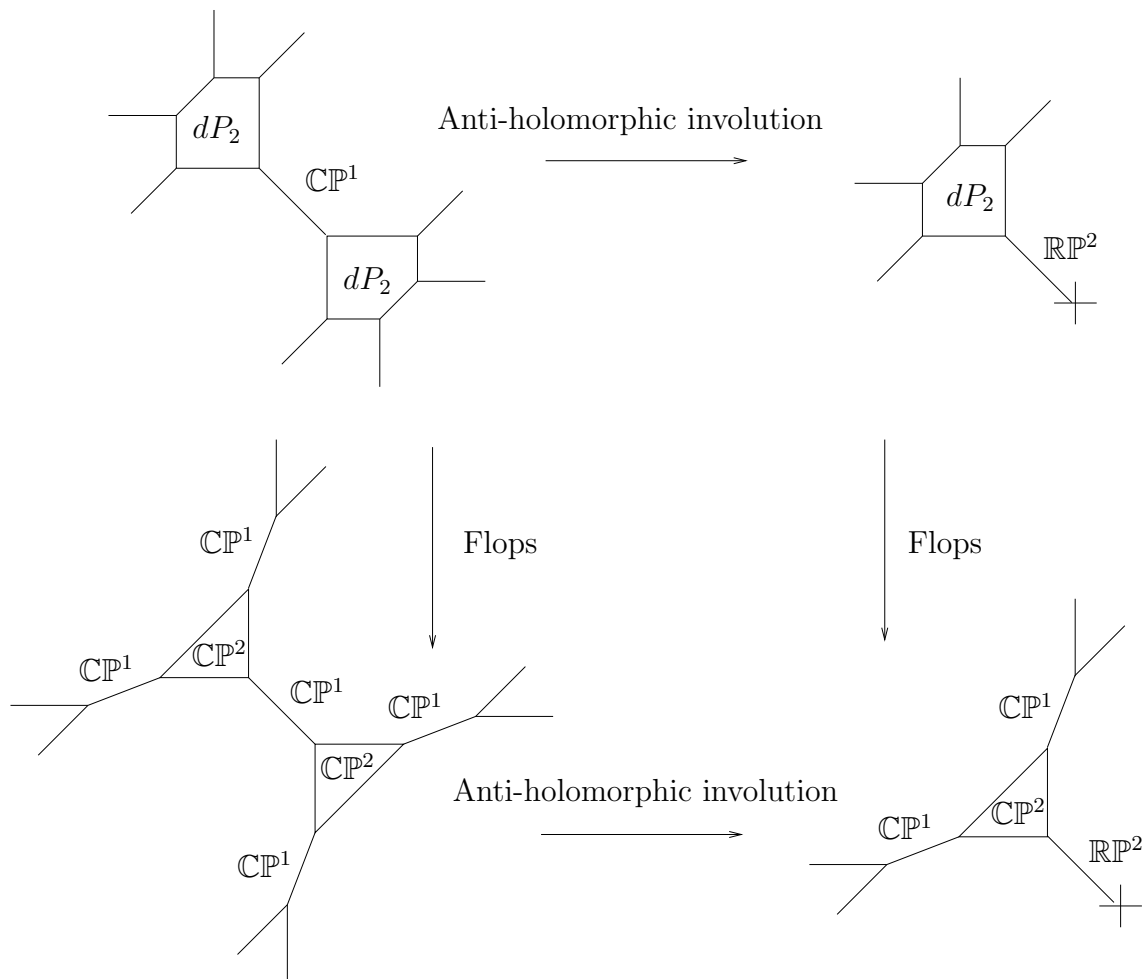


Figure 4.2: The geometry on the closed topological strings side. The orientifolding action acts from left to right, while flopping the CP^1 's acts top-down. The RP^2 is represented by a cross at the end of the toric leg.

It is often useful [22] to consider a related Calabi-Yau threefold \tilde{X} obtained from X by flopping the two exceptional curves outside of the compact divisors. The “commuting square” of geometries (where the arrows correspond either to flopping or to quotienting by the anti-holomorphic involution) is presented in figure 4.2.

We can now follow the logic in [22, 23, 24, 25] and consider a geometric transition in which each of the resolved conifolds (or their orientifolds) that exist locally in the geometry are replaced by deformed conifolds (or their orientifolds). In the above example, this means that we contract two $\mathbb{C}\mathbb{P}^1$'s and a $\mathbb{R}\mathbb{P}^2$ and we replace them with three spheres carrying $U(N)$ and $SO(N)/Sp(N)$ Chern-Simons theories, respectively. The transition is represented in figure 4.3. In the next section we will see how to obtain the closed string amplitudes in the orientifold from Chern-Simons theory.

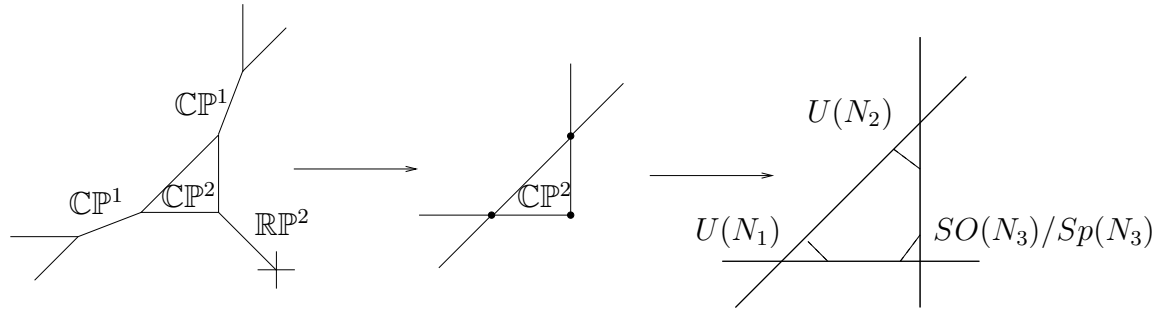


Figure 4.3: The geometric transition. The two $\mathbb{C}\mathbb{P}^1$'s and the $\mathbb{R}\mathbb{P}^2$ of the left figure are shrunk to singular points in the middle diagram, and then deformed into three \mathbb{S}^3 .

4.3 Closed String Amplitudes from Chern-Simons Theory

4.3.1 Results from Chern-Simons Theory with Classical Gauge Groups

As we will see in a moment, in order to compute the free energies of topological strings on orientifolds via geometric transitions we have to compute the Chern-Simons invariants of the unknot and the Hopf link of linking number +1 in arbitrary representations of $U(N)$, $SO(N)$ and $Sp(N)$. Some general results from Chern-Simons theory and the topological vertex have been regrouped in appendix A.2. In this section we will denote $q = e^{ig_s}$ and

$$\lambda = q^{N+a}, \quad (4.17)$$

where

$$a = \begin{cases} 0 & \text{for } U(N), \\ -1 & \text{for } SO(N), \\ 1 & \text{for } Sp(N). \end{cases} \quad (4.18)$$

Notice that the 't Hooft parameter of the classical gauge groups can be written as

$$t = (N + a)g_s \quad (4.19)$$

therefore $\lambda = e^t$. For an arbitrary gauge group G it is a well known result that the Chern-Simons invariant of the unknot in an arbitrary representation R is given by the so-called *quantum dimension* of R [68]:

$$\mathcal{W}_R = \frac{S_{0R}}{S_{00}} = \dim_q R, \quad (4.20)$$

where S_{0R} , S_{00} are entries of the S matrix of the Wess-Zumino-Witten model with the corresponding gauge group and at level k (recall that k is related to the string coupling constant by (4.10)). The general definition of the quantum dimension is given in (A.3).

The expression (A.3) can be written more explicitly for the different classical gauge groups. Let R be a representation corresponding to a Young tableau with row lengths $\{\mu_i\}_{i=1,\dots,d(\mu)}$, with $\mu_1 \geq \mu_2 \geq \dots$ and where $d(\mu)$ denotes the number of rows. Then the quantum dimension of a representation R of $U(N)$ reads (see for example [69])

$$\dim_q^{U(N)} R = \prod_{1 \leq i < j \leq d(\mu)} \frac{[\mu_i - \mu_j + j - i]}{[j - i]} \prod_{i=1}^{d(\mu)} \frac{\prod_{v=-i+1}^{\mu_i-1} [v]_\lambda}{\prod_{w=1}^{\mu_i} [w - i + d(\mu)]}, \quad (4.21)$$

where the quantum number $[x]$ is defined in (A.4), and we defined

$$[x]_\lambda = \lambda^{1/2} q^{x/2} - \lambda^{-1/2} q^{-x/2}, \quad (4.22)$$

and $\lambda = q^N$ for $U(N)$ representations.

We can also find explicit expressions for the quantum dimensions of $SO(N)$ and

$Sp(N)$ representations

$$\begin{aligned}
\dim_q^{SO(N)} R &= \prod_{1 \leq i < j \leq d(\mu)} \frac{[\mu_i - \mu_j + j - i][\mu_i + \mu_j + 1 - i - j]_\lambda}{[j - i][1 - i - j]_\lambda} \\
&\quad \times \prod_{i=1}^{d(\mu)} \frac{[\mu_i - i]_\lambda^{SO(N)}}{[-i]_\lambda^{SO(N)}} \prod_{v=1}^{\mu_i} \frac{[\mu_i + 1 - i - v - d(\mu)]_\lambda}{[v - i + d(\mu)]}, \\
\dim_q^{Sp(N)} R &= \prod_{1 \leq i < j \leq d(\mu)} \frac{[\mu_i - \mu_j + j - i][\mu_i + \mu_j + 1 - i - j]_\lambda}{[j - i][1 - i - j]_\lambda} \\
&\quad \times \prod_{i=1}^{d(\mu)} \frac{[1 - i]_\lambda^{Sp(N)} [2\mu_i - 2i + 1]_\lambda}{[1 - i + \mu_i]_\lambda^{Sp(N)} [1 - 2i]_\lambda} \\
&\quad \times \prod_{v=1}^{\mu_i} \frac{[\mu_i + 1 - i - v - d(\mu)]_\lambda}{[v - i + d(\mu)]}, \tag{4.23}
\end{aligned}$$

where we defined

$$[x]_\lambda^{SO(N)} = \lambda^{1/4} q^{\frac{1}{4}(2x+1)} - \lambda^{-1/4} q^{-\frac{1}{4}(2x+1)}, \tag{4.24}$$

and

$$[x]_\lambda^{Sp(N)} = \lambda^{1/4} q^{\frac{1}{4}(2x-1)} - \lambda^{-1/4} q^{-\frac{1}{4}(2x-1)}, \tag{4.25}$$

with $\lambda = q^{N+a}$ which leads to $\lambda = q^{N-1}$ for $SO(N)$ and $\lambda = q^{N+1}$ for $Sp(N)$. Using (4.23) one can show that

$$\dim_q^{Sp(N)} R = (-1)^{\ell(R)} \dim_q^{SO(-N)} R^T, \tag{4.26}$$

where R^T is the transposed or conjugate representation, related to R by exchanging rows with columns, $SO(-N)$ is meant in the sense of analytic continuation, and $\ell(R)$ is the number of boxes of the Young tableau. This relation is part of the “ $SO(N) = Sp(-N)$ ” equivalence [70]. A relation similar to (4.26) holds for usual dimensions [71].

Using (4.21) and (4.23) one can also infer the following formula for quantum dimensions of representations of $SO(N)$ and $Sp(N)$ in terms of quantum dimensions of representations of $U(N)$:

$$\dim_q^{SO(N)/Sp(N)} R = \sum_{Q=Q^t} (-1)^{1/2(\ell(Q) \mp r(Q))} \dim_q^{U(N)}(R/Q), \tag{4.27}$$

where the skew quantum dimension is defined, as in (A.8), by

$$\dim_q^{U(N)}(R/Q) = \sum_{R'} N_{R'Q}^R \dim_q^{U(N)} R' \tag{4.28}$$

and $N_{R_1 R_2}^R$ are the usual Littlewood-Richardson coefficients that appear in the tensor product of $U(N)$ representations: $R_1 \otimes R_2 = \sum_R N_{R_1 R_2}^R R$. In (4.27) the sum is over self-conjugate representations, i.e. representations that are equal to their transpose, and starts with the trivial representation: $\{\cdot, \square, \begin{smallmatrix} \square & \\ & \square \end{smallmatrix}, \begin{smallmatrix} \square & & \\ & \square & \\ & & \square \end{smallmatrix}, \dots\}$. $r(Q)$ denotes the rank of Q , which is defined as the number of boxes in the leading diagonal of the Young tableau [72]. The $-$ sign is for $SO(N)$ representations while the $+$ sign is for $Sp(N)$ representations.

As we will see in the following sections, the relations between quantum dimensions of representations of $SO(N)$ and $Sp(N)$ (4.26) and (4.27) are responsible for the fact that partition functions of $SO(N)$ and $Sp(N)$ differ only by an overall sign in front of the unoriented contributions with an odd number of crosscaps, which leads to the interpretation that they correspond to different choices of sign for the crosscap states. Basically, the first term in the sum of the right hand side of (4.27) is responsible for oriented contributions to the partition functions, so they are the same for $SO(N)$, $Sp(N)$ and $U(N)$ gauge groups. The other terms in the sum are responsible for unoriented contributions to the partition function, and the difference of sign in the exponent of the (-1) factor leads to a relative minus sign between unoriented contributions with an odd number of crosscaps of the $SO(N)$ and $Sp(N)$ partition functions.

Another important ingredient we will need is the framing of knots and links [68]. Given a knot invariant in representation R , we can change its framing by p units (where p is an integer) if we multiply it by

$$(-1)^{\ell(R)p} q^{pC_R/2} \quad (4.29)$$

where C_R is the quadratic Casimir of the representation R . The quadratic Casimirs have the following expressions for the different classical gauge groups:

$$C_R = \kappa_R + (N + a)\ell(R), \quad (4.30)$$

where a is given by (4.18), and

$$\kappa_R = \sum_i \mu_i(\mu_i - 2i + 1). \quad (4.31)$$

The framing factor can then be written as

$$(-1)^{\ell(R)p} \lambda^{p\ell(R)/2} q^{p\kappa_R/2}. \quad (4.32)$$

The sign in (4.29) is not standard in the context of Chern-Simons theory, but as shown in [73, 69], it is crucial in the context of topological string theory in order to

guarantee integrality properties in the resulting amplitudes. To incorporate a change of framing in a link, we just change the framings of each of its components according to the rule (4.29) as well.

In our computations we will also need the invariants of Hopf links with linking number $+1$. For arbitrary gauge group \mathcal{G} , the invariant of the Hopf link with linking number $+1$ is given by the normalized inverse S matrix [68], and it can be written in terms of quantum dimensions as (see for example [74])

$$\mathcal{W}_{R_1 R_2} = \frac{S_{R_1 R_2}^{-1}}{S_{00}} = \sum_{R \in R_1 \otimes R_2} q^{\frac{1}{2}(C_R - C_{R_1} - C_{R_2})} \dim_q R, \quad (4.33)$$

where the sum is over all representations R occurring in the decomposition of the tensor product of R_1 and R_2 . In the $U(N)$ case, we can replace the Casimir operators C_{R_i} appearing in (4.33) by κ_{R_i} , since $\ell(R) = \ell(R_1) + \ell(R_2)$ in the decomposition of a tensor product of irreducible representations of $U(N)$. However this relation between the number of boxes of Young tableaux does not hold in the $SO(N)$ and $Sp(N)$ cases. We thus find

$$\begin{aligned} \mathcal{W}_{R_1 R_2}^{U(N)} &= \sum_R N_{R_1 R_2}^R q^{\frac{1}{2}(\kappa_R - \kappa_{R_1} - \kappa_{R_2})} \dim_q^{U(N)} R, \\ \mathcal{W}_{R_1 R_2}^{SO(N)/Sp(N)} &= \sum_R M_{R_1 R_2}^R \lambda^{\frac{1}{2}(\ell(R) - \ell(R_1) - \ell(R_2))} q^{\frac{1}{2}(\kappa_R - \kappa_{R_1} - \kappa_{R_2})} \\ &\quad \times \dim_q^{SO(N)/Sp(N)} R, \end{aligned} \quad (4.34)$$

where we have denoted by $M_{R_1 R_2}^R$ the tensor product coefficients for irreducible representations of $SO(N)$ and $Sp(N)$, which turn out to be the same for $SO(N)$ and $Sp(N)$.

To compute (4.34) we need the values of $M_{R_1 R_2}^R$, in other words, we have to decompose any tensor product of $SO(N)$ or $Sp(N)$ representations into a sum of irreducible representations. This can be done with a technique first developed by Littlewood in [72]. Let us first consider $SO(N)$ representations. Let $[R]$ be the character of the representations R , as a function of the eigenvalues of an $SO(N)$ matrix, and let $\{R\}$ be the Schur function of these eigenvalues labeled by the same representation. One can prove the following formulae [72]:

$$\begin{aligned} [R] &= \{R\} + \sum_{R_1 \in \{\delta\}} (-1)^{\ell(R_1)/2} N_{R_1 R_2}^R \{R_2\}, \\ \{R\} &= [R] + \sum_{R_1 \in \{\gamma\}} N_{R_1 R_2}^R [R_2], \end{aligned} \quad (4.35)$$

where $\{\delta\}$ and $\{\gamma\}$ are subsets of Young tableaux that we describe in appendix A.1. By using these relations one can express each character $[R][R']$ in the product as a sum of Schur functions, then multiply these with the usual Littlewood-Richardson coefficients, and finally reexpress the Schur functions in terms of a sum of characters by the second equation of (4.35). For example,

$$\begin{aligned} [\square][\square] &= (-1 + \{\square\square\})(\{\square\}) \\ &= \{\square\square\} + \{\begin{smallmatrix} \square \\ \square \end{smallmatrix}\} - \{\square\} \\ &= [\square\square] + [\square] + [\begin{smallmatrix} \square \\ \square \end{smallmatrix}] + [\square] - [\square] = [\square] + [\square\square] + [\begin{smallmatrix} \square \\ \square \end{smallmatrix}], \end{aligned} \quad (4.36)$$

where the Young tableaux are associated to irreducible representations of $SO(N)$. To compute the decompositions for $Sp(N)$ representations, one only has to replace the subsets $\{\delta\}$ and $\{\gamma\}$ respectively by the subsets $\{\beta\}$ and $\{\alpha\}$, which are also explained in appendix A.1 [71]. Using this technique one can decompose any tensor products of $SO(N)$ and $Sp(N)$ representations into a sum of irreducible representations, which is needed in the computation of expectation values of Hopf links using (4.34). One finds that the decomposition of tensor products is always the same for $SO(N)$ and $Sp(N)$ representations, justifying our claim above.

The procedure we have described turns out to be rather involved, and fortunately there is a more direct way of computing $M_{R_1 R_2}^R$ through the following formula [75, 76]:

$$M_{R_1 R_2}^R = \sum_{Q, T, U} N_{QT}^{R_1} N_{QU}^{R_2} N_{TU}^R, \quad (4.37)$$

which expresses these coefficients in terms of usual Littlewood-Richardson coefficients. This formula allows to easily compute the invariants of Hopf links for SO/Sp gauge groups for any pair of representations.

As shown in [22, 17], the Hopf link invariant $\mathcal{W}_{R_1 R_2}^{U(N)}$ plays a crucial rôle in the computation of oriented string amplitudes. It is a Laurent polynomial in $\lambda^{\frac{1}{2}}$ whose highest power is $\lambda^{(\ell(R_1) + \ell(R_2))/2}$:

$$\mathcal{W}_{R_1 R_2}^{U(N)} = \lambda^{(\ell(R_1) + \ell(R_2))/2} W_{R_1 R_2}(q) + \dots, \quad (4.38)$$

where the dots refer to terms with lower powers of λ . The leading part of $\mathcal{W}_{R_1 R_2}^{U(N)}$, which we have denoted by $W_{R_1 R_2}$, can be computed in terms of Schur polynomials in an infinite number of variables (see for example [17, 77, 78] for more details):

$$W_{R_1 R_2}(q) = s_{R_2}(x_i = q^{-i + \frac{1}{2}}) s_{R_1}(x_i = q^{\mu_i^{R_2} - i + \frac{1}{2}}), \quad (4.39)$$

where $\{\mu_i^{R_2}\}_{i=1,\dots,d(\mu^{R_2})}$ is the partition corresponding to R_2 . We will also denote $W_R = W_{R_1 R_2} = s_R(x_i = q^{-i+\frac{1}{2}})$. By looking at the formula in (4.34) for $\mathcal{W}_{R_1 R_2}^{SO(N)/Sp(N)}$, one can see that it is a Laurent polynomial in $\lambda^{\frac{1}{2}}$, whose highest power is also $\lambda^{(\ell(R_1)+\ell(R_2))/2}$, and which has the same leading coefficient $W_{R_1 R_2}(q)$.

More results about Schur functions and their relations to Chern-Simons invariants and the topological vertex are presented in appendix A.2. In the following we will often use this point of view, especially in chapter 5.

4.3.2 Computation of Open String Amplitudes

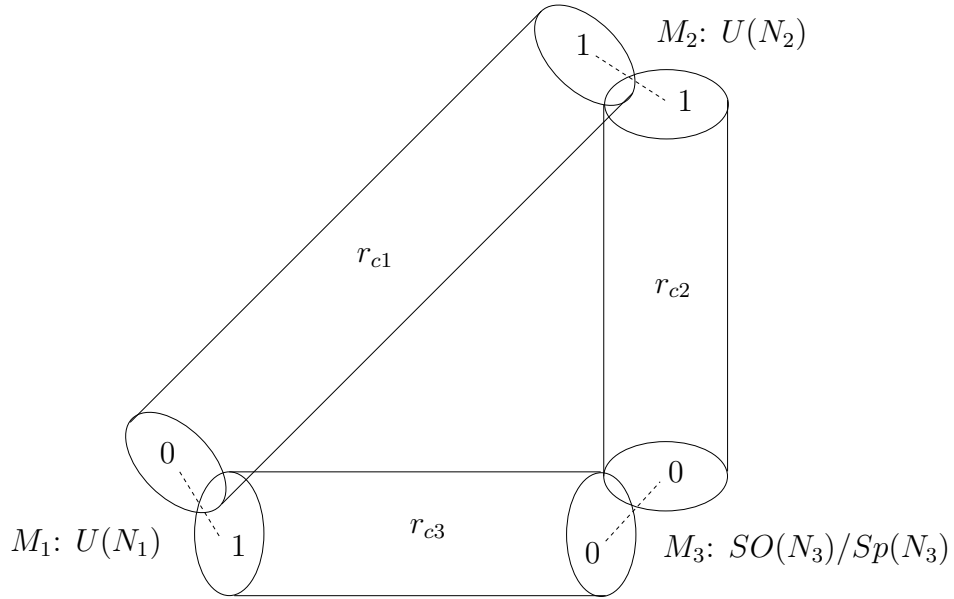


Figure 4.4: The deformed geometry. M_i $i = 1, 2, 3$ are the three spheres and r_{ci} are the Kähler parameters of the cylindrical instantons. The gauge groups of the Chern-Simons theories on the spheres and the framings of the unknots are also indicated.

We will now follow the results in [22, 24, 25] to compute the open topological string amplitudes in the geometry described in section 4.2, which is shown in figure 4.4. There are N_i D-branes wrapped around the three \mathbf{S}^3 's M_i , $i = 1, 2, 3$. This geometry is similar to the one considered for example in [22]; the main difference being that one of the spheres in our geometry, more precisely M_3 , is left invariant by the anti-holomorphic involution, thus leading to a $SO(N)$ or $Sp(N)$ Chern-Simons theory.

For open strings with both ends on the same \mathbf{S}^3 , the dynamics is described by a Chern-Simons theory as usual. For M_1 and M_2 , the Chern-Simons theories respectively have gauge groups $U(N_1)$ and $U(N_2)$, while for M_3 it has gauge group $SO(N_3)$ or $Sp(N_3)$. However, there are also cylindrical open string instantons coupling the Chern-Simons theories on different spheres [79]. Schematically, the path integral becomes

$$Z = \int \prod_{i=1}^3 \mathcal{D}A_i e^{\sum_{i=1}^3 S_i^{CS}(A_i) + S_{inst}}, \quad (4.40)$$

where $S_i^{CS}(A_i)$, $i = 1, 2, 3$ are the Chern-Simons actions for the three \mathbf{S}^3 's. The instanton sector, S_{inst} , can be computed by using localization (as in [24, 25]) or by using the techniques of [22]. We will follow here the procedure of [22]. As explained there, the bifundamental strings stretching between two three sphere \mathbf{S}^3 's give a massive complex scalar field, with mass proportional to the complexified Kähler parameter r_c corresponding to the “distance” between the two spheres. After integrating out this scalar field one finds an operator which corresponds to a primitive annulus of size r_c together with its multicovers. The boundaries of the annulus are on the two three-spheres between which the bifundamental strings are stretched. These cylindrical instantons and the geometry are shown in figure 4.4. Inserting one operator for each cylindrical instanton we find

$$e^{S_{inst}} = \mathcal{O}(U_3, U_1) \mathcal{O}(V_1, V_2) \mathcal{O}(U_2, V_3), \quad (4.41)$$

where we have defined the holonomy variables

$$U_i = P \exp \oint_{\Xi_i} A_i, \quad V_i = P \exp \oint_{\Gamma_i} A_i, \quad i = 1, 2, 3, \quad (4.42)$$

and the Ξ_i, Γ_i , $i = 1, 2, 3$ are the boundary components of the cylindrical instantons, which are unknots in the corresponding three-spheres. The operators in (4.41) are given by

$$\mathcal{O}(A, B, r_c) = \sum_R \text{Tr}_R A e^{-\ell(R)r_c} \text{Tr}_R B, \quad (4.43)$$

where the sum is over all representations, including the trivial one.

The careful reader may note that the operator (4.43) is only equivalent to the usual operator [29, 22]

$$\exp \sum_{n=1}^{\infty} \frac{e^{-nr_c}}{n} \text{Tr} A^n \text{Tr} B^n \quad (4.44)$$

in the $U(N)$ case. In the more general case where the gauge group is $SO(N)$ or $Sp(N)$, the two operators are not equivalent. It turns out that (4.43) is the good operator to use; it would be interesting to investigate further why this is so.

We can now write the total free energy $\mathcal{F} = -\log Z$ (with Z given in (4.40)) as

$$\mathcal{F} = \sum_{i=1}^3 \mathcal{F}(M_i) + \mathcal{F}_{inst}, \quad (4.45)$$

where $\mathcal{F}(M_i)$ are the free energies of the Chern-Simons theories in the spheres M_i , $i = 1, 2, 3$, and \mathcal{F}_{inst} is:

$$\mathcal{F}_{inst} = -\ln \left\{ \sum_{R_1, R_2, R_3} e^{-\sum_{i=1}^3 \ell(R_i) r_{ci}} K_{R_3 R_1}(\mathcal{L}_1) K_{R_1 R_2}(\mathcal{L}_2) K_{R_2 R_3}(\mathcal{L}_3) \right\}, \quad (4.46)$$

where \mathcal{L}_i is the link formed by the knots (Ξ_i, Γ_i) and

$$\begin{aligned} K_{R_3 R_1}(\mathcal{L}_1) &= \frac{\langle R_3 | V_{M_1} | R_1 \rangle}{Z_{M_1}}, \\ K_{R_1 R_2}(\mathcal{L}_2) &= \frac{\langle R_1 | V_{M_2} | R_2 \rangle}{Z_{M_2}}, \\ K_{R_2 R_3}(\mathcal{L}_3) &= \frac{\langle R_2 | V_{M_3} | R_3 \rangle}{Z_{M_3}}. \end{aligned} \quad (4.47)$$

It was shown in [22] (using our notation as in figure 4.4) that

$$V_{M_1} = TS^{-1}, \quad V_{M_2} = ST^{-1}S, \quad V_{M_3} = S^{-1}, \quad (4.48)$$

which means that the three links \mathcal{L}_i , $i = 1, 2, 3$ are Hopf links with linking number +1 and that the framings are as follows: $(\Gamma_1, \Xi_3, \Gamma_3)$ are canonically framed, i.e. with framings $(0, 0, 0)$, while (Ξ_1, Ξ_2, Γ_2) have framings $(1, 1, 1)$, as shown in figure 4.4. We can thus write

$$\begin{aligned} K_{R_3 R_1}(\mathcal{L}_1) &= (-1)^{\ell(R_3)} q^{\frac{\kappa_{R_3}}{2}} \frac{S_{R_3 R_1}^{-1}}{S_{00}} = (-1)^{\ell(R_3)} q^{\frac{\kappa_{R_3}}{2}} \mathcal{W}_{R_3 R_1}, \\ K_{R_1 R_2}(\mathcal{L}_2) &= (-1)^{\ell(R_1) + \ell(R_2)} q^{\frac{1}{2}(\kappa_{R_1} + \kappa_{R_2})} \frac{S_{R_1 R_2}^{-1}}{S_{00}} = (-1)^{\ell(R_1) + \ell(R_2)} q^{\frac{1}{2}(\kappa_{R_1} + \kappa_{R_2})} \mathcal{W}_{R_1 R_2} \\ K_{R_2 R_3}(\mathcal{L}_3) &= \frac{S_{R_2 R_3}^{-1}}{S_{00}} = \mathcal{W}_{R_1 R_3}, \end{aligned} \quad (4.49)$$

where the λ dependent pieces of (4.32) have been absorbed in a redefinition of r_{ci} . Therefore (4.46) becomes

$$\begin{aligned} \mathcal{F}_{inst} &= -\ln \left\{ 1 + \sum_{R_1, R_2, R_3} (-1)^{\sum_{i=1}^3 \ell_i} e^{-\sum_{i=1}^3 \ell(R_i) r_{ci}} q^{\frac{1}{2}(\kappa_{R_1} + \kappa_{R_2} + \kappa_{R_3})} \right. \\ &\quad \left. \times \mathcal{W}_{R_3 R_1}(\mathcal{L}_1) \mathcal{W}_{R_1 R_2}(\mathcal{L}_2) \mathcal{W}_{R_2 R_3}(\mathcal{L}_3) \right\}, \end{aligned} \quad (4.50)$$

where we singled out the term coming from $R_1, R_2, R_3 = \cdot$, i.e. the three representations being the trivial representation.

4.3.3 Duality Map and Closed String Amplitudes

Let us first recall the variables we have defined so far. We first defined the Chern-Simons variables $q = e^{ig_s}$ and $\lambda_i = q^{N_i+a_i}$, with $g_s = \frac{2\pi}{k_i+y}$ being the same for the three theories. We denote the three Kähler parameters of the cylindrical instantons by r_{ci} , $i = 1, 2, 3$ and the three 't Hooft parameters of the different gauge groups by t_i . To compare the amplitudes on both sides of the duality, we have to relate the open string parameters t_i and r_{ci} to the following closed string parameters: t , which is the Kähler parameter of \mathbb{CP}^2 , and s_i , $i = 1, 2, 3$, which are the Kähler parameters of the two \mathbb{CP}^1 's and the \mathbb{RP}^2 . The duality map reads

$$\begin{aligned} t &= r_{c1} - \frac{t_1 + t_2}{2} = r_{c2} - \frac{t_2 + t_3}{2} = r_{c3} - \frac{t_1 + t_3}{2}, \\ t_1 &= s_1, \quad t_2 = s_2, \quad t_3 = s_3. \end{aligned} \quad (4.51)$$

Let now q_i be $q_i = e^{-s_i} = e^{-t_i}$, $i = 1, 2$, $Q = e^{-s_3} = e^{-t_3}$ and let ℓ be $\ell(R_1) + \ell(R_2) + \ell(R_3)$. We can rewrite the open string partition function (4.50) using (4.51):

$$\begin{aligned} \mathcal{F}_{inst} &= -\ln \left\{ 1 + \sum_{\ell} (-1)^{\ell} e^{-\ell t} q^{\frac{1}{2}(\kappa_{R_1} + \kappa_{R_2} + \kappa_{R_3})} q_1^{\frac{\ell(R_1) + \ell(R_3)}{2}} q_2^{\frac{\ell(R_1) + \ell(R_2)}{2}} Q^{\frac{\ell(R_2) + \ell(R_3)}{2}} \right. \\ &\quad \left. \times \mathcal{W}_{R_3 R_1}^{U(N)} \mathcal{W}_{R_1 R_2}^{U(N)} \mathcal{W}_{R_2 R_3}^{SO(N)/Sp(N)} \right\}, \end{aligned} \quad (4.52)$$

where the Hopf link invariants in the last line are evaluated at $\lambda = q_i^{-1}$, $i = 1, 2$, and $\lambda = Q^{-1}$ respectively. Notice that the leading power of λ in $\mathcal{W}_{R_1 R_2}^{U(N)}$ and in $\mathcal{W}_{R_1 R_2}^{SO(N)/Sp(N)}$ is in both cases $\lambda^{(\ell(R_1) + \ell(R_2))/2}$, therefore the above expression for \mathcal{F}_{inst} gives a power series in q_i and Q with positive integer coefficients, as it should. We can now expand the logarithm to find

$$\mathcal{F}_{inst} = \sum_{\ell=1}^{\infty} Z_{\ell}^{(c)} e^{-\ell t}, \quad (4.53)$$

where the connected coefficient $Z_{\ell}^{(c)}$ are given by

$$Z_{\ell}^{(c)} = \sum_{1 \leq d \leq \ell} \frac{(-1)^{d+1}}{d} \sum_{m_1 + m_2 + \dots + m_d = \ell} Z_{m_1} Z_{m_2} \dots Z_{m_d}. \quad (4.54)$$

These coefficients give the instanton partition function order by order in the Kähler parameter e^{-t} . Using the formulae given above for Hopf link invariants with classical gauge groups, we can explicitly compute the coefficients $Z_{\ell}^{(c)}$. The contributions independent of the Kähler parameter t are given by the sum of Chern-Simons free energies on $\mathbf{S}^3 \sum_{i=1}^3 \mathcal{F}_{CS}(M_i)$, which have already been computed in [20, 16].

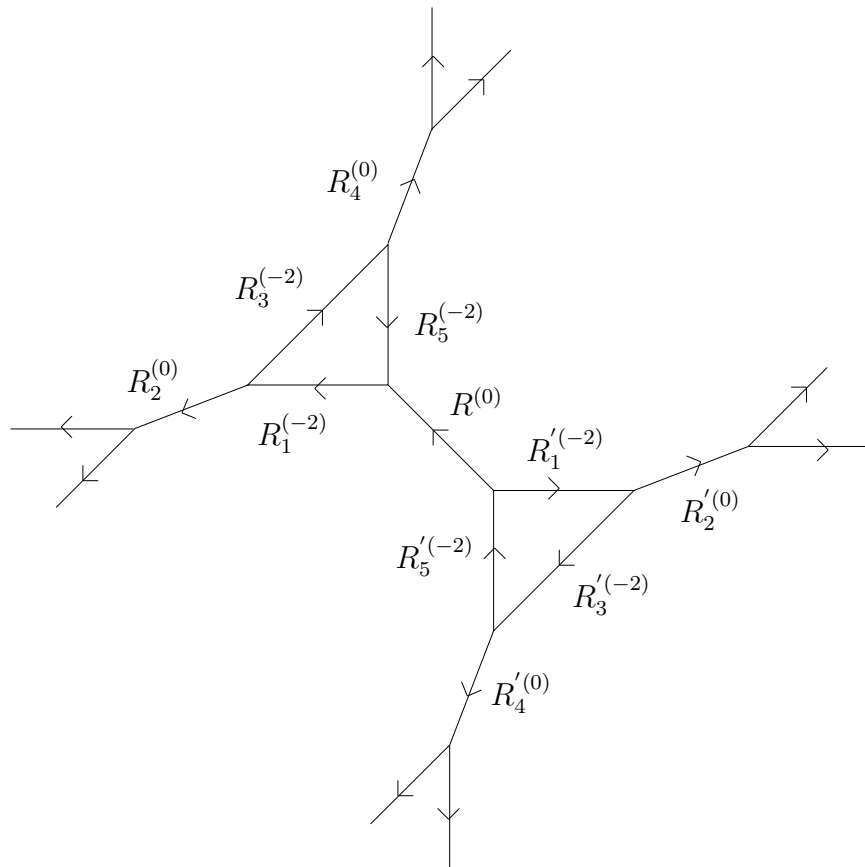


Figure 4.5: The geometry in the topological vertex formalism. In brackets next to the representations are the framings in the corresponding propagator.

4.3.4 The Oriented Contribution

As we explained in section 4.1, \mathcal{F}_{inst} contains contributions due to oriented and to unoriented instantons. In order to compute the closed, unoriented string amplitudes we have to subtract the oriented part, which we must compute independently. The covering space X is the Calabi-Yau manifold depicted in figure 4.5. The oriented amplitude can be computed using the topological vertex formalism [17]. Using the formulae and gluing rules explained in [17] we find

$$Z(X) = \sum_R \mathcal{O}_R(t, q_1, q_2) \mathcal{O}_{R^T}(t, q_1, q_2) (-1)^{\ell(R)} Q^{\ell(R)}, \quad (4.55)$$

where $q_i = e^{-s_i}$, $i = 1, 2$ and $Q = e^{-s_3}$. t is the Kähler parameter of the \mathbb{CP}^2 , s_1 and s_2 are the Kähler parameters of the two \mathbb{CP}^1 's attached to the \mathbb{CP}^2 , and s_3 is the Kähler parameter of the \mathbb{CP}^1 between the two \mathbb{CP}^2 's. Notice that we have identified the Kähler parameters in the way prescribed by the involution. In (4.55) we introduced the operator

$$\begin{aligned} \mathcal{O}_R(t, q_1, q_2) &= \sum_{R_i} C_{RR_5 R_1^T} C_{R_1 R_3^T R_2^T} C_{R_3 R_5^T R_4^T} C_{R_2} \cdot C_{R_4} \cdot (-1)^{\sum_i \ell(R_i)} \\ &\times q^{\kappa(R_1) + \kappa(R_3) + \kappa(R_5)} e^{-(\ell(R_1) + \ell(R_3) + \ell(R_5))t} q_1^{\ell(R_2)} q_2^{\ell(R_4)}, \end{aligned} \quad (4.56)$$

where $C_{R_i R_j R_k}$ is the topological vertex amplitude, which can be expressed in terms of the quantities (4.39):

$$C_{R_1 R_2 R_3} = \sum_{Q_1, Q_3, Q} N_{QQ_1}^{R_1} N_{QQ_3}^{R_3^T} q^{\kappa_{R_2}/2 + \kappa_{R_3}/2} \frac{W_{R_2^T Q_1} W_{R_2 Q_3}}{W_{R_2}}. \quad (4.57)$$

More results about the topological vertex and its relation to Chern-Simons invariants and Schur functions are given in appendix A.2.

Using (4.55) we can express again the free energy as a sum over connected coefficients

$$\mathcal{F}(X) = -\log Z(X) = \sum_{\ell, \ell_1, \ell_2, \ell_3} Z_{\ell, \ell_1, \ell_2, \ell_3}^{(c)} q_1^{\ell_1} q_2^{\ell_2} Q^{\ell_3} e^{-\ell t}. \quad (4.58)$$

The free energy computed in (4.53) should equal, according to (4.2),

$$\mathcal{F}_{inst} = \frac{1}{2} \mathcal{F}(X) + \mathcal{F}(X/I, g_s)_{unor}, \quad (4.59)$$

where $\mathcal{F}(X)$ is given in (4.58). This determines the unoriented part, which should have the structure given in (4.6). We will encode the resulting oriented and unoriented Gopakumar-Vafa invariants in the following generating functionals

$$\begin{aligned}\mathcal{F}_d^{g,0} &= \frac{1}{2} \sum_{d_1, d_2, d_Q} n_{d, d_1, d_2, d_Q}^{g,0} q_1^{d_1} q_2^{d_2} Q^{d_Q}, \\ \mathcal{F}_d^{g,1} &= \sum_{d_1, d_2, d_Q} n_{d, d_1, d_2, d_Q}^{g,1} q_1^{d_1} q_2^{d_2} Q^{d_Q/2}, \\ \mathcal{F}_d^{g,2} &= \sum_{d_1, d_2, d_Q} n_{d, d_1, d_2, d_Q}^{g,2} q_1^{d_1} q_2^{d_2} Q^{d_Q},\end{aligned}\tag{4.60}$$

where d is the degree in e^{-t} , and the superscripts g, c with $c = 0, 1, 2$ denote the genus and the number of crosscaps, respectively. Of course, $c = 0$ is the oriented contribution obtained from (4.58) (multiplied by the factor of $1/2$), and in the second equation of (4.60) d_Q must be odd. In order to compute these functionals, we have to remove multicoverings according to (4.5) and (4.6). It is important to note that the requirement that the partition function satisfies the good integrality properties leading to (4.60) is highly non-trivial.

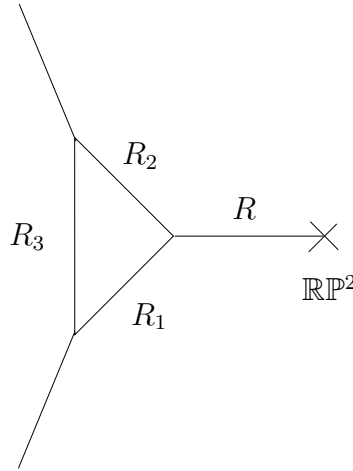


Figure 4.6: Toric diagram for local $\mathbb{C}\mathbb{P}^2$ attached to an $\mathbb{R}\mathbb{P}^2$.

We present the results for the functionals given by (4.60) in appendix B.2. For the sake of brevity, here we present the results only in the limiting case where we take the volumes of the two $\mathbb{C}\mathbb{P}^1$'s attached to the $\mathbb{C}\mathbb{P}^2$ to infinity, as in [22]. We thus obtain the answer for the simpler geometry whose toric diagram is depicted in figure 4.6. This geometry already captures all the interesting features of the unoriented and oriented generating functionals.

To take this limit, one can directly consider the generating functionals (4.60) and set $q_{1,2} = 0$, which corresponds to sending the two Kähler parameters to infinity. One can also obtain this limit by taking the leading piece of the $U(N)$ Hopf link invariants in (4.52), in the sense explained in (4.38). The free energy of this geometry is just:

$$\mathcal{F} = -\ln \left\{ 1 + \sum_{\ell} (-1)^{\ell} e^{-\ell t} q^{\frac{1}{2}(\kappa_{R_1} + \kappa_{R_2} + \kappa_{R_3})} Q^{\frac{\ell(R_2) + \ell(R_3)}{2}} W_{R_3 R_1} W_{R_1 R_2} \mathcal{W}_{R_2 R_3}^{SO(N)/Sp(N)} \right\}. \quad (4.61)$$

The result can now be encoded in the simpler generating functionals

$$\begin{aligned} \mathcal{F}_d^{g,0} &= \frac{1}{2} \sum_{d_Q} n_{d,d_Q}^{g,0} Q^{d_Q}, \\ \mathcal{F}_d^{g,1} &= \sum_{d_Q} n_{d,d_Q}^{g,1} Q^{d_Q/2}, \\ \mathcal{F}_d^{g,2} &= \sum_{d_Q} n_{d,d_Q}^{g,2} Q^{d_Q}, \end{aligned} \quad (4.62)$$

with the same restrictions as for (4.60). We present here the all genus results we obtain up to degree 6 in e^{-t} . At this order $n_{d,d_Q}^{g,c} = 0 \forall g \geq 11$ (all the invariants $n_{d,d_Q}^{g,c}$ with $d \leq 6$ that are not shown in the tables are understood to be zero). The results in tables 4.1–4.24 correspond to $Sp(N)$ gauge group; to obtain the $SO(N)$ result it suffices to change the sign of the invariants with $c = 1$.

$c = 0$	$d_Q = 0$	1	2	3	4	5
$d = 0$	0	1	0	0	0	0
1	6	-4	0	0	0	0
2	-12	14	-2	0	0	0
3	54	-84	30	0	0	0
4	-384	725	-392	51	0	0
5	3390	-7540	5434	-1368	84	0
6	-34128	87776	-79198	29466	-4040	124

Table 4.1: Invariants $n_{d,d_Q}^{0,0}$ at genus 0, up to $d = 6$.

$c = 1$	$d_Q = 1$	3	5	7	9	11
$d = 0$	1	0	0	0	0	0
1	-2	0	0	0	0	0
2	5	-3	0	0	0	0
3	-32	30	-4	0	0	0
4	286	-369	112	-5	0	0
5	-3038	5016	-2410	328	-6	0
6	35870	-72150	47554	-11528	819	-7

Table 4.2: Invariants $n_{d,d_Q}^{0,1}$ at genus 0, up to $d = 6$.

$c = 2$	$d_Q = 2$	3	4	5
$d = 3$	1	0	0	0
4	-11	2	0	0
5	131	-66	7	0
6	-1690	1460	-333	12

Table 4.3: Invariants $n_{d,d_Q}^{0,2}$ at genus 0, up to $d = 6$.

$c = 0$	$d_Q = 0$	1	2	3	4
$d = 3$	20	-18	0	0	0
4	-462	612	-168	0	0
5	8904	-15210	7380	-930	0
6	-161896	336636	-228532	56536	-3851

Table 4.4: Invariants $n_{d,d_Q}^{1,0}$ at genus 1, up to $d = 6$.

$c = 1$	$d_Q = 1$	3	5	7	9
$d = 3$	-9	7	0	0	0
4	288	-315	59	0	0
5	-6984	9954	-3630	282	0
6	152622	-269501	145467	-25672	1014

Table 4.5: Invariants $n_{d,d_Q}^{1,1}$ at genus 1, up to $d = 6$.

$c = 2$	$d_Q = 2$	3	4	5
$d = 4$	-6	0	0	0
5	201	-55	1	0
6	-5180	3180	-438	2

Table 4.6: Invariants $n_{d,d_Q}^{1,2}$ at genus 1, up to $d = 6$.

$c = 0$	$d_Q = 0$	1	2	3	4
$d = 4$	-204	216	-24	0	0
5	10860	-15444	5154	-276	0
6	-388044	690273	-365536	60235	-1800

Table 4.7: Invariants $n_{d,d_Q}^{2,0}$ at genus 2, up to $d = 6$.

$c = 1$	$d_Q = 1$	3	5	7	9
$d = 4$	108	-103	9	0	0
5	-7506	9474	-2567	95	0
6	329544	-521400	231550	-29010	554

Table 4.8: Invariants $n_{d,d_Q}^{2,1}$ at genus 2, up to $d = 6$.

$c = 2$	$d_Q = 2$	3	4
$d = 4$	-1	0	0
5	146	-18	0
6	-8296	3520	-274

Table 4.9: Invariants $n_{d,d_Q}^{2,2}$ at genus 2, up to $d = 6$.

$c = 0$	$d_Q = 0$	1	2	3	4
$d = 4$	-30	28	0	0	0
5	7344	-9094	2036	-30	0
6	-581706	913220	-381934	40728	-408

Table 4.10: Invariants $n_{d,d_Q}^{3,0}$ at genus 3, up to $d = 6$.

$c = 1$	$d_Q = 1$	3	5	7	9
$d = 4$	14	-12	0	0	0
5	-4519	5133	-977	11	0
6	447502	-642780	233460	-19781	139

Table 4.11: Invariants $n_{d,d_Q}^{3,1}$ at genus 3, up to $d = 6$.

$c = 2$	$d_Q = 2$	3	4
$d = 5$		58	-2
6		-8489	2352

Table 4.12: Invariants $n_{d,d_Q}^{3,2}$ at genus 3, up to $d = 6$.

$c = 0$	$d_Q = 0$	1	2	3	4
$d = 5$		2772	-3084	424	0
6		-580800	821490	-270708	17600

Table 4.13: Invariants $n_{d,d_Q}^{4,0}$ at genus 4, up to $d = 6$.

$c = 1$	$d_Q = 1$	3	5	7	9
$d = 5$		-1542	1599	-191	0
6		407661	-536973	157255	-8372

Table 4.14: Invariants $n_{d,d_Q}^{4,1}$ at genus 4, up to $d = 6$.

$c = 2$	$d_Q = 2$	3	4
$d = 5$		12	0
6		-5862	976

Table 4.15: Invariants $n_{d,d_Q}^{4,2}$ at genus 4, up to $d = 6$.

$c = 0$	$d_Q = 0$	1	2	3	$c = 1$	$d_Q = 1$	3	5	7
$d = 5$		540	-552	36	0	$d = 5$		-276	265
6		-393714	509724	-130496	4684	6		254310	-309962

Table 4.16: Invariants $n_{d,d_Q}^{5,c}$ at genus 5, with $c = 0, 1$, up to $d = 6$.

$c = 2$	$d_Q = 2$	3	4
$d = 5$		1	0
6		-2758	245

Table 4.17: Invariants $n_{d,d_Q}^{5,2}$ at genus 5, up to $d = 6$.

$c = 0$	$d_Q = 0$	1	2	3	$c = 1$	$d_Q = 1$	3	5	7
$d = 5$		42	-40	0	0	$d = 5$		-20	18
6		-180780	216960	-41904	696	6		108440	-123342

Table 4.18: Invariants $n_{d,d_Q}^{6,c}$ at genus 6, with $c = 0, 1$, up to $d = 6$.

$c = 2$	$d_Q = 2$	3
$d = 5$		0 0
6		-868 34

Table 4.19: Invariants $n_{d,d_Q}^{6,2}$ at genus 6, up to $d = 6$.

$c = 0$	$d_Q = 0$	1	2	3	$c = 1$	$d_Q = 1$	3	5	7
$d = 6$	-55076	61896	-8532	44	$d = 6$	30948	-33110	4156	-18

Table 4.20: Invariants $n_{d,d_Q}^{7,c}$ at genus 7, with $c = 0, 1$, up to $d = 6$.

$c = 2$	$d_Q = 2$	3
$d = 6$		-174 2

Table 4.21: Invariants $n_{d,d_Q}^{7,2}$ at genus 7, up to $d = 6$.

$c = 0$	$d_Q = 0$	1	2	$c = 1$	$d_Q = 1$	3	5	$c = 2$	$d_Q = 2$
$d = 6$	-10620	11268	-992	$d = 6$	5634	-5710	458	$d = 6$	-20

Table 4.22: Invariants $n_{d,d_Q}^{8,c}$ at genus 8, with $c = 0, 1, 2$, up to $d = 6$.

$c = 0$	$d_Q = 0$	1	2	$c = 1$	$d_Q = 1$	3	5	$c = 2$	$d_Q = 2$
$d = 6$	-1170	1180	-50	$d = 6$	590	-570	22	$d = 6$	-1

Table 4.23: Invariants $n_{d,d_Q}^{9,c}$ at genus 9, with $c = 0, 1, 2$, up to $d = 6$.

$c = 0$	$d_Q = 0$	1	$c = 1$	$d_Q = 1$	3
$d = 6$	-56	54	$d = 6$	27	-25

Table 4.24: Invariants $n_{d,d_Q}^{10,c}$ at genus 10, with $c = 0, 1$, up to $d = 6$.

4.4 Unoriented Localization

As explained in section 4.1, to compute the full partition function of closed topological strings on the geometry before the geometric transition, we have to sum both over holomorphic maps from orientable Riemann surfaces to the Calabi-Yau space X as well as maps from non-orientable worldsheets to the orientifolded space X/I .

In [26] it was developed a method for summing unoriented world-sheet instantons for closed topological strings based on localization with respect to a torus action on a moduli space of equivariant holomorphic maps. Although in [26] this moduli space has not been constructed, a computational definition for its virtual fundamental cycle was given. Concretely, this reduces to enumerating all fixed loci under an induced torus action on the moduli space and assigning a local contribution to each component of the fixed locus using an equivariant version of the localization theorem of [80]. Moreover, in [26] it was shown that the fixed loci can be represented in terms of Kontsevich graphs [81] with involution.

This method does not rely on large N duality, and therefore may provide an independent check of our large N duality proposal for orientifolds. Namely, we can employ the localization techniques of [26] to compute one crosscap and two crosscaps contributions to the full closed topological string partition function on the orientifolded geometry before the geometric transition.

We can use the computation in [26] to confirm the one crosscap invariants for low degree and genus obtained from the Chern-Simons computation. There, it was computed the unoriented free energy for a $\mathbb{C}\mathbb{P}^2$ with a $\mathbb{R}\mathbb{P}^2$ attached. This is exactly the limiting geometry for which we presented our results in tables 4.1–4.24, related to the full geometry of section 4.1 by sending the two Kähler parameters of the $\mathbb{C}\mathbb{P}^1$'s of the full geometry to infinity. In our variables, the result of [26] reads

$$\begin{aligned} \mathcal{F} = & \frac{1}{g_s} (Q^{1/2} - 2e^{-t}Q^{1/2} + 5e^{-2t}Q^{1/2} + \dots + \frac{1}{9}Q^{3/2} - 3e^{-2t}Q^{3/2} + \frac{268}{9}e^{-3t}Q^{3/2} + \dots) \\ & + g_s \left(\frac{1}{24}Q^{1/2} - \frac{1}{12}e^{-t}Q^{1/2} + \dots \right). \end{aligned} \quad (4.63)$$

By expanding $q = e^{ig_s}$ in powers of g_s , it is straightforward to show that the contributions with $c = 1$ in tables 4.1–4.24 are in agreement with (4.63).

In the following we will compute some Klein bottle amplitudes using unoriented localization. We will find agreement with the Chern-Simons and with the topological

vertex computations. We will perform the computations in the Calabi-Yau geometry \tilde{X} . In the patch $\{z_1 \neq 0, z_7 \neq 0, z_{10} \neq 0\}$ we introduce local coordinates

$$z = \frac{z_1^3 z_4}{z_7 z_{10}^3}, \quad u = \frac{z_6 z_7 z_{10}^2}{z_1}, \quad v = \frac{z_5 z_7 z_{10}^2}{z_1}. \quad (4.64)$$

Using (4.16) we obtain the weights of the local coordinates

$$\lambda_z = 6\lambda_1 + 2\lambda_4, \quad \lambda_u = -3\lambda_1 - \lambda_4 + \lambda_6, \quad \lambda_v = -3\lambda_1 - \lambda_4 + \lambda_5. \quad (4.65)$$

Note that the compatibility of the involution with the torus action implies $\lambda_z + \lambda_u + \lambda_v = 0$.

We will denote the contributions of the fixed loci by $C_{\chi,d,h}$, where χ is the Euler characteristic of the unoriented source Riemann surface and d and h are the degrees of the map with respect to the \mathbb{RP}^2 and hyperplane class of \mathbb{CP}^2 respectively.

4.4.1 Unoriented Localization at 2 Crosscaps and Degree 2 \mathbb{RP}^2

The computation at degree 0 hyperplane class has been performed in [26]. Let us recall the graphs and their contributions.

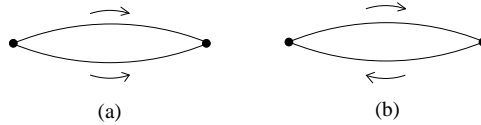


Figure 4.7: Two crosscaps and no hyperplane at degree 2 \mathbb{RP}^2 .

Note that in case (b) the anti-holomorphic involution exchanges the two components of the source curve. In [26] it has been postulated that such an operation will introduce an additional minus sign. Therefore the contributions of the two graphs are

$$C_{0,2,0}^{(a)} = \frac{\lambda_u \lambda_v}{4\lambda_z^2}, \quad C_{0,2,0}^{(b)} = -\frac{\lambda_u \lambda_v}{4\lambda_z^2}. \quad (4.66)$$

Let us consider now the degree 1 hyperplane class configurations. The graphs allowed are presented in figure 4.8.

The allowed configurations are obtained by performing bubbings at the nodes of the graphs in figure 4.7 and inserting degree 1 hyperplane graphs; we will call such configurations type I graphs. These come in pairs, each one admits a mirror graph.

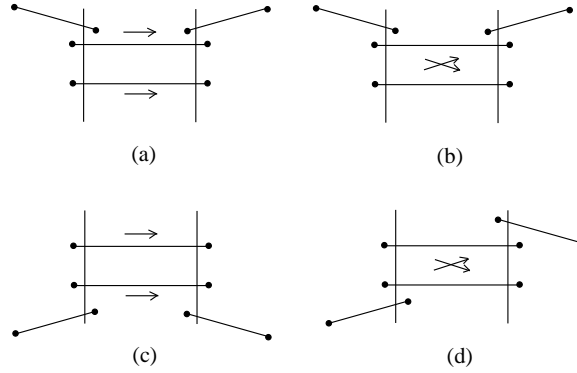


Figure 4.8: Two crosscaps and one hyperplane at degree 2 $\mathbb{R}P^2$. Mirror pairs are $\{(a), (c)\}$ and $\{(b), (d)\}$ respectively.

From now on, we will draw a single graph for each mirror pair. The contributions of the above configurations are given by

$$C_{0,2,1}^{(a)} = \frac{\lambda_v^2}{2\lambda_z^2}, \quad C_{0,2,1}^{(b)} = -\frac{\lambda_v^2}{2\lambda_z^2}, \quad C_{0,2,1}^{(c)} = \frac{\lambda_u^2}{2\lambda_z^2}, \quad C_{0,2,1}^{(d)} = -\frac{\lambda_u^2}{2\lambda_z^2} \quad (4.67)$$

where we have used again the sign rule postulated in [26]. The graph contributions add up to zero.

The discussion is similar at degree 2 hyperplane class. The type I graphs appearing cancel in pairs due to the same sign rule as above. There also appear new configurations, which we will call type II graphs, and which we present in figure 4.9.

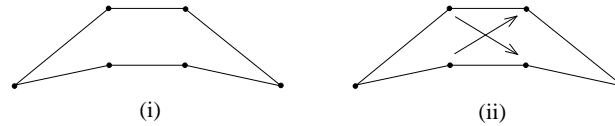


Figure 4.9: Two crosscaps and two hyperplanes at degree 2 $\mathbb{R}P^2$: type II graphs.

Their contributions are given by

$$C_{0,2,2}^{(i)} = \frac{(\lambda_u - 2\lambda_v)(\lambda_v - \lambda_u)}{2\lambda_v^2}, \quad C_{0,2,2}^{(ii)} = -\frac{(\lambda_u - 2\lambda_v)(\lambda_v - \lambda_u)}{2\lambda_v^2} \quad (4.68)$$

and therefore they cancel due to the same sign rule that we used previously.

At degree 3 hyperplane class, we obtain again pairs of graphs of type I and type II that cancel each other. In figure 4.10 we draw some new type II graphs whose analogues at higher $\mathbb{R}P^2$ degree will play an important rôle.

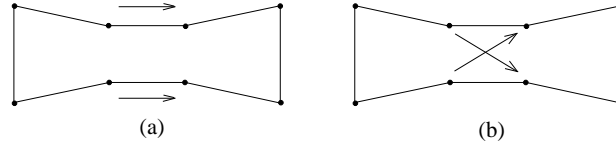


Figure 4.10: Two crosscaps and three hyperplanes at degree 2 $\mathbb{R}P^2$: type II graphs.

The contributions of the two graphs of figure 4.10 are: $C_{0,2,3}^{(a)} = -C_{0,2,3}^{(b)} = 1$. To conclude, we obtain that up to degree 3 hyperplane class, the 2 crosscaps degree 2 $\mathbb{R}P^2$ Gromov-Witten invariants vanish. In fact, this will be true at any hyperplane class degree.

4.4.2 Unoriented Localization at 2 Crosscaps and Degree 4 $\mathbb{R}P^2$

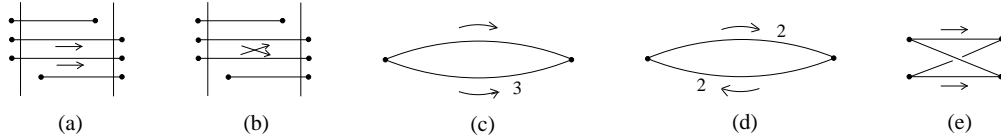


Figure 4.11: Two crosscaps and no hyperplane at degree 4 $\mathbb{R}P^2$.

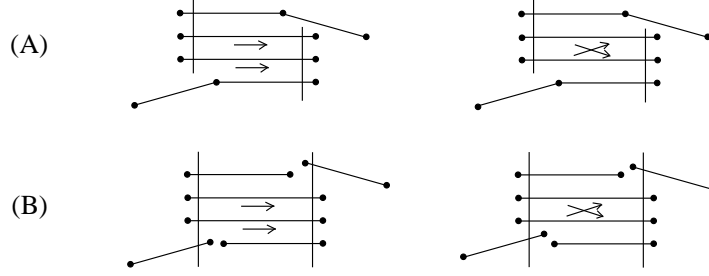
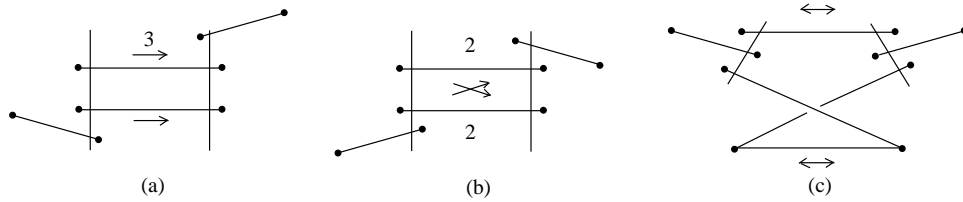
At degree 0 hyperplane class this computation has been performed in [26]. We list the graphs in figure 4.11. The contributions of the graphs are:

$$\begin{aligned}
 C_{0,4,0}^{(a)} &= \frac{1}{2} \frac{\lambda_u^2 \lambda_v^2}{\lambda_z^4}, & C_{0,4,0}^{(b)} &= -\frac{1}{2} \frac{\lambda_u^2 \lambda_v^2}{\lambda_z^4}, & C_{0,4,0}^{(c)} &= \frac{1}{8} \frac{\lambda_u \lambda_v (2\lambda_z^2 - 9\lambda_u \lambda_v)}{\lambda_z^4}, \\
 C_{0,4,0}^{(d)} &= -\frac{1}{4} \frac{\lambda_u \lambda_v (\lambda_z^2 - 4\lambda_u \lambda_v)}{\lambda_z^4}, & C_{0,4,0}^{(e)} &= \frac{1}{8} \frac{\lambda_u^2 \lambda_v^2}{\lambda_z^4}.
 \end{aligned}
 \tag{4.69}$$

Note that $C_{0,4,0}^{(a)} + C_{0,4,0}^{(b)} = 0$ and $C_{0,4,0}^{(c)} + C_{0,4,0}^{(d)} + C_{0,4,0}^{(e)} = 0$.

At degree 1 hyperplane class there appear new configurations, which we will call type III graphs; they are obtained by adding to the first two graphs in figure 4.11 degree 1 hyperplane lines as shown in figure 4.12.

Using again the sign rule in [26], the two graphs in each line of figure 4.12 add up to zero. We now turn to type I graphs; they are presented in figure 4.13 and their

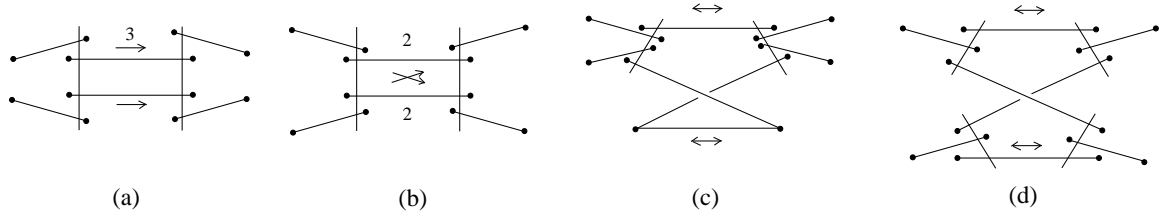
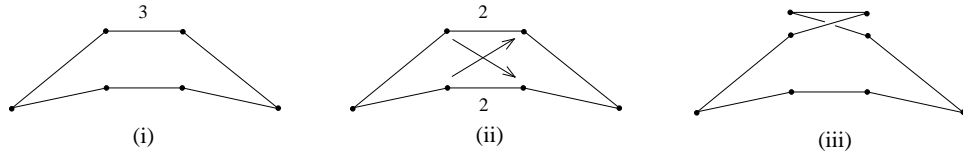

 Figure 4.12: Two crosscaps and one hyperplane at degree 4 $\mathbb{R}P^2$: type III graphs.

 Figure 4.13: Two crosscaps and one hyperplane at degree 4 $\mathbb{R}P^2$: type I graphs.

contributions are:

$$\begin{aligned}
 C_{0,4,1}^{(a)} &= \frac{1}{2} \left(2 - 9 \frac{\lambda_u \lambda_v}{\lambda_z^2} \right) \left(\frac{\lambda_u^2}{\lambda_z^2} + \frac{\lambda_v^2}{\lambda_z^2} \right), & C_{0,4,1}^{(b)} &= \left(-1 + 4 \frac{\lambda_u \lambda_v}{\lambda_z^2} \right) \left(\frac{\lambda_u^2}{\lambda_z^2} + \frac{\lambda_v^2}{\lambda_z^2} \right), \\
 C_{0,4,1}^{(c)} &= \frac{\lambda_u \lambda_v}{2 \lambda_z^2} \left(\frac{\lambda_u^2}{\lambda_z^2} + \frac{\lambda_v^2}{\lambda_z^2} \right). & &
 \end{aligned} \tag{4.70}$$

It is easy to check that $C_{0,4,1}^{(a)} + C_{0,4,1}^{(b)} + C_{0,4,1}^{(c)} = 0$. This is in fact the same cancellation that took place at degree 0 hyperplane class between the contributions of the corresponding three graphs. Again, we see that at degree 1 hyperplane class there is nothing essentially new compared to degree 0 hyperplane class.

Let us now consider the case of degree 2 hyperplane class. We can split the allowed configurations in graphs of type I and III above. Configurations of type III are built by starting with the graphs (a) and (b) in figure 4.11 and further adding in all possible ways degree 2 graphs in $\mathbb{C}P^2$. They will always cancel in pairs. Configurations of type I are constructed by starting with the graphs (c), (d) and (e) in figure 4.11, performing a bubbling at a pair of identified nodes and inserting degree 2 graphs in $\mathbb{C}P^2$. The contributions of the graphs with degree 2 multicoverings of one of the hyperplane sections cancel as before; there also appear configurations as in figure 4.14. However, their contributions also add up to zero, and this will be true for any quartet of type I graphs as in figure 4.14.

Figure 4.14: Two crosscaps and two hyperplanes at degree 4 \mathbb{RP}^2 : type I graphs.Figure 4.15: Two crosscaps and two hyperplanes at degree 4 \mathbb{RP}^2 : type II graphs.

There are also type II graphs, which are constructed by starting with the graphs (c), (d) and (e) in figure 4.11. A triplet of such graphs is presented in figure 4.15. The total contribution of these three graphs is

$$C_{0,4,2}^{(i)} + C_{0,4,2}^{(ii)} + C_{0,4,2}^{(iii)} = -\frac{(\lambda_u - \lambda_v)^2(\lambda_u + \lambda_v + \lambda_z)Q_9(\lambda_u, \lambda_v, \lambda_z)}{4\lambda_u^2\lambda_v^2\lambda_z^2(2\lambda_u + \lambda_z)^2(2\lambda_v + \lambda_z)^2(3\lambda_u + \lambda_z)(3\lambda_v + \lambda_z)}, \quad (4.71)$$

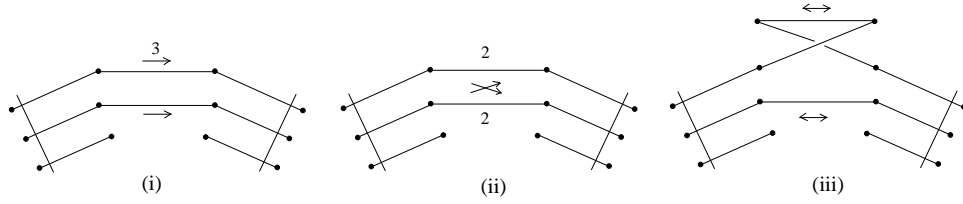
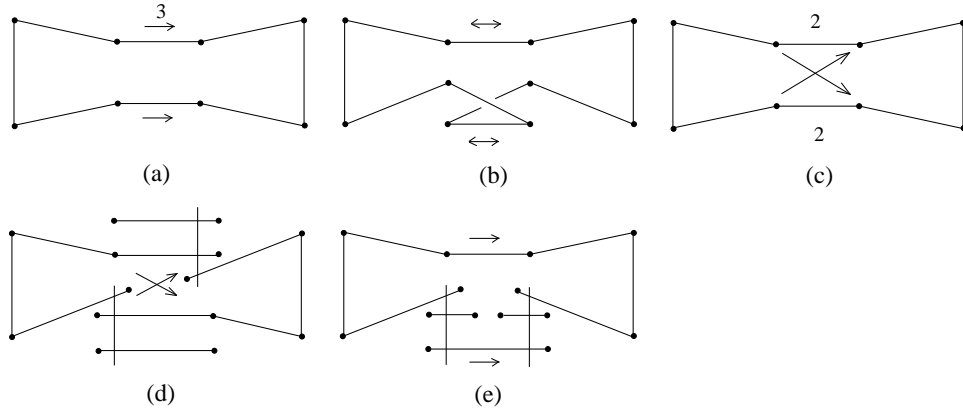
where $Q_9(\lambda_u, \lambda_v, \lambda_z)$ is a degree 9 homogeneous polynomial in $\lambda_u, \lambda_v, \lambda_z$. We recall that consistency of the anti-holomorphic involution with the torus action implies $\lambda_u + \lambda_v + \lambda_z = 0$, and therefore the sum of the graphs in figure 4.15 is zero. This will also be true for the other possible triplet of type II graphs. We conclude that up to degree 2 hyperplane class, the two crosscaps degree 4 \mathbb{RP}^2 Gromov–Witten invariants vanish.

At degree 3 hyperplane class there appear all three types of graphs. We claim that the type I and III graphs sum up to zero, as above. Besides sets of type II graphs that have analogues at lower degree hyperplane class, and whose contributions add up to zero in a similar fashion, at degree 3 hyperplane class there also are new collections of graphs. Such a set is presented in figure 4.16.

The total contribution of the above three graphs is

$$C_{0,4,3}^{(i)} + C_{0,4,3}^{(ii)} + C_{0,4,3}^{(iii)} = \frac{\lambda_u(\lambda_u + \lambda_v + \lambda_z)(\lambda_u - \lambda_v)^2(\lambda_u - 2\lambda_v)^2Q_3(\lambda_u, \lambda_v, \lambda_z)}{2\lambda_z^2\lambda_v^4(2\lambda_v + \lambda_z)^2(3\lambda_v + \lambda_z)}, \quad (4.72)$$

where $Q_3(\lambda_u, \lambda_v, \lambda_z)$ is a degree 3 homogeneous polynomial in $\lambda_u, \lambda_v, \lambda_z$. But $\lambda_u + \lambda_v + \lambda_z = 0$, and these graphs sum up to zero.


 Figure 4.16: Two crosscaps and three hyperplanes at degree 4 $\mathbb{R}P^2$: type II graphs.

 Figure 4.17: Two crosscaps and three hyperplanes at degree 4 $\mathbb{R}P^2$: type II graphs.

However, at degree 3 hyperplane class there is a unique set of type II graphs, presented in figure 4.17, whose total contribution does not vanish. The contributions of these graphs are given by

$$\begin{aligned}
 C_{0,4,3}^{(a)} &= 1 - 3 \frac{\lambda_u \lambda_v}{\lambda_z^2}, & C_{0,4,3}^{(b)} &= \frac{\lambda_u \lambda_v}{\lambda_z^2}, & C_{0,4,3}^{(c)} &= 2 \frac{\lambda_u \lambda_v}{\lambda_z^2}, \\
 C_{0,4,3}^{(d)} &= -1 + 2 \frac{\lambda_u \lambda_v}{\lambda_z^2}, & C_{0,4,3}^{(e)} &= 1 - 2 \frac{\lambda_u \lambda_v}{\lambda_z^2}.
 \end{aligned} \tag{4.73}$$

We see that the sum of the above expressions is equal to 1, which is the Gromov-Witten invariant $n_{3,2}^{0,2}$ of table 4.3. It is straightforward to perform now a similar computation but taking also into account the two $(-1, -1)$ curves that are transversal to the $\mathbb{C}P^2$. The result is that at degree 3 hyperplane class we obtain the following contribution to the free energy from 2 crosscap configurations

$$\mathcal{F}_3^{0,2} = Q^2 - q_1 Q^2 - q_2 Q^2 + q_1 q_2 Q^2. \tag{4.74}$$

This is in agreement with the Chern-Simons theory result presented in appendix B.2.

4.5 Topological Vertex Computation

Using large N duality, it was recently proposed [17] that the free energy of closed topological strings on a toric manifold can be computed using a cubic field theory, namely a topological vertex and gluing rules. In this section we present a prescription to compute all genus topological string amplitudes on orientifolds with an external “ \mathbb{RP}^2 leg” by using the topological vertex formalism. We will also explicitly show that this prescription is equivalent to the large N dual Chern-Simons computation.

4.5.1 General Prescription

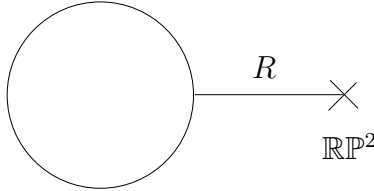


Figure 4.18: Toric diagram for the quotient X/I of a local, toric Calabi-Yau manifold with a single \mathbb{RP}^2 .

Consider a quotient X/I of a local, toric Calabi-Yau manifold X by an involution I which can be represented as in figure 4.18. We have a bulk geometry, represented by the blob, attached to an \mathbb{RP}^2 through an edge associated to the representation R . Let us denote by \mathcal{O}_R the amplitude for the blob with the external leg. We propose the following formula for the total partition function:

$$Z = \sum_{R=R^T} \mathcal{O}_R Q^{\ell(R)/2} (-1)^{\frac{1}{2}(\ell(R) \mp r(R))} \quad (4.75)$$

where the sum is over all self-conjugate representations R . Here $r(R)$ denotes the rank of R , as in (4.27), and $Q = e^{-s}$ is the exponentiated Kähler parameter corresponding to the \mathbb{RP}^2 . The \mp sign is correlated with the choice of \pm sign for the crosscaps, and corresponds to the SO/Sp gauge duals, respectively.

The prescription (4.75) comes from the action of the involution I on the partition function on the covering space, which is given by

$$Z = \sum_R \mathcal{O}_R(t_i) \mathcal{O}_{R^T}(t_i) Q^{\ell(R)} (-1)^{\ell(R)}. \quad (4.76)$$

where the Kähler parameters have been identified in the way prescribed by the involution. The involution I maps one half of the toric diagram onto the other half, reversing the orientation of the middle leg. The resulting partition function is the one given by (5.36).

We are presently investigating in more details the origin of (4.75). Having a clear understanding of this formula will probably allow us to define a similar prescription for involutions with a fixed locus, like the I^+ of [21].

The restriction to self-conjugate representations may appear surprising at first sight. But in the topological vertex formalism, inverting the orientation of one edge sends R to its transpose R^T (and also introduces a factor of $(-1)^{\ell(R)}$). Therefore, since the \mathbb{RP}^2 leg is unoriented, its partition function must sum only over self-conjugate representations, which are the only representations consistent with the involution I .

It is interesting to note that the formula (4.75) is very similar to the formula for quantum dimensions of SO/Sp gauge group in terms of $U(N)$ quantum dimensions (4.27). Both formulas share the constraint $R = R^T$ and the factor of $(-1)^{\frac{1}{2}(\ell(R) \mp r(R))}$. This gives a geometrical argument, from the topological vertex formalism, for the appearance of SO/Sp gauge groups on the Chern-Simons side.

4.5.2 Examples

We now consider two examples of the above prescription. This will lead us to prove an identity between the topological vertex and SO/Sp Chern-Simons expectation values of Hopf links.

4.5.2.1 Orientifold of the Resolved Conifold

The simplest example is the orientifold of the resolved conifold first considered in [20], which we reviewed in section 4.2. In that case, the toric diagram is very simple and has been drawn in the left hand side of figure 4.1. The rule (4.75) gives:

$$F = -\log \left\{ \sum_{R=R^T} C_{..R} Q^{\ell(R)/2} (-1)^{\frac{1}{2}(\ell(R) \mp r(R))} \right\}. \quad (4.77)$$

This should equal the free energy of Chern-Simons on the sphere for the gauge groups SO/Sp (4.9).

Using (A.7), (A.9) and (A.17), we can rewrite (4.77) as

$$\begin{aligned}
F &= -\log \left\{ \sum_{R=R^T} s(Q^{1/2}q^{-\rho})(-1)^{\frac{1}{2}(\ell(R)\pm r(R))} \right\} \\
&= -\log \left\{ \prod_{i=1}^{\infty} (1 \mp Q^{1/2}q^{i-1/2}) \prod_{1 \leq i < j < \infty} (1 - Qq^{i+j-1}) \right\} \\
&= -\log \left\{ \frac{\prod_{i=1}^{\infty} (1 \mp Q^{1/2}q^{i-1/2})^{1/2} \prod_{i,j=1}^{\infty} (1 - Qq^{i+j-1})^{1/2}}{\prod_{i=1}^{\infty} (1 \pm Q^{1/2}q^{i-1/2})^{1/2}} \right\} \quad (4.78)
\end{aligned}$$

Using (A.19) we find that it becomes

$$\begin{aligned}
F &= \frac{1}{2} \sum_{n=1}^{\infty} \frac{Q^n}{n(q^{n/2} - q^{-n/2})^2} \pm \frac{1}{2} \sum_{n=1}^{\infty} \frac{((-1)^n - 1)Q^{n/2}}{n(q^{n/2} - q^{-n/2})} \\
&= \frac{1}{2} \sum_{n=1}^{\infty} \frac{Q^n}{n(q^{n/2} - q^{-n/2})^2} \mp \sum_{n=1, n \text{ odd}}^{\infty} \frac{Q^{n/2}}{n(q^{n/2} - q^{-n/2})} \quad (4.79)
\end{aligned}$$

which is exactly $-\log S_{00}^{\text{SO}(N)/\text{Sp}(N)}$ as given by (4.9).

4.5.2.2 Local \mathbb{CP}^2 Attached to \mathbb{RP}^2

The second example to consider is the local \mathbb{CP}^2 attached to a single \mathbb{RP}^2 , whose toric diagram is drawn in figure 4.6, and which was discussed before from the point of view of geometric transitions. The amplitude for this geometry is given by (4.75) with

$$\mathcal{O}_R = \sum_{R_i} q^{\sum_i \kappa_{R_i}} (-1)^{\sum_i \ell(R_i)} C_{\cdot R_3 R_1^T} C_{\cdot R_2 R_3^T} C_{R_1 R_2^T R} e^{-t \sum_i \ell(R_i)}, \quad (4.80)$$

and t is the Kähler parameter of the local \mathbb{CP}^2 . If we now compare this expression to the one obtained by geometric transition in (4.61), we find that both amplitudes are equal if

$$\frac{1}{S_{00}^{\text{SO}(N)/\text{Sp}(N)}} \sum_{R=R^T} C_{R_1 R_2^T R} Q^{\ell(R)/2} (-1)^{\frac{1}{2}(\ell(R)\mp r(R))} = q^{-\frac{\kappa_{R_2}}{2}} Q^{\frac{1}{2}(\ell(R_1)+\ell(R_2))} \mathcal{W}_{R_1 R_2}^{\text{SO}(N)/\text{Sp}(N)}, \quad (4.81)$$

where we have taken into account that the partition function of the geometry in figure 4.6 also includes a t -independent piece which equals $S_{00}^{\text{SO}(N)/\text{Sp}(N)}$. The r.h.s. of (4.81) involves the Hopf link invariant for the gauge groups SO/Sp , where we put $\lambda = Q^{-1}$. Notice that $Q^{\frac{1}{2}(\ell(R_1)+\ell(R_2))} \mathcal{W}_{R_1 R_2}^{\text{SO}(N)/\text{Sp}(N)}$ is a polynomial in $Q^{\frac{1}{2}}$, while the l.h.s. of (4.81) is *a priori* an infinite series in $Q^{\frac{1}{2}}$.

4.5.3 A Theorem Relating the Topological Vertex and SO/Sp Chern-Simons Invariants

We can now prove the following theorem that relates the topological vertex to SO/Sp Chern-Simons invariants of the Hopf link.

Theorem 4.1. *Let X/I be the quotient of a local, toric Calabi-Yau manifold X by an involution I without fixed points, which can be represented as in figure 4.18. The topological vertex formula for the total partition function given by (4.75) is equivalent to the total partition function obtained by large N SO/Sp geometric transition.*

We saw in section 4.5.2.2 that in the case of the local $\mathbb{C}P^2$ attached to $\mathbb{R}P^2$, the theorem is proved if the identity (4.81) holds. In fact, it is straightforward to show that if (4.81) holds then the topological vertex rule given in the theorem to compute amplitudes on orientifolds agrees with the results of large N SO/Sp transitions for all the geometries of the form depicted in figure 4.18. Therefore, to prove the theorem we only have to prove the following lemma.

Lemma 4.2. *Let $C_{R_2^T R R_1}$ be the topological vertex of [17] defined in (A.6) and (A.7), $\mathcal{W}_{R_1 R_2}^{SO(N)/Sp(N)}$ be the SO/Sp Chern-Simons expectation value of the Hopf link with linking number $+1$ (after setting the Chern-Simons variable λ defined in (4.17) to be $\lambda = Q^{-1}$), and $S_{00}^{SO(N)/Sp(N)}$ be the partition function of SO/Sp Chern-Simons theory on \mathbf{S}^3 . Then the following identity holds:*

$$\frac{1}{S_{00}^{SO(N)/Sp(N)}} \sum_{R=R^T} C_{R_1 R_2^T R} Q^{\ell(R)/2} (-1)^{\frac{1}{2}(\ell(R) \mp r(R))} = q^{-\frac{\kappa R_2}{2}} Q^{\frac{1}{2}(\ell(R_1) + \ell(R_2))} \mathcal{W}_{R_1 R_2}^{SO(N)/Sp(N)}. \quad (4.82)$$

We will only consider here the Sp case for the sake of clarity, but the proof for the SO case is similar.

Let us start by considering (4.82) for $R_1 = \cdot$ being the trivial representation and $R_2 = \mu$ being any representation. We must show that

$$\frac{1}{S_{00}^{Sp(N)}} \sum_{R=R^T} C_{\cdot \mu^T R} Q^{\frac{1}{2}(\ell(R) - \ell(\mu))} q^{\frac{\kappa \mu}{2}} (-1)^{\frac{1}{2}(\ell(R) + r(R))} = \mathcal{W}_{\mu}^{Sp(N)}. \quad (4.83)$$

Using (A.7) and (A.9) the l.h.s can be rewritten as

$$\frac{1}{S_{00}^{Sp(N)}} s_{\mu}(Q^{-1/2} q^{\rho}) \sum_{R=R^T} (-1)^{\frac{1}{2}(\ell(R) - r(R))} s_R(Q^{1/2} q^{-\ell(\mu) - \rho}). \quad (4.84)$$

From (A.17), the first line of (4.78) and the definition of $W_R(q) = s_R(q^\rho)$ in terms of q -numbers (see for instance eq. (7.5) of [17]), we find, after some algebra:

$$Q^{-\ell(\mu)/2} \prod_{1 \leq i < j \leq d(\mu)} \frac{[l_i + l_j - i - j + 1]_{Q^{-1}} [l_i - l_j + j - i]}{[-i - j + 1]_{Q^{-1}} [j - i]} \\ \times \prod_{i=1}^{d(\mu)} \frac{[1 - i]_{Q^{-1}}^{\text{Sp}(N)} [2l_i - 2i + 1]_{Q^{-1}} \prod_{v=1}^{l_i} Q^{1/2} \frac{[l_i - i - v - d(\mu) + 1]_{Q^{-1}}}{[v - i + d(\mu)]}}{[l_i + 1 - i]_{Q^{-1}}^{\text{Sp}(N)} [-2i + 1]_{Q^{-1}}} \quad (4.85)$$

where $d(\mu)$ is the number of rows of μ , and we used the q -numbers defined in (A.4), (4.22) and (4.25). One can see that the two factors of Q cancel out of (4.85), and the remaining expression is exactly the definition of the $Sp(N)$ quantum dimension of μ for $\lambda = Q^{-1}$, as given by (4.23). But $\mathcal{W}_\mu^{\text{Sp}(N)} = \dim_q^{\text{Sp}(N)} \mu(\lambda = Q^{-1})$. Therefore (4.83) is proved.

We are now in position to prove (4.82) in the general case, namely we have to show that

$$\frac{1}{S_{00}^{\text{Sp}(N)}} \sum_{R=R^T} C_{R_1 R_2^T R} Q^{\ell(R)/2} (-1)^{\frac{1}{2}(\ell(R)+r(R))} = q^{-\frac{\kappa_{R_2}}{2}} Q^{\frac{1}{2}(\ell(R_1)+\ell(R_2))} \mathcal{W}_{R_1 R_2}^{\text{Sp}(N)}. \quad (4.86)$$

Let us first rewrite the Hopf link expectation value in terms of quantum dimensions, using (4.34). The r.h.s. becomes:

$$\sum_{\mu, \lambda_1, \lambda_2, \lambda_3} N_{\lambda_1 \lambda_2}^{R_1} N_{\lambda_1 \lambda_3}^{R_2} N_{\lambda_2 \lambda_3}^\mu q^{\frac{1}{2}(\kappa_{R_1} - \kappa_\mu)} Q^{\frac{1}{2}(\ell(\mu))} \mathcal{W}_\mu^{\text{Sp}(N)}, \quad (4.87)$$

where we expressed the Sp tensor product coefficients in terms of Littlewood-Richardson coefficients using (4.37). We can now rewrite the r.h.s. using (4.83) and (A.7) as

$$\frac{1}{S_{00}^{\text{Sp}(N)}} \sum_{R=R^T} Q^{\frac{1}{2}\ell(R)} (-1)^{\frac{1}{2}(\ell(R)+r(R))} s_{R^T}(q^\rho) q^{\frac{1}{2}(\kappa_{R_1} + \kappa_R)} \\ \times \sum_{\mu, \lambda_1, \lambda_2, \lambda_3} N_{\lambda_1 \lambda_2}^{R_1} N_{\lambda_1 \lambda_3}^{R_2} N_{\lambda_2 \lambda_3}^\mu s_{\mu^T}(q^{\ell(R)+\rho}) \quad (4.88)$$

The sum in the second line can be explicitly evaluated by using (A.9), (A.10), the definition of skew Schur functions (A.8) and the fact that $s_{R_1}(x) s_{R_2}(x) = \sum_R N_{R_1 R_2}^R s_R(x)$:

$$\sum_{\mu, \lambda_1, \lambda_2, \lambda_3} N_{\lambda_1 \lambda_2}^{R_1} N_{\lambda_1 \lambda_3}^{R_2} N_{\lambda_2 \lambda_3}^\mu s_{\mu^T}(q^{\ell(R)+\rho}) = \sum_{\lambda_1} s_{R_1^T/\lambda_1^T}(q^{\ell(R)+\rho}) s_{R_2^T/\lambda_1^T}(q^{\ell(R)+\rho}) \quad (4.89)$$

Inserting (4.89) in (4.88) gives (using the fact that $R = R^T$):

$$\frac{1}{S_{00}^{\text{Sp}(N)}} \sum_{R=R^T} Q^{\frac{1}{2}\ell(R)} (-1)^{\frac{1}{2}(\ell(R)+r(R))} \\ \times \left[q^{\frac{1}{2}(\kappa_{R_1} + \kappa_R)} s_{R^T}(q^\rho) \sum_{\lambda_1} s_{R_2^T/\lambda_1}(q^{\ell(R^T)+\rho}) s_{R_1^T/\lambda_1}(q^{\ell(R)+\rho}) \right] \quad (4.90)$$

The term in brackets is exactly the definition of $C_{R_2^T R R_1}$ in terms of Schur functions (see (A.7)). Therefore (4.90) is equal to the l.h.s. of (4.86) and lemma 4.2 is proved.

As we explained lemma 4.2 implies theorem 4.1; thus we have just shown that the topological vertex prescription (4.75) is equivalent to computations using large N SO/Sp transitions. We will use extensively the prescription (4.75) and the identity (4.82) in chapter 5.

Chapter 5

Open Topological Strings on Orientifolds

In this chapter we study open topological strings on orientifolds of toric Calabi-Yau threefolds. In other words, we consider orientifolds of toric Calabi-Yau threefolds with D-branes.

We first explore the BPS content of open topological string amplitudes on orientifolds and formulate their structural properties. We then compute explicitly the amplitudes for various examples in section 5.2: the SO/Sp framed unknot, the SO/Sp framed Hopf link, and an outer brane in \mathbb{CP}^2 attached to \mathbb{RP}^2 . The independent localization computations we provide for all these examples corroborate our methods and proposals. In section 5.3 we apply our results to formulate structural properties of the coloured Kauffman polynomial.

5.1 Open Topological String Amplitudes in Orientifolds

5.1.1 BPS Structure of Topological String Amplitudes

We saw in section 4.1.2 that closed topological string amplitudes have an integrality structure which expresses them in terms of numbers of BPS states. The aim of this section is to formulate the BPS structure of open topological string amplitudes. First, let us briefly review the known results for open strings.

The structure of the open string amplitudes was found in [29, 30] and is much more delicate than in the closed string case – which was explored in section 4.1.2. To define an open string amplitude we have to specify boundary conditions through a set of submanifolds of X , S_1, \dots, S_L . To each of these submanifolds we associate a source V_ℓ , $\ell = 1, \dots, L$, which is a $U(M)$ matrix. The total partition function is given by

$$Z(V_1, \dots, V_L) = \sum_{R_1, \dots, R_L} Z_{(R_1, \dots, R_L)} \prod_{\alpha=1}^L \text{Tr}_{R_\alpha} V_\alpha, \quad (5.1)$$

where R_α denote representations of $U(M)$ and we are considering the limit $M \rightarrow \infty$. The amplitudes $Z_{(R_1, \dots, R_L)}$ can be computed in the noncompact, toric case by using the topological vertex [17]. According to the correspondence proposed in [29], they are given in some cases by invariants of links whose components are coloured by representations R_1, \dots, R_L . The free energy is defined as usual by

$$\mathcal{F}(V_1, \dots, V_L) = -\log Z(V_1, \dots, V_L) \quad (5.2)$$

and is understood as a series in traces of V in different representations. We define the generating function $f_{(R_1, \dots, R_L)}(q, \lambda)$ through the following equation:

$$\mathcal{F}(V) = -\sum_{n=1}^{\infty} \sum_{R_1, \dots, R_L} \frac{1}{n} f_{(R_1, \dots, R_L)}(q^n, e^{-nt}) \prod_{\alpha=1}^L \text{Tr}_{R_\alpha} V_\alpha^n \quad (5.3)$$

The main result of [30] is that $f_{(R_1, \dots, R_L)}(q, e^{-t})$ is given by:

$$f_{(R_1, \dots, R_L)}(q, e^{-t}) = (q^{\frac{1}{2}} - q^{-\frac{1}{2}})^{L-2} \sum_{g \geq 0} \sum_{\beta} \sum_{R'_1, R'_1 \dots, R'_L, R'_L} \prod_{\alpha=1}^L c_{R_\alpha R'_\alpha R''_\alpha} S_{R'_\alpha}(q) \times N_{(R'_1, \dots, R'_L), g, \beta} (q^{\frac{1}{2}} - q^{-\frac{1}{2}})^{2g} e^{-\beta t}. \quad (5.4)$$

In this formula $R_\alpha, R'_\alpha, R''_\alpha$ label representations of the symmetric group S_ℓ , which can be labeled by a Young tableau with a total of ℓ boxes. $c_{R R' R''}$ are the Clebsch-Gordon coefficients of the symmetric group, and the monomials $S_R(q)$ are defined as follows. If R is a hook representation

$$\begin{array}{|c|c|c|c|c|} \hline \square & \square & \square & \square & \square \\ \hline \square & & & & \\ \hline \square & & & & \\ \hline \end{array} \quad (5.5)$$

with ℓ boxes in total, and with $\ell - d$ boxes in the first row, then

$$S_R(q) = (-1)^d q^{-\frac{\ell-1}{2}+d}, \quad (5.6)$$

and it is zero otherwise. Finally, $N_{(R_1, \dots, R_L), g, \beta}$ are *integers* associated to open string amplitudes. They compute the net number of BPS domain walls of charge β and spin

g transforming in the representations R_α of $U(M)$, where we are using the fact that representations of $U(M)$ can also be labeled by Young tableaux. It is also useful to introduce a generating functional for these degeneracies as in [30]:

$$\widehat{f}_{(R_1, \dots, R_L)}(q, e^{-t}) = \sum_{g \geq 0} \sum_{\beta} N_{(R_1, \dots, R_L), g, \beta} (q^{\frac{1}{2}} - q^{-\frac{1}{2}})^{2g+L-2} e^{-\beta \cdot t}. \quad (5.7)$$

We then have the relation:

$$f_{(R_1, \dots, R_L)}(q, e^{-t}) = \sum_{R'_1, \dots, R'_L} \prod_{\alpha=1}^L M_{R_\alpha R'_\alpha}(q) \widehat{f}_{(R_1, \dots, R_L)}(q, e^{-t}), \quad (5.8)$$

where the matrix $M_{RR'}(q)$ is given by

$$M_{RR'}(q) = \sum_{R''} c_{RR'R''} S_{R''}(q) \quad (5.9)$$

and it is symmetric and invertible [30]. The $f_{(R_1, \dots, R_L)}$ introduced in (5.74) can be extracted from $Z_{(R_1, \dots, R_L)}$ through a procedure spelled out in detail in [82, 83, 30]. One has, for example,

$$f_{\square\square} = Z_{\square\square} - Z_{\square} \cdot Z_{\square}, \quad (5.10)$$

where \cdot denotes the trivial representation. As it was emphasized in [82, 83, 30], this structure result has interesting consequences for knot theory, since it implies a series of integrality results for knot and link invariants. We will come back to this issue in section 5.3.

5.1.2 BPS Structure of Topological Strings on Orientifolds

We want to understand now the corresponding BPS structure of open topological string amplitudes on orientifolds without fixed points, like the ones considered in [20, 21]. In chapter 4 the closed case was studied in detail, in the noncompact case, by using large N transitions and the topological vertex. In particular, the BPS structure was formulated in section 4.1.2 Let us now recall some of the results that we found.

Let us denote by X/I the orientifold obtained by an involution on X . The total free energy has in this case the structure

$$\mathcal{F}(X/I, g_s) = \frac{1}{2} \mathcal{F}(X, g_s) + \mathcal{F}(X/I, g_s)_{\text{unor}}, \quad (5.11)$$

where g_s is the string coupling constant. In the r.h.s. of this equation, the first summand is the contribution of the untwisted sector, and it involves the free energy

$\mathcal{F}(X, g_s)$ of the covering X of X/I , after suitably identifying the Kähler classes in the way prescribed by the involution I . This piece of the free energy has the expansion given by (4.5). The second summand, that we call the unoriented part $\mathcal{F}(X/I, g_s)_{\text{unor}}$, is the contribution of the twisted sector, and involves the counting of holomorphic maps from closed non-orientable Riemann surfaces to the orientifold X/I . The Euler characteristic of a closed Riemann surface of genus g and c crosscaps is $\chi = -2g + 2 - c$ where c is the number of crosscaps. We then have

$$\mathcal{F}(X/I, g_s)_{\text{unor}} = \mathcal{F}(X/I, g_s)_{\text{unor}}^{c=1} + \mathcal{F}(X/I, g_s)_{\text{unor}}^{c=2}, \quad (5.12)$$

which corresponds to the contributions of one and two crosscaps. Following the arguments in [28] we predict the following structure

$$\begin{aligned} \mathcal{F}(X/I, g_s)_{\text{unor}}^{c=1} &= \pm \sum_{d \text{ odd}} \sum_{g=0}^{\infty} \sum_{\beta} n_{\beta}^{g,c=1} \frac{1}{d} (q^{\frac{d}{2}} - q^{-\frac{d}{2}})^{2g-1} e^{-d\beta \cdot t}, \\ \mathcal{F}(X/I, g_s)_{\text{unor}}^{c=2} &= \sum_{d \text{ odd}} \sum_{g=0}^{\infty} \sum_{\beta} n_{\beta}^{g,c=2} \frac{1}{d} (q^{\frac{d}{2}} - q^{-\frac{d}{2}})^{2g} e^{-d\beta \cdot t}, \end{aligned} \quad (5.13)$$

where $n_{\beta}^{g,c}$ are integers. The \pm sign in the $c = 1$ free energy is due to the two different choices for the sign of the crosscaps, and the restriction to d odd comes, in the case of $c = 1$, from the geometric absence of even multicoverings. In the $c = 2$ case this was concluded from examination of different examples. The structure results in (5.11), (5.12) and (5.13) were tested in chapter 4 through detailed computations in noncompact geometries.

We now address the generalization to open string amplitudes in orientifolds. We first consider for simplicity the case of a single boundary condition in the orientifold X/I associated to a topological D-brane wrapping a submanifold S . As in the closed string case, the total open string amplitude will have a contribution from untwisted sectors, and a contribution from twisted sectors. We will then write

$$\mathcal{F}(V) = \frac{1}{2} \mathcal{F}_{\text{or}}(V) + \mathcal{F}_{\text{unor}}(V), \quad (5.14)$$

The contribution from the untwisted sector, $\mathcal{F}_{\text{or}}(V)$, involves the covering geometry, which will be given by X , the submanifold S , and its image under the involution $I(S)$. In other words, the covering amplitude will involve now *two* different sets of D-branes, in general. The covering geometry with two sets of branes has the total partition function

$$Z_{\text{cov}}(V_1, V_2) = \sum_{R_1, R_2} \mathcal{C}_{R_1 R_2} \text{Tr}_{R_1} V_1 \text{Tr}_{R_2} V_2, \quad (5.15)$$

where V_1, V_2 are the sources corresponding to S and $I(S)$ and represent open string moduli. Since the two D-branes in S and $I(S)$ are related by an involution, the two-brane amplitude in (5.15) is symmetric under their exchange, *i.e.* we have

$$\mathcal{C}_{R_1 R_2} = \mathcal{C}_{R_2 R_1}. \quad (5.16)$$

In order to obtain $\mathcal{F}_{\text{or}}(V)$ we have to make the identification of *both* closed and open string moduli under the involution I . This means identifying the Kähler parameters that appear in $\mathcal{C}_{R_1 R_2}$ (the closed background) but also setting $V_1 = V_2 = V$ (the open background). We then find

$$Z_{\text{or}}(V) = \sum_R Z_R^{\text{or}} \text{Tr}_R V \quad (5.17)$$

where

$$Z_R^{\text{or}} = \sum_{R_1, R_2} N_{R_1 R_2}^R \mathcal{C}_{R_1 R_2} = \sum_{R'} \mathcal{C}_{R/R'}. \quad (5.18)$$

Here we have used that

$$\text{Tr}_{R_1} V \text{Tr}_{R_2} V = \sum_R N_{R_1 R_2}^R \text{Tr}_R V \quad (5.19)$$

and $N_{R_1 R_2}^R$ are tensor product coefficients. In (5.18) we also used these coefficients to define skew coefficients with labels R/R' , as in (A.8). If we denote $\mathcal{C}_R \equiv \mathcal{C}_{R\cdot}$, we have for example

$$Z_{\square}^{\text{or}} = 2\mathcal{C}_{\square}, \quad Z_{\square\square}^{\text{or}} = 2\mathcal{C}_{\square\square} + \mathcal{C}_{\square\square}, \quad Z_{\square\Box}^{\text{or}} = 2\mathcal{C}_{\square\Box} + \mathcal{C}_{\square\square}. \quad (5.20)$$

It turns out that the quantities Z_R^{or} defined in this way have the integrality properties of a one-brane amplitude, as it should. One finds, for example,

$$\widehat{f}_{\square}^{\text{or}} = 2\widehat{f}_{\square}^{\text{cov}}, \quad \widehat{f}_{\square\square}^{\text{or}} = 2\widehat{f}_{\square\square}^{\text{cov}} - \frac{1}{q^{\frac{1}{2}} - q^{-\frac{1}{2}}} \widehat{f}_{\square\square}^{\text{cov}}, \quad \widehat{f}_{\square\Box}^{\text{or}} = 2\widehat{f}_{\square\Box}^{\text{cov}} - \frac{1}{q^{\frac{1}{2}} - q^{-\frac{1}{2}}} \widehat{f}_{\square\square}^{\text{cov}}. \quad (5.21)$$

In these equations, the superscript “cov” refers to quantities computed from the two-brane amplitude $\mathcal{C}_{R_1 R_2}$ according to the general rules for open string amplitudes in the usual, oriented case explained above. One can easily verify from the integrality properties of $\widehat{f}_{R_1 R_2}$ as a 2-brane amplitude that indeed $\widehat{f}_R^{\text{or}}$ has the integrality properties of a one-brane amplitude. In fact, using the identity

$$\sum_{R', R'_1, R'_2} M_{RR'}^{-1} N_{R'_1 R'_2}^{R'} M_{R'_1 R_1} M_{R'_2 R_2} = \frac{1}{q^{-\frac{1}{2}} - q^{\frac{1}{2}}} N_{R_1 R_2}^R \quad (5.22)$$

we can write

$$\widehat{f}_R^{\text{or}} = \sum_{R_1 R_2} N_{R_1 R_2}^R \widehat{f}_{R_1 R_2}^{\text{cov}}, \quad (5.23)$$

where we put $\widehat{f}_R \equiv (q^{-\frac{1}{2}} - q^{\frac{1}{2}}) \widehat{f}_R$.

We would like to determine now the structural properties of $\mathcal{F}_{\text{unor}}(V)$. This is indeed very easy. The analysis of [30] to determine the structural properties of $F(V)$ in the usual oriented case was based on an analysis of the Hilbert space associated to an oriented Riemann surface $\Sigma_{g,\ell}$ with ℓ holes ending on S and in the relative homology class $\beta \in H_2(X, S)$. The relevant Hilbert space turns out to be

$$\text{Sym}(F^{\otimes \ell} \otimes H^*(J_{g,\ell}) \otimes H^*(\mathcal{M}_{g,\ell,\beta})) \quad (5.24)$$

where $J_{g,\ell} = \mathbf{T}^{2g+\ell-1}$ is the Jacobian of $\Sigma_{g,\ell}$, F is a copy of the fundamental representation of the gauge group, $\mathcal{M}_{g,\ell,\beta}$ is the moduli space of geometric deformations of the Riemann surface inside the Calabi–Yau manifold, and Sym means that we take the completely symmetric piece with respect to permutations of the ℓ holes. Since the bulk of the Riemann surface is not relevant for the action of the permutation group, we can factor out the cohomology of the Jacobian \mathbf{T}^{2g} . The projection onto the symmetric piece can easily be done using the Clebsch-Gordon coefficients $c_{R R' R''}$ of the permutation group S_ℓ [76], and one finds

$$\sum_{R R' R''} c_{R R' R''} \mathbf{S}_R(F^{\otimes \ell}) \otimes \mathbf{S}_{R'}(H^*((\mathbf{S}^1)^{\ell-1})) \otimes \mathbf{S}_{R''}(H^*(\mathcal{M}_{g,\ell,\beta})) \quad (5.25)$$

where \mathbf{S}_R is the Schur functor that projects onto the corresponding subspace. The space $\mathbf{S}_R(F^{\otimes \ell})$ is nothing but the vector space underlying the irreducible representation R of $U(M)$. $\mathbf{S}_{R'}(H^*((\mathbf{S}^1)^{\ell-1}))$ gives the hook Young tableau, and the Euler characteristic of $\mathbf{S}_{R''}(H^*(\mathcal{M}_{g,\ell,\beta}))$ is the integer invariant $N_{R'',g,\beta}$. Therefore, the above decomposition corresponds very precisely to (5.4) (here we are considering for simplicity the one-brane case).

In the case of an *unoriented* Riemann surface, the above argument goes through, with the only difference that now the Jacobian is $J_{g,c,\ell} = \mathbf{T}^{2g-1+\ell+c}$, where $c = 1, 2$ denotes the number of crosscaps. Therefore, the analysis of the cohomology associated to the boundary is the same. We then conclude that

$$\mathcal{F}_{\text{unor}}(V) = - \sum_R \sum_{d \text{ odd}} \frac{1}{d} f_R^{\text{unor}}(q^d, e^{-dt}) \text{Tr}_R V^d, \quad (5.26)$$

and using again (5.8) one can obtain new functions

$$\widehat{f}_R^{\text{unor}} = \sum_{R'} M_{RR'}^{-1} f_{R'}^{\text{unor}} \quad (5.27)$$

with contributions from one and two crosscaps:

$$\widehat{f}_R^{\text{unor}} = \widehat{f}_R^{c=1} + (q^{\frac{1}{2}} - q^{-\frac{1}{2}})\widehat{f}_R^{c=2}, \quad (5.28)$$

and we finally have

$$\widehat{f}_R^c(q, e^{-t}) = \sum_{g, \beta} N_{R, g, \beta}^c (q^{\frac{1}{2}} - q^{-\frac{1}{2}})^{2g} e^{-\beta t}. \quad (5.29)$$

Each crosscap contributes then an extra factor of $q^{\frac{1}{2}} - q^{-\frac{1}{2}}$, as in the closed case.

In real life, what one computes is the total amplitude in the l.h.s. of (5.14), in terms of

$$\mathcal{F}(V) = -\log Z(V) = -\log\left(\sum_R Z_R \text{Tr}_R V\right), \quad (5.30)$$

and one wants to find the unoriented contribution to the amplitude after subtracting the oriented contribution. The above formulae give a precise prescription to compute f_R^{unor} . The results one finds, up to three boxes, are the following:

$$\begin{aligned} f_{\square}^{\text{unor}} &= Z_{\square} - \mathcal{C}_{\square}, \\ f_{\square\square}^{\text{unor}} &= Z_{\square\square} - \frac{1}{2}Z_{\square}^2 - \mathcal{C}_{\square\square} + \frac{1}{2}\mathcal{C}_{\square}^2 - \frac{1}{2}f_{\square\square}^{\text{cov}}, \\ f_{\square\square\square}^{\text{unor}} &= Z_{\square\square\square} - \frac{1}{2}Z_{\square}^3 - \mathcal{C}_{\square\square\square} + \frac{1}{2}\mathcal{C}_{\square}^3 - \frac{1}{2}f_{\square\square\square}^{\text{cov}}, \end{aligned} \quad (5.31)$$

and

$$\begin{aligned} f_{\square\square\square}^{\text{unor}} &= Z_{\square\square\square} - Z_{\square\square}Z_{\square} + \frac{1}{3}Z_{\square}^3 - \mathcal{C}_{\square\square\square} + \mathcal{C}_{\square\square}\mathcal{C}_{\square} - \frac{1}{3}\mathcal{C}_{\square}^3 \\ &\quad - \frac{1}{3}f_{\square\square\square}^{\text{unor}}(q^3, Q^3) - f_{\square\square\square}^{\text{cov}}, \\ f_{\square\square\square\square}^{\text{unor}} &= Z_{\square\square\square\square} - Z_{\square\square\square}Z_{\square} - Z_{\square\square}Z_{\square}^2 + \frac{2}{3}Z_{\square}^4 - \mathcal{C}_{\square\square\square\square} + \mathcal{C}_{\square\square}\mathcal{C}_{\square}^2 + \mathcal{C}_{\square\square}\mathcal{C}_{\square} + \frac{2}{3}\mathcal{C}_{\square}^4 \\ &\quad + \frac{1}{3}f_{\square\square\square\square}^{\text{unor}}(q^3, Q^3) - \frac{1}{2}(f_{\square\square\square\square}^{\text{cov}} + f_{\square\square\square\square}^{\text{cov}}), \\ f_{\square\square\square\square\square}^{\text{unor}} &= Z_{\square\square\square\square\square} - Z_{\square\square\square\square}Z_{\square} + \frac{1}{3}Z_{\square}^5 - \mathcal{C}_{\square\square\square\square\square} - \mathcal{C}_{\square\square\square}\mathcal{C}_{\square} + \frac{1}{3}\mathcal{C}_{\square}^5 \\ &\quad - \frac{1}{3}f_{\square\square\square\square\square}^{\text{unor}}(q^3, Q^3) - f_{\square\square\square\square\square}^{\text{cov}}. \end{aligned} \quad (5.32)$$

The above considerations are easily extended to the case in which we have L sets of D-branes in the orientifold geometry. The covering amplitude involves now $2L$ D-branes, and reads

$$Z_{\text{cov}} = \sum_{R_1, S_1, \dots, R_L, S_L} \mathcal{C}_{R_1 S_1 \dots R_L S_L} \text{Tr}_{R_1} V_1 \text{Tr}_{S_1} W_1 \cdots \text{Tr}_{R_L} V_L \text{Tr}_{S_L} W_L. \quad (5.33)$$

The oriented amplitude is obtained by identifying the moduli in pairs under I , and is given by

$$Z_{Q_1 \dots Q_L}^{\text{or}} = \sum_{R_i, S_i} N_{R_1 S_1}^{Q_1} \cdots N_{R_L S_L}^{Q_L} \mathcal{C}_{R_1 S_1 \dots R_L S_L}. \quad (5.34)$$

The equations (5.14), (5.26) and (5.29) generalize in an obvious way, but now we have

$$\widehat{f}_{(R_1 \dots R_L)}^c(q, e^{-t}) = \sum_{g, \beta} N_{(R_1, \dots, R_L), g, \beta}^c (q^{\frac{1}{2}} - q^{-\frac{1}{2}})^{2g+L-1} e^{-\beta t}, \quad (5.35)$$

where the extra $L - 1$ factors of $q^{\frac{1}{2}} - q^{-\frac{1}{2}}$ have the same origin as in (5.7).

5.2 Examples of Open String Amplitudes

In this section we study in detail some examples and verify the above formulae for the unoriented part of the free energy. In order to do that, we have to compute the total amplitudes Z_R in orientifold geometries. These amplitudes can be obtained in three ways: by using the unoriented localization methods developed in section 4.4 and in [26], by using mirror symmetry [21], and by using Chern-Simons theory and the topological vertex. For the examples of open string amplitudes studied in this section we will use the topological vertex of [17], which can be adapted to the orientifold case as was proposed in section 4.5, and also localization. We first summarize very briefly the results of section 4.5 on the topological vertex on orientifolds, and then we study in detail three examples. Finally we check some of the topological vertex results with unoriented localization.

5.2.1 The topological vertex on orientifolds

Let us consider a quotient X/I of a local, toric Calabi-Yau manifold X by an involution I without fixed points, as was represented in figure 4.18. Theorem 4.1 tells us that the following topological vertex formula for the total partition function is equivalent to the large N Chern-Simons result:

$$Z = \sum_{S=S^T} \mathcal{O}_S Q^{\ell(S)/2} (-1)^{\frac{1}{2}(\ell(S) \mp r(S))} \quad (5.36)$$

where the sum is over all self-conjugate representations S . In section 4.5 the above prescription was used to compute closed string amplitudes. Moreover, to prove Theorem 4.1, we proved the following identity, which was stated in Lemma 4.2:

$$\frac{1}{S_{00}^{SO(N)/Sp(N)}} \sum_{R=R^T} C_{R_1 R_2^T R} Q^{\ell(R)/2} (-1)^{\frac{1}{2}(\ell(R) \mp r(R))} = q^{-\frac{\kappa_{R_2}}{2}} Q^{\frac{1}{2}(\ell(R_1) + \ell(R_2))} \mathcal{W}_{R_1 R_2}^{SO(N)/Sp(N)}, \quad (5.37)$$

where $C_{R_2^T R R_1}$ is the topological vertex of [17] defined in (A.6) and (A.7), $\mathcal{W}_{R_1 R_2}^{SO(N)/Sp(N)}$ is the SO/Sp Chern-Simons expectation value of the Hopf link with linking number +1 (after setting the Chern-Simons variable λ defined in (4.17) to be $\lambda = Q^{-1}$), and $S_{00}^{SO(N)/Sp(N)}$ is the partition function of SO/Sp Chern-Simons theory on \mathbf{S}^3 . In the examples that follow we will use (5.36) to compute open string amplitudes on orientifolds, making use as well of the identity (5.37).

5.2.2 The SO/Sp framed unknot

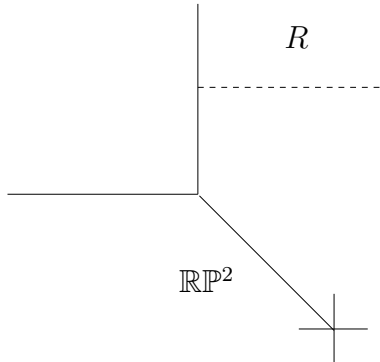


Figure 5.1: A D-brane in an outer leg of the orientifold of the resolved conifold.

We start again with the simplest non-trivial Calabi-Yau orientifold, namely the orientifold of the resolved conifold. This geometry was studied in section 4.2.

Let us now put a D-brane in an *outer* leg of the orientifold geometry. In the oriented case, the open string amplitude labelled by R is computed by the Chern-Simons invariant of the framed unknot with gauge group $U(N)$ (see for example [18, 69]). We want to study now the unoriented case. In order to extract the unoriented string amplitudes, we have to compute both the total amplitudes Z_R and the covering amplitudes $\mathcal{C}_{R_1 R_2}$. Let us start analyzing the covering amplitude.

The covering geometry involves both the original D-brane and its image under the involution I , and a simple analysis shows that we have to consider *two* D-branes in

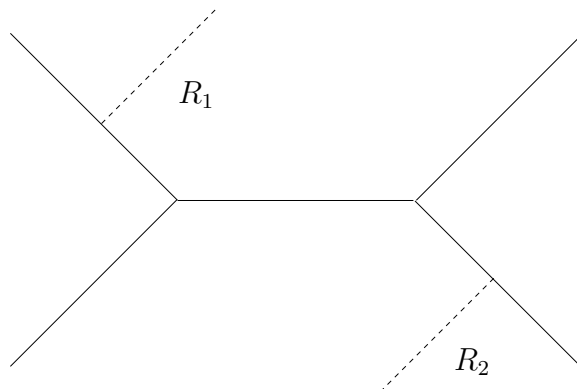


Figure 5.2: The covering configuration contains two D-branes.

opposite legs as depicted in figure 5.2. The amplitude for this two-brane configuration can be computed by using the topological vertex of [17] (see appendix A.2 for a list of useful formulae and properties of the vertex). A simple application of the rules in [17] gives

$$\mathcal{C}_{R_1 R_2} = \frac{1}{Z_{\mathbb{P}^1}} \sum_R C_{R_1 R} C_{R^T \cdot R_2} (-Q)^{\ell(R)} = \frac{1}{Z_{\mathbb{P}^1}} \sum_R W_{R_1 R^T} W_{R R_2} (-Q)^{\ell(R)} \quad (5.38)$$

where $Q = e^{-t}$, $Z_{\mathbb{P}^1}$ is the partition function of the resolved conifold

$$Z_{\mathbb{P}^1} = \prod_{k=1}^{\infty} (1 - Qq^k)^k, \quad (5.39)$$

and the quantities $W_{R_1 R_2}$ are defined in (A.5). The above quotient of series can be computed in a closed way by using the techniques of [78, 84], and in fact one obtains two equivalent expressions. The first expression is

$$\mathcal{C}_{R_1 R_2} = W_{R_1} W_{R_2} \prod_k (1 - q^k Q)^{C_k(R_1, R_2)} \quad (5.40)$$

where the coefficients $C_k(R_1, R_2)$ are given by (A.14) or (A.15). Notice that (5.40) is a Laurent polynomial in $q^{\pm\frac{1}{2}}$ and a *polynomial* in Q . There is, however, a second expression for $\mathcal{C}_{R_1 R_2}$ which involves skew quantum dimensions as defined in (4.28). The derivation uses the representation of the vertex in terms of skew Schur functions given in (A.7). Define first, as in (4.20):

$$\mathcal{W}_R = (\dim_q^{U(N)} R)(\lambda = Q^{-1}), \quad (5.41)$$

where λ is again the Chern-Simons variable (4.17), and the quantum dimension is defined in (A.3) (an explicit formula was given in (4.21)). Then we have, after using

(A.11),

$$\mathcal{C}_{R_1 R_2} = q^{\frac{\kappa_{R_1} + \kappa_{R_2}}{2}} Q^{\frac{\ell(R_1) + \ell(R_2)}{2}} \sum_R (-1)^{\ell(R)} \mathcal{W}_{R_1^T/R} \mathcal{W}_{R_2^T/R^T}. \quad (5.42)$$

We now compute the total amplitude for the configuration depicted in figure 5.1. To do this we can use (5.36), where \mathcal{O}_S is now an open string amplitude given by C_{RS} . One finds

$$\begin{aligned} Z_R &= \frac{1}{Z_{X/I}} \sum_{R'=R^T} C_{RR'} Q^{\ell(R')/2} (-1)^{\frac{1}{2}(\ell(R') \mp r(R'))} \\ &= q^{\frac{\kappa_R}{2}} \mathcal{W}_{R^T}^{SO/Sp}, \end{aligned} \quad (5.43)$$

where we have used the formula (5.37) to express the amplitude in terms of SO/Sp quantum dimensions. We then see that the *total* brane amplitude in figure 5.1 is given by the Chern-Simons invariant of an unknot for gauge groups SO/Sp . To obtain the unoriented piece of this amplitude, we have to subtract the covering contribution, which involves a nontrivial combination of quantum dimensions for $U(N)$. For a *framed* D-brane one should simply change

$$\begin{aligned} Z_R &\rightarrow (-1)^{\ell(R)p} q^{\frac{p\kappa_R}{2}} Z_R, \\ \mathcal{C}_{R_1 R_2} &\rightarrow (-1)^{(\ell(R_1) + \ell(R_2))p} q^{p \frac{\kappa_{R_1} + \kappa_{R_2}}{2}} \mathcal{C}_{R_1 R_2}, \end{aligned} \quad (5.44)$$

since in the covering configuration one has to put the same framing in both legs, by symmetry.

We can now compute f_R^{unor} by using the results of the previous section. We will present explicit results only up to three boxes. The first thing one finds is that $f_R^{c=2}$ vanishes at this order in R . For $f_R^{c=1}$ one finds (we present here the results for $SO(N)$; for $Sp(N)$ one only has to change the overall sign of the $c = 1$ contributions):

$$\begin{aligned} \widehat{f}_{\square}^{c=1} &= (-1)^p Q^{1/2}, \\ \widehat{f}_{\square\square}^{c=1} &= \frac{q^{1-p} (1 - q^p - q^{1+p} + q^{1+2p}) Q^{1/2} (-1 + Q)}{(q-1)^2 (q+1)}, \\ \widehat{f}_{\square\square\square}^{c=1} &= q^{-p} \frac{(1 - q^{1+p} - q^{2+p} + q^{3+2p}) Q^{1/2} (-1 + Q)}{(q-1)^2 (q+1)}, \end{aligned}$$

and

$$\begin{aligned} \widehat{f}_{\square\square\square}^{c=1} &= \frac{(-1)^p q^{2-3p} (-1 + q^p) (-1 + q^{1+p}) Q^{1/2} (-1 + Q)}{(-1 + q)^4 (1 + q)^2 (1 + q^2 + q^4)} \\ &\quad \times [-q + q^{2p} + q^{1+p} (-1 - q + 2q^p - q^{2p}) + q^{2(1+p)} (2 + q - q^p - q^{2p})] \end{aligned}$$

$$\begin{aligned}
& + Q(1 + q^p - q^{2p} + q^{1+p}(1 - 2q^p) + q^{2(1+p)}(-2 - q + q^p) \\
& \quad + q^{3(1+p)}(1 + q^p)), \\
\widehat{f}_{\begin{array}{|c|} \hline \square \\ \hline \end{array}}^{c=1} &= \frac{(-1)^p q^{-3p} (-1 + q^{1+p}) Q^{1/2}}{(-1 + q)^4 (1 + q)^2 (1 + q^2 + q^4)} \\
& \times [q(-1 + q^p)(1 + q^p + q^{1+p}(1 - 2q^p) + q^{2(1+p)}(-2 - 2q) \\
& \quad + q^{3(1+p)}(1 + q) + q^{4(1+p)}) \\
& \quad - Q(1 + q)(-1 + q^{1+p}(-1 + 3q^p) + q^{2(1+p)}(2 + 3q - 3q^p) \\
& \quad + q^{3(1+p)}(-2 - 3q^2) + q^{4(1+p)} + q^{5(1+p)}) \\
& \quad + Q^2(-1 + q^{1+p}(-1 + 2q^p) + q^{2(1+p)}(2 + 3q + q^2 - q^p) \\
& \quad + q^{3(1+p)}(-3 - 2q - 2q^2) + q^{5+4p} + q^{6+5p})], \\
\widehat{f}_{\begin{array}{|c|} \hline \square \\ \hline \end{array}}^{c=1} &= \frac{(-1)^p q^{-1-3p} (1 - q^{1+p} - q^{2+p} + q^{3+2p}) Q^{1/2} (-1 + Q)}{(-1 + q)^4 (1 + q)^2 (1 + q^2 + q^4)} \\
& \times [-q(1 + q^{1+p}(1 + q - q^p) + q^{2(1+p)}(-2 - 2q - q^2) \\
& \quad + q^{3(1+p)}(1 + q) + q^{5+4p}) \\
& \quad + Q(1 + q^{1+p}(1 + q) + q^{2(1+p)}(-1 - 2q - 2q^2 - q^3) \\
& \quad + q^{3(1+p)}(q^2 + q^3) + q^{7+4p})].
\end{aligned}$$

One can indeed check that, for any integer p , the above polynomials are of the form predicted in (5.29) (they are polynomials in $(q^{1/2} - q^{-1/2})^2$ with integer coefficients).

5.2.3 \mathbb{CP}^2 Attached to \mathbb{RP}^2

The next example we consider is the orientifold studied in chapter 4 and in [26], with a D-brane located in an outer leg. In this case, the covering space consists of two \mathbb{CP}^2 's connected by a \mathbb{CP}^1 , with two D-branes in opposite legs (the geometry is shown in figure 5.3). Let us now define the following operator corresponding to the \mathbb{CP}^2 with an outer D-brane:

$$\mathcal{O}_{RS} = \sum_{R_i} q^{\sum_i \kappa_{R_i}} (-1)^{\sum_i \ell(R_i)} C_{SR_3 R_1^T} C_{\cdot R_2 R_3^T} C_{R_1 R_2^T R} e^{-t \sum_i \ell(R_i)} \quad (5.45)$$

where S is the representation attached to the D-brane. Using the topological vertex rules we can write, for arbitrary framing p (Z_{closed} is the amplitude without D-branes):

$$\mathcal{C}_{S_1 S_2} = \frac{1}{Z_{\text{closed}}^{\text{cov}}} \sum_R (-1)^{p(\ell(S_1) + \ell(S_2))} q^{\frac{p}{2}(\kappa_{S_1} + \kappa_{S_2})} \mathcal{O}_{RS_1} \mathcal{O}_{R^T S_2} (-Q)^{\ell(R)} \quad (5.46)$$

and

$$Z_{\text{closed}}^{\text{cov}} = 1 + \sum_R \mathcal{O}_R \cdot \mathcal{O}_{R^T} \cdot (-Q)^{\ell(R)}, \quad (5.47)$$

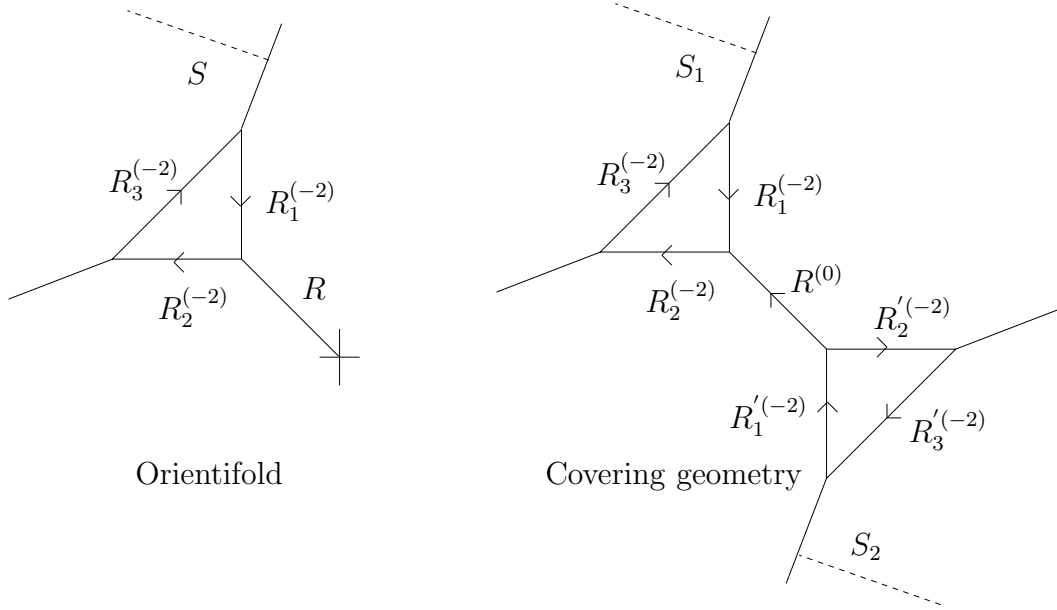


Figure 5.3: A D-brane in an outer leg of the orientifold of the two \mathbb{CP}^2 's connected by a \mathbb{CP}^1 .

where in the last equation we have singled out the term where all the representations are trivial. As we do not have a closed expression for $\mathcal{C}_{S_1 S_2}$ we have to evaluate Z_{or} order by order in Q and e^{-t} .

Let us compute now Z_S by using the topological vertex rules for orientifolds developed in section 4.5. We find that

$$Z_S = \frac{1}{Z_{\text{closed}}} (-1)^{p\ell(S)} q^{\frac{p\kappa_S}{2}} \sum_{R=R^T} \mathcal{O}_{RS} Q^{\ell(R)/2} (-1)^{\frac{1}{2}(\ell(R) \mp r(R))} \quad (5.48)$$

where

$$Z_{\text{closed}} = 1 + \sum_{R=R^T} \mathcal{O}_R Q^{\ell(R)/2} (-1)^{\frac{1}{2}(\ell(R) \mp r(R))}. \quad (5.49)$$

Using the results in the previous section, we can compute the functions $\widehat{f}_S^c(q, Q, e^{-t})$. We find the following results at low order, for arbitrary framing p (again we present

the results for $SO(N)$):

$$\begin{aligned}
\widehat{f}_{\square}^{c=1} &= (-1)^p \left[-Q^{1/2} e^{-t} + 4Q^{1/2} e^{-2t} - (35 + 8z) Q^{1/2} e^{-3t} \right. \\
&\quad + (400 + 344z + 112z^2 + 13z^3) Q^{1/2} e^{-4t} - 2Q^{3/2} e^{-2t} \\
&\quad + (30 + 6z) Q^{3/2} e^{-3t} - (488 + 359z + 104z^2 + 11z^3) Q^{3/2} e^{-4t} \\
&\quad \left. - 3Q^{5/2} e^{-3t} + (132 + 59z + 8z^2) Q^{5/2} e^{-4t} + \dots \right], \\
\widehat{f}_{\square}^{c=2} &= -(-1)^p \left[Q^2 e^{-3t} - (15 + 7z + z^2) Q^2 e^{-4t} + 2Q^4 e^{-4t} + \dots \right], \\
\widehat{f}_{\square\square}^{c=1} &= \frac{q^{-p+1}(-1+q^p)(-q+q^p)}{(q-1)^2(q+1)} Q^{1/2} e^{-t} - \frac{3q^{-p+1}(-1+q^p)^2}{(q-1)^2} Q^{1/2} e^{-2t} + \dots, \\
\widehat{f}_{\square\square}^{c=2} &= \frac{q^{-p+1}(q^p-1)^2}{(q-1)^2} Q^2 e^{-3t} + \dots, \\
\widehat{f}_{\square}^{c=1} &= \frac{q^{-p+1}(q^p-1)(q^{1+p}-1)}{(q-1)^2(q+1)} Q^{1/2} e^{-t} - \frac{3q^{-p}(q^{1+p}-1)^2}{(q-1)^2} Q^{1/2} e^{-2t} + \dots, \\
\widehat{f}_{\square}^{c=2} &= \frac{q^{-p}(q^{1+p}-1)^2}{(q-1)^2} Q^2 e^{-3t} + \dots,
\end{aligned}$$

where $z \equiv (q^{\frac{1}{2}} - q^{-\frac{1}{2}})^2$.

By comparing with (5.29), it is easy to see that the results above have the expected polynomial form with integer coefficients for any p . In contrast to the example above of a D-brane in the orientifold of the conifold, in this example there are nonzero amplitudes with an even number of crosscaps.

5.2.4 SO/Sp Hopf Link Invariant

Our third and final example is the orientifold of the resolved conifold with two adjacent D-branes in the outer legs. The covering geometry now involves four sets of D-branes in the outer legs of the resolved conifold, oppositely identified by the involution. The geometry is shown in figure 5.4.

Using the topological vertex, we find for the covering amplitude (for arbitrary framings p_1 and p_2):

$$\begin{aligned}
\mathcal{C}_{P_1 P_2 P_3 P_4} &= \frac{1}{Z_{\mathbb{P}^1}} \sum_R (-1)^{p_1(\ell(P_1)+\ell(P_3))+p_2(\ell(P_2)+\ell(P_4))} \\
&\quad \times q^{\frac{p_1}{2}(\kappa_{P_1}+\kappa_{P_2})+\frac{p_2}{2}(\kappa_{P_2}+\kappa_{P_4})} (-Q)^{\ell(R)} C_{RT P_1 P_2} C_{RP_3 P_4} \quad (5.50)
\end{aligned}$$

To obtain the oriented amplitude from (5.50) we have to identify the moduli P_1 (P_2) with P_3 (P_4) as explained in (5.34). We can rewrite (5.50) by using the expression of

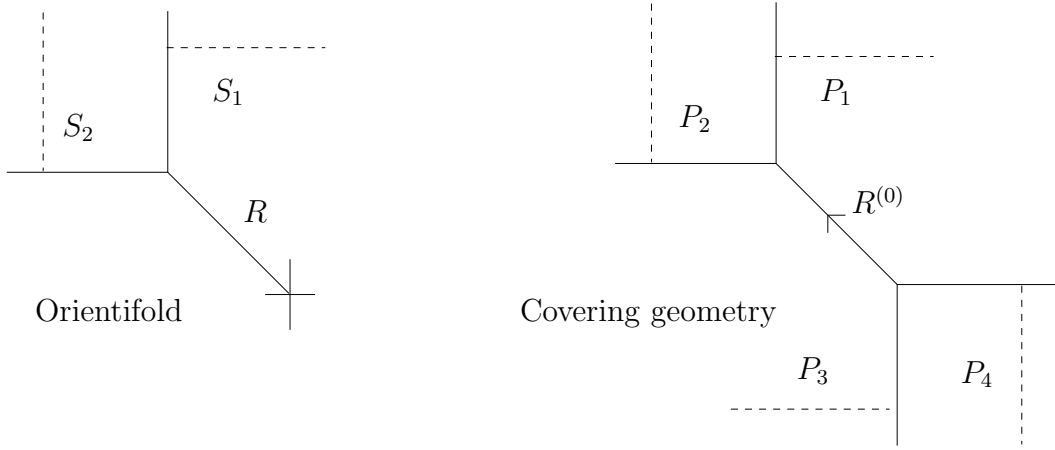


Figure 5.4: Two adjacent D-branes in the outer legs of the orientifold of the resolved conifold.

the topological vertex in terms of Schur functions (A.7):

$$\begin{aligned} \mathcal{C}_{P_1 P_2 P_3 P_4} &= \frac{1}{Z_{\mathbb{P}^1}} q^{\frac{1}{2}(\sum_{i=1}^4 \kappa_{R_i})} s_{R_1^T}(q^\rho) s_{R_3^T}(q^\rho) \sum_{\eta_1, \eta_2} (-Q)^{\ell(\eta_1)} s_{R_2^T/\eta_1}(q^{\ell(R_1)+\rho}) s_{R_4^T/\eta_2}(q^{\ell(R_3)+\rho}) \\ &\quad \times \sum_R s_{R^T/\eta_1}(-Q q^{\ell(R_1^T)+\rho}) s_{R/\eta_2}(q^{\ell(R_3^T)+\rho}). \end{aligned} \quad (5.51)$$

By using the identities (A.10), (A.11) and (A.16) we finally obtain that

$$\begin{aligned} \mathcal{C}_{P_1 P_2 P_3 P_4} &= q^{\frac{1}{2}(\sum_{i=1}^4 \kappa_{R_i})} s_{R_1^T}(q^\rho) s_{R_3^T}(q^\rho) \prod_k (1 - Q q^k)^{C_k(R_1^T, R_3^T)} \\ &\quad \times \sum_\eta (-Q)^{\ell(\eta)} s_{R_2^T/\eta^T}(q^{\ell(R_1)+\rho}, Q q^{-\ell(R_3^T)-\rho}) s_{R_4^T/\eta}(q^{\ell(R_3)+\rho}, Q q^{-\ell(R_1^T)-\rho}), \end{aligned} \quad (5.52)$$

where we defined the functions

$$s_{R/Q}(x, y) = \sum_\eta s_{R/\eta}(x) s_{\eta/Q}(y), \quad (5.53)$$

and the coefficients $C_k(R_1^T, R_3^T)$ are defined in (A.14) or (A.15). Notice that (5.52) is a polynomial in Q .

Now that we have our final expression for the covering amplitude, let us look at the full amplitude. The vertex rules for orientifolds tell us that, for the amplitude where there are two D-branes in the outer legs, one has (for arbitrary framings p_1 and p_2)

$$\begin{aligned} Z_{S_1 S_2} &= \frac{1}{Z_{X/I}} \sum_{R=R^T} (-1)^{p_1 \ell(S_1) + p_2 \ell(S_2)} q^{\frac{1}{2}(p_1 \kappa_{S_1} + p_2 \kappa_{S_2})} C_{S_1 S_2 R} Q^{\ell(R)/2} (-1)^{\frac{1}{2}(\ell(R) \mp r(R))} \\ &= (-1)^{p_1 \ell(S_1) + p_2 \ell(S_2)} q^{\frac{1}{2}(p_1 \kappa_{S_1} + p_2 \kappa_{S_2})} q^{\frac{1}{2} \kappa_{S_2}} Q^{\frac{1}{2}(\ell(S_1) + \ell(S_2))} \mathcal{W}_{S_1 S_2^t}^{SO(N)/Sp(N)}, \end{aligned} \quad (5.54)$$

where we used again (5.37). This time, we see that the *total* amplitude of the two D-brane configuration in the orientifold of the conifold is given by the SO/Sp Chern-Simons invariants of the Hopf link.

By subtracting the oriented piece from the unoriented amplitude, and using the results of the previous section, we can compute the $N_{(S_1, S_2), g, \beta}^c$ integer invariants through the $\widehat{f}_{S_1 S_2}^c$ functions. As noted in (5.7) we now expect a slightly different structure for the $\widehat{f}_{S_1 S_2}^c$ functions than the one given by (5.29), since $L = 2$. Namely, we expect

$$\widehat{f}_{S_1 S_2}^c = \sum_{g, \beta} N_{(S_1, S_2), g, \beta}^c (q^{\frac{1}{2}} - q^{-\frac{1}{2}})^{2g+1} Q^\beta. \quad (5.55)$$

with the $\widehat{f}_{S_1 S_2}^c$ functions defined as in (5.28).

We obtain the following results for $SO(N)$:

$$\begin{aligned} \widehat{f}_{\square\square}^{c=1} &= (-1)^{p_1+p_2} Q^{1/2} (1-Q)(q^{1/2} - q^{-1/2}), \\ \widehat{f}_{\square\square}^{c=1} &= \frac{(-1)^{2p_1+p_2} Q^{1/2} (1-Q) q^{-p_1-1/2}}{q-1} (-q + 2q^{1+p_1} - q^{1+2p_1} \\ &\quad + Q(q^2 + q^{2p_1} - 2q^{1+p_1})), \\ \widehat{f}_{\square\square}^{c=1} &= \frac{(-1)^{2p_1+p_2} Q^{1/2} (1-Q) q^{-p_1-1/2}}{q-1} (-(-1 + q^{1+p_1})^2 + Qq(-1 + q^{p_1})^2). \end{aligned} \quad (5.56)$$

It is straightforward to show that for any fixed framings p_1 and p_2 the \widehat{f} functions (5.56) have the structure predicted by (5.55) with integer invariants $N_{(S_1, S_2), g, \beta}^c$. Up to the order $\ell(S_1) + \ell(S_2) = 3$ the contributions with two crosscaps vanish.

5.2.5 Localization Computations

In the previous subsections we found many open BPS invariants using the topological vertex prescription of section 4.5 and the structure predictions of section 5.1. As far as we are aware these invariants have never been computed before. Therefore it would be nice to have an independent check of our results which does not rely on large N duality.

In section 4.4 and in [26] localization techniques were defined to compute closed unoriented Gromov-Witten invariants of Calabi-Yau orientifolds. In this section we will extend these techniques to the case of *open* unoriented Gromov-Witten invariants, therefore providing an alternative and independent way to compute the invariants of the previous subsections.

In order to compare our results with localization computations we have to extract open Gromov-Witten invariants from the f polynomials. First let us recall the definition of the f functions (5.74):

$$\mathcal{F}^c(V_1, \dots, V_L) = - \sum_{d=1}^{\infty} \sum_{R_1, \dots, R_L} \frac{1}{d} f_{(R_1, \dots, R_L)}^c(q^d, e^{-dt}) \prod_{\alpha=1}^L \text{Tr}_{R_\alpha} V_\alpha^d \quad (5.57)$$

where we added the superscript c for the number of crosscaps. As usual, we can also work in the \vec{k} basis. In this basis the free energy reads (see [83]):

$$\mathcal{F}^c(V_1, \dots, V_L) = - \sum_{\{\vec{k}^\alpha\}} W_{(\vec{k}^{(1)}, \dots, \vec{k}^{(L)})}^{(\text{conn}),c} \prod_{\alpha} \frac{1}{z_{\vec{k}^{(\alpha)}}} \Upsilon_{\vec{k}^{(\alpha)}}(V_\alpha), \quad (5.58)$$

where we defined the connected vevs $W_{(\vec{k}^{(1)}, \dots, \vec{k}^{(L)})}^{(\text{conn}),c}$, and $z_{\vec{k}} = \prod_m k_m! m^{k_m}$. Since $q = e^{ig_s}$, we can expand the r.h.s. of (5.58) in g_s . We find a series with the structure [83]:

$$\begin{aligned} \mathcal{F}^c(V_1, \dots, V_L) &= \sum_{g=0}^{\infty} i^{\sum_{\alpha=1}^L |\vec{k}^{(\alpha)}| + c} F_{g, (\vec{k}^{(1)}, \dots, \vec{k}^{(L)})}^c g_s^{2g-2+c+\sum_{\alpha=1}^L |\vec{k}^{(\alpha)}|} \Upsilon_{\vec{k}^{(\alpha)}}(V_\alpha) \\ &= - \left(\prod_{\alpha} \frac{1}{z_{\vec{k}^{(\alpha)}}} \right) W_{(\vec{k}^{(1)}, \dots, \vec{k}^{(L)})}^{(\text{conn}),c} \Upsilon_{\vec{k}^{(\alpha)}}(V_\alpha), \end{aligned} \quad (5.59)$$

where $F_{g, (\vec{k}^{(1)}, \dots, \vec{k}^{(L)})}^c$ is the generating functional for open Gromov-Witten invariants at genus g , with c crosscaps and fixed boundary conditions given by $(\vec{k}^{(1)}, \dots, \vec{k}^{(L)})$. The factor of $i^{\sum_{\alpha=1}^L |\vec{k}^{(\alpha)}| + c}$ is necessary to compare Chern-Simons (or topological vertex) results with localization computations [69]. Thus, we see that to extract open Gromov-Witten invariants we have to compute the connected vevs $W_{(\vec{k}^{(1)}, \dots, \vec{k}^{(L)})}^{(\text{conn}),c}$ from the f functions. Such a relation has been found in [83]:

$$W_{(\vec{k}^{(1)}, \dots, \vec{k}^{(L)})}^{(\text{conn}),c} = \sum_{d|\vec{k}^{(\alpha)}, d \text{ odd}} d^{\sum_{\alpha} |\vec{k}^{(\alpha)}| - 1} \sum_{\{R_\alpha\}} \prod_{\alpha=1}^L \chi_{R_\alpha}(C(\vec{k}_{1/d}^{(\alpha)})) f_{(R_1, \dots, R_L)}^c(q^d, e^{-dt}), \quad (5.60)$$

where $C(\vec{k})$ is the conjugacy class associated to a vector \vec{k} , which has k_j cycles of length j , and χ_R is the character of the symmetric group S_ℓ . In (5.60) the vector $\vec{k}_{1/d}$ is defined as follows. Fix a vector \vec{k} , and consider all the positive integers d that satisfy the following condition: $d|j$ for every j with $k_j \neq 0$. When this happens, we will say that “ d divides \vec{k} ”, and we will denote this as $d|\vec{k}$. We can then define the vector $\vec{k}_{1/d}$ whose components are $(\vec{k}_{1/d})_i = k_{di}$. In (5.60) the integer d has to divide all the vectors $\vec{k}^{(\alpha)}$, $\alpha = 1, \dots, L$. Note that in (5.60) the sum is only over d odd: this is because in the unoriented case only odd multicovers contribute.

Using (5.59) and (5.60) one can find expressions for the generating functionals of open Gromov-Witten invariants in terms of f functions. Let us define the all genera generating functionals for open Gromov-Witten invariants with c crosscaps and fixed boundary conditions given by $(\vec{k}^{(1)}, \dots, \vec{k}^{(L)})$:

$$F_{(\vec{k}^{(1)}, \dots, \vec{k}^{(L)})}^c = \sum_{g=0}^{\infty} F_{g, (\vec{k}^{(1)}, \dots, \vec{k}^{(L)})}^c g_s^{2g-2+c+\sum_{\alpha=1}^L |\vec{k}^{(\alpha)}|}. \quad (5.61)$$

For configurations with one representation ($L = 1$), one finds

$$\begin{aligned} F_{(1,0,\dots)}^c &= i^{1-c} f_{\square}^c, & F_{(2,0,\dots)}^c &= \frac{i^{-c}}{2} (f_{\square\square}^c + f_{\square}^c), & F_{(0,1,0,\dots)}^c &= \frac{i^{1-c}}{2} (f_{\square\square}^c - f_{\square}^c) \\ F_{(3,0,\dots)}^c &= -\frac{i^{1-c}}{6} (f_{\square\square\square}^c + 2f_{\square\square}^c + f_{\square}^c), & F_{(1,1,0,\dots)}^c &= \frac{i^{-c}}{2} (f_{\square\square}^c - f_{\square}^c) \\ F_{(0,0,1,0,\dots)}^c &= \frac{i^{1-c}}{3} (f_{\square\square\square}^c - f_{\square\square}^c + f_{\square}^c + f_{\square}^c(q^3, e^{-3t})), \end{aligned} \quad (5.62)$$

For configurations with two representations ($L = 2$), one finds

$$\begin{aligned} F_{((1,0,\dots),(1,0,\dots))}^c &= i^{-c} f_{\square\square}^c, & F_{((2,0,\dots),(1,0,\dots))}^c &= -\frac{i^{1-c}}{2} (f_{\square\square\square}^c + f_{\square\square}^c), \\ F_{((0,1,0,\dots),(1,0,\dots))}^c &= \frac{i^{-c}}{2} (f_{\square\square\square}^c - f_{\square\square}^c). \end{aligned} \quad (5.63)$$

Using the above formulae, we can compute the $F_{(\vec{k}^{(1)}, \dots, \vec{k}^{(L)})}^c$ generating functionals and put them in the form of (5.61) by expanding in g_s . This will extract the open Gromov-Witten invariants from our previous results.

5.2.5.1 The SO/Sp Framed Unknot

The topological vertex gives the following results:

$$\begin{aligned} F_{(1,0,0,\dots)}^{c=1} &= (-1)^p Q^{1/2}, \\ F_{(2,0,0,\dots)}^{c=1} &= \frac{1}{2} [(1+p)^2 Q^{1/2} (1-Q)] g_s - \frac{1}{48} [(1+p)^2 (1+4p+2p^2) Q^{1/2} (1-Q)] g_s^3 + \dots, \\ F_{(0,1,0,\dots)}^{c=1} &= [(1+p) Q^{1/2} (1-Q)] - \frac{1}{24} [(3+11p+12p^2+4p^3) Q^{1/2} (1-Q)] g_s^2 + \dots, \\ F_{(3,0,0,\dots)}^{c=1} &= \frac{1}{6} [(-1)^p Q^{1/2} (1+p)^3 (1+3p-6Q(1+p)+Q^2(5+3p))] g_s^2 + \dots, \\ F_{(1,1,0,\dots)}^{c=1} &= [(-1)^p Q^{1/2} (1+p)^2 (1+2p-4Q(1+p)+Q^2(3+2p))] g_s + \dots, \\ F_{(0,0,1,\dots)}^{c=1} &= \frac{1}{6} [(-1)^p Q^{1/2} (3(1+p)(2+3p+Q^2(4+3p)) - 2Q(8+18p+9p^2))] + \dots \end{aligned}$$

In order to compare with the localization computation, we introduce first some notation. We will consider the following real torus action on the resolved conifold X :

$$e^{i\phi} \cdot (z_1, z_2, z_3, z_4) = (e^{i\lambda_1\phi} z_1, e^{i\lambda_2\phi} z_2, e^{i\lambda_3\phi} z_3, e^{i\lambda_4\phi} z_4). \quad (5.64)$$

The weights of the torus action on the local coordinates $z = z_1/z_2$, $u = z_2 z_3$, $v = z_2 z_4$ are given by $\lambda_z = \lambda_1 - \lambda_2$, $\lambda_u = \lambda_2 + \lambda_3$, $\lambda_v = \lambda_2 + \lambda_4$ respectively. Note that from the compatibility of the torus action with the anti-holomorphic involution it follows that $\lambda_u + \lambda_v + \lambda_z = 0$. Now we can present the localization results:

$$\begin{aligned} F_{(1,0,0,\dots)}^{c=1} &= Q^{\frac{1}{2}}, \\ F_{(2,0,0,\dots)}^{c=1} &= \frac{1}{2} \left[\left(\frac{a}{a-1} \right)^2 Q^{\frac{1}{2}} (1-Q) \right] g_s - \frac{1}{48} \left[\frac{a^2(a^2+2a-1)}{(a-1)^4} Q^{\frac{1}{2}} (1-Q) \right] g_s^3 + \dots, \\ F_{(0,1,0,\dots)}^{c=1} &= \left[\frac{a}{a-1} Q^{\frac{1}{2}} (1-Q) \right] - \frac{1}{24} \left[\frac{a(a+1)(3a-1)}{(a-1)^3} Q^{\frac{1}{2}} (1-Q) \right] g_s^2 + \dots, \\ F_{(3,0,0,\dots)}^{c=1} &= -\frac{1}{6} \left[Q^{1/2} \left(\frac{a}{a-1} \right)^3 \left(\frac{a+2}{a-1} - \frac{6a}{a-1} Q + \dots \right) \right] g_s^2 + \dots, \\ F_{(1,1,0,\dots)}^{c=1} &= -\left[Q^{1/2} \left(\frac{a}{a-1} \right)^2 \left(\frac{a+1}{a-1} - \frac{4a}{a-1} Q + \dots \right) \right] g_s + \dots, \\ F_{(0,0,1,\dots)}^{c=1} &= -\frac{1}{6} \left[Q^{1/2} \left(\frac{3a(2a+1)}{(a-1)^2} - \frac{2(8a^2+2a-1)}{(a-1)^2} Q + \dots \right) \right] + \dots \end{aligned}$$

where $a = -\lambda_v/\lambda_z$. After making the substitution $a = 1 + \frac{1}{p}$, we find that the above results coincide with the expressions obtained from the vertex computation up to factors of $\pm(-1)^p$. The sign difference is due to different choice of conventions between the vertex and the localization computations. As an example, we present in figure 5.5 the graphs contributing to the unoriented open Gromov–Witten invariant for genus 1 maps with degree 3 $\mathbb{R}\mathbb{P}^2$ and winding vector $(0, 1, 0, \dots)$, as well as their contributions.

The contributions of these graphs are computed according to the rules explained in [26]. We obtain:

$$\begin{aligned} C_{(0,1,0,\dots)}^{(1,3),(a)} &= \frac{(\lambda_u - 2\lambda_v)(2\lambda_u - \lambda_v)\lambda_v(\lambda_u + 2\lambda_v)(\lambda_u^3 + 6\lambda_u^2\lambda_v + \lambda_u\lambda_v^2 + 2\lambda_v^3)}{48\lambda_u^3\lambda_z^4}, \\ C_{(0,1,0,\dots)}^{(1,3),(b)} &= -\frac{(\lambda_u - 2\lambda_v)\lambda_v^2(\lambda_u + 2\lambda_v)}{48\lambda_u^2\lambda_z^2}, & C_{(0,1,0,\dots)}^{(1,3),(c)} &= \frac{\lambda_v^2(\lambda_u + 2\lambda_v)}{24\lambda_u\lambda_z^2}, \\ C_{(0,1,0,\dots)}^{(1,3),(d)} &= -\frac{\lambda_v^2(2\lambda_u + \lambda_v)(\lambda_u + 2\lambda_v)}{24\lambda_z^4}, & C_{(0,1,0,\dots)}^{(1,3),(e)} &= \frac{\lambda_v^3(\lambda_u + 2\lambda_v)(\lambda_u^3 - 2\lambda_u\lambda_v^2 - 2\lambda_v^3)}{12\lambda_u^3\lambda_z^4}, \\ C_{(0,1,0,\dots)}^{(1,3),(f)} &= -\frac{(\lambda_u + 2\lambda_v)\lambda_v^3(\lambda_u - 2\lambda_v)}{6\lambda_u\lambda_z^4}, & C_{(0,1,0,\dots)}^{(1,3),(g)} &= \frac{(\lambda_u + 2\lambda_v)\lambda_v^3(\lambda_u - 2\lambda_v)}{2\lambda_u\lambda_z^4}. \end{aligned}$$

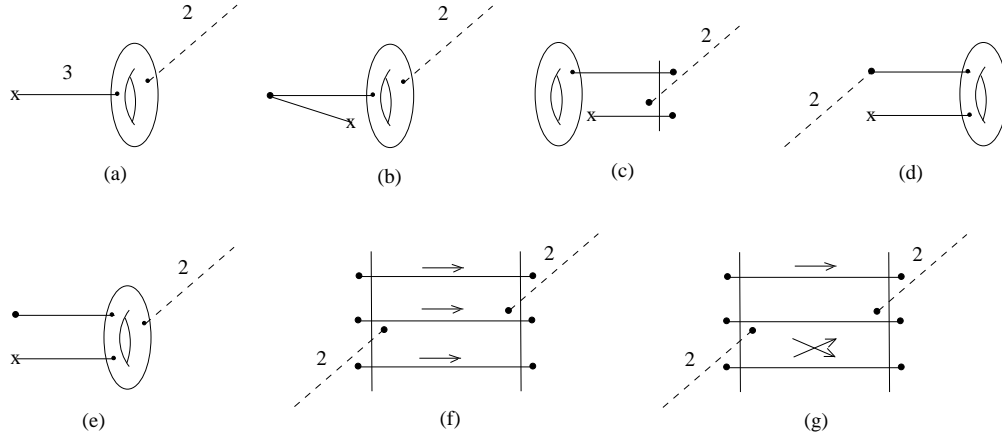


Figure 5.5: One crosscap, genus 1 and three crosscaps, genus 0 at degree 3 \mathbb{RP}^2 , and winding vector $(0, 1, 0, \dots)$.

which sum up to $\frac{1}{24} \frac{a(a+1)(3a-1)}{(a-1)^4}$.

5.2.5.2 \mathbb{CP}^2 Attached to \mathbb{RP}^2

The topological vertex gives the following results:

$$\begin{aligned}
 F_{(1,0,\dots)}^{c=1} &= (-1)^p Q^{1/2} e^{-t} [-1 - 2(-2 + Q)e^{-t} + (-35 + 30Q - 3Q^2)e^{-2t} \\
 &\quad + 4(100 - 122Q + 33Q^2)e^{-3t} + \dots] + \dots, \\
 F_{(1,0,\dots)}^{c=2} &= -(-1)^p Q^2 e^{-3t} [1 + (-15 + 2Q^2)e^{-t} + \dots] g_s + \dots, \\
 F_{(2,0,\dots)}^{c=1} &= \frac{1}{2} Q^{1/2} e^{-t} [-p^2 + (3 + 6p + 6p^2)e^{-t} + \dots] g_s + \dots, \\
 F_{(2,0,\dots)}^{c=2} &= -\frac{1}{2} Q^2 e^{-3t} [1 + 2p + 2p^2 + \dots] g_s^2 + \dots, \\
 F_{(0,1,0,\dots)}^{c=1} &= Q^{1/2} e^{-t} [-p + (3 + 6p)e^{-t} + \dots] + \dots, \\
 F_{(0,1,0,\dots)}^{c=2} &= -Q^2 e^{-3t} [1 + 2p + \dots] g_s + \dots.
 \end{aligned}$$

For the localization computations, we will use the same notation as in section 4.4. We present below some of the localization computations we performed. First, we obtain

$$F_{(2,0,\dots)}^{c=1} = \frac{1}{2} Q^{1/2} e^{-t} \left[- \left(\frac{\lambda_v - \lambda_u}{\lambda_v - 2\lambda_u} \right)^2 + \left(\frac{3(2\lambda_u^2 - 2\lambda_u\lambda_v + \lambda_v^2)}{(2\lambda_u - \lambda_v)^2} \right) e^{-t} + \dots \right] g_s + \dots.$$

We present in figure 5.6 the graphs contributing at degree 2 hyperplane class in

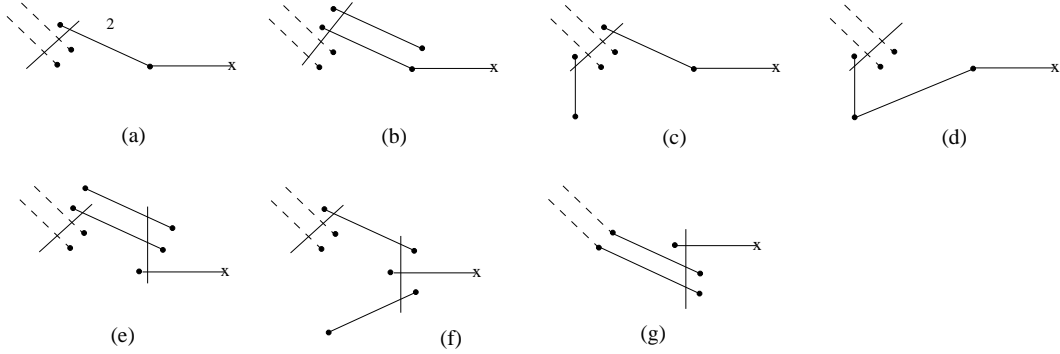


Figure 5.6: One crosscap graphs at degree 1 \mathbb{RP}^2 , degree 2 hyperplane and winding vector $(2, 0, \dots)$.

the expression above. Their contributions are:

$$\begin{aligned}
 C_{(-1,1,2)}^{(2,0,0,\dots),(a)} &= \frac{\lambda_v(\lambda_u - \lambda_v)^2(3\lambda_u - 2\lambda_v)}{\lambda_u^2(\lambda_v - 2\lambda_u)^2}, & C_{(-1,1,2)}^{(2,0,0,\dots),(b)} &= \frac{(\lambda_u - \lambda_v)^4}{\lambda_u^2(\lambda_v - 2\lambda_u)^2}, \\
 C_{(-1,1,2)}^{(2,0,0,\dots),(c)} &= \frac{2\lambda_u^2 - 2\lambda_u\lambda_v + \lambda_v^2}{2(\lambda_v - 2\lambda_u)^2}, & C_{(-1,1,2)}^{(2,0,0,\dots),(d)} &= \frac{\lambda_u^2}{2(\lambda_v - 2\lambda_u)^2}, \\
 C_{(-1,1,2)}^{(2,0,0,\dots),(e)} &= \frac{\lambda_v^2(\lambda_u - \lambda_v)^2}{2\lambda_u^2(\lambda_v - 2\lambda_u)^2}, & C_{(-1,1,2)}^{(2,0,0,\dots),(f)} &= \frac{(\lambda_u - \lambda_v)^2}{2(\lambda_v - 2\lambda_u)^2}, & C_{(-1,1,2)}^{(2,0,0,\dots),(g)} &= \frac{\lambda_v^2}{2\lambda_u^2}.
 \end{aligned}$$

which sum up to $\frac{1}{2} \left(\frac{3(2\lambda_u^2 - 2\lambda_u\lambda_v + \lambda_v^2)}{(2\lambda_u - \lambda_v)^2} \right)$.

In the expressions above, the subscript of the contributions is (χ, d_1, d_2) where χ is the unoriented genus of the closed component of the map and d_1 and d_2 are the \mathbb{RP}^2 and hyperplane degrees respectively. Then, for the same winding vector, at 2 crosscaps we obtain

$$F_{(2,0,\dots)}^{c=2} = -\frac{1}{2}Q^2 e^{-3t} \left[\frac{2\lambda_u^2 - 2\lambda_u\lambda_v + \lambda_v^2}{(\lambda_v - 2\lambda_u)^2} + \dots \right] + \dots$$

The two crosscaps configurations were discussed at length in section 4.4. The graphs come in sets and there is a single set such that the sum of the contributions of the corresponding graphs does not vanish. That set is presented in figure 5.7. The contributions of the graphs are

$$\begin{aligned}
 C_{(0,4,3)}^{(2,0,0,\dots),(a)} &= -\frac{(\lambda_u^2 - \lambda_u\lambda_v + \lambda_v^2)(2\lambda_u^2 - 2\lambda_u\lambda_v + \lambda_v^2)}{2\lambda_z^2(\lambda_v - 2\lambda_u)^2}, \\
 C_{(0,4,3)}^{(2,0,0,\dots),(b)} &= \frac{1}{2}C_{(0,4,3)}^{(2,0,0,\dots),(c)} = -\frac{\lambda_u\lambda_v(2\lambda_u^2 - 2\lambda_u\lambda_v + \lambda_v^2)}{2\lambda_z^2(\lambda_v - 2\lambda_u)^2}, \\
 C_{(0,4,3)}^{(2,0,0,\dots),(d)} &= -C_{(0,4,3)}^{(2,0,0,\dots),(e)} = \frac{(\lambda_u^2 + \lambda_v^2)(2\lambda_u^2 - 2\lambda_u\lambda_v + \lambda_v^2)}{2\lambda_z^2(\lambda_v - 2\lambda_u)^2}.
 \end{aligned}$$

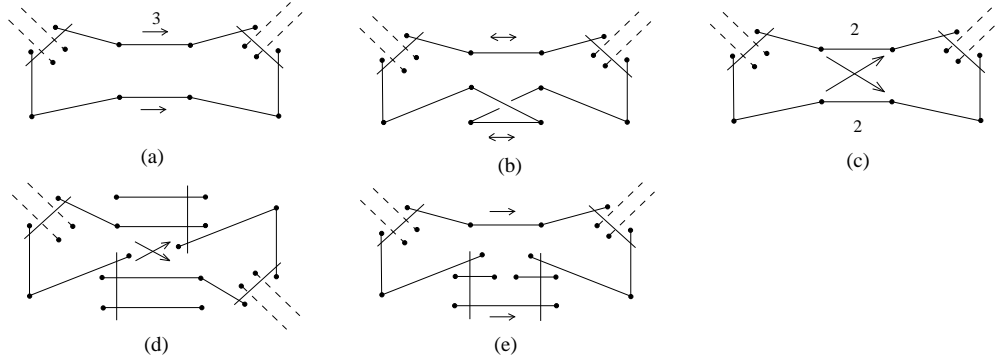


Figure 5.7: Two crosscaps graphs at degree 4 \mathbb{RP}^2 , degree 3 hyperplane and winding vector $(2, 0, \dots)$.

which sum up to $-\frac{1}{2} \left(\frac{2\lambda_u^2 - 2\lambda_u\lambda_v + \lambda_v^2}{(\lambda_v - 2\lambda_u)^2} \right)$.

We also obtain

$$F_{(0,1,0,\dots)}^{c=1} = Q^{1/2} e^{-t} \left[\frac{\lambda_v - \lambda_u}{\lambda_v - 2\lambda_u} - 3 \left(\frac{\lambda_v}{\lambda_v - 2\lambda_u} \right) e^{-t} + \dots \right] + \dots,$$

$$F_{(0,1,0,\dots)}^{c=2} = Q^2 e^{-3t} \left[\left(\frac{\lambda_v}{\lambda_v - 2\lambda_u} \right) + \dots \right] + \dots.$$

We note that for this geometry we obtain agreement with the vertex computation if we set $p = -\frac{\lambda_v - \lambda_u}{\lambda_v - 2\lambda_u}$.

5.2.5.3 SO/Sp Hopf Link Invariant

The results obtained from the topological vertex are:

$$F_{((1,0,\dots),(1,0,\dots))}^{c=1} = (-1)^{p_1+p_2} Q^{1/2} (1-Q) g_s - \frac{1}{24} (-1)^{p_1+p_2} Q^{1/2} (1-Q) g_s^3 + \dots,$$

$$F_{((2,0,\dots),(1,0,\dots))}^{c=1} = \frac{1}{2} (-1)^{p_2} Q^{1/2} [1 + 2p_1 + 2p_1^2 - 2Q(1 + 2p_1^2) + Q^2(1 - 2p_1 + 2p_1^2)] g_s^2 + \dots,$$

$$F_{((0,1,0,\dots),(1,0,\dots))}^{c=1} = (-1)^{p_2} Q^{1/2} [1 + 2p_1 - 4Qp_1 - Q^2(1 - 2p_1)] g_s + \dots.$$

The localization results are:

$$F_{((1,0,\dots),(1,0,\dots))}^{c=1} = Q^{1/2} (1-Q) g_s - \frac{1}{24} Q^{1/2} (1-Q) g_s^3 + \dots,$$

$$F_{((2,0,\dots),(1,0,\dots))}^{c=1} = -\frac{1}{2} Q^{1/2} \left[\frac{\lambda_u^2 + 2\lambda_u\lambda_v + 2\lambda_v^2}{\lambda_u^2} - 2Q \left(\frac{\lambda_u^2 + 2\lambda_v^2}{\lambda_u^2} \right) + Q^2 \left(\frac{\lambda_u^2 - 2\lambda_u\lambda_v + 2\lambda_v^2}{\lambda_u^2} \right) \right] g_s^2 + \dots,$$

$$F_{((0,1,0,\dots),(1,0,\dots))}^{c=1} = Q^{1/2} \left[\frac{\lambda_u + 2\lambda_v}{\lambda_u} - 4Q \left(\frac{\lambda_v}{\lambda_u} \right) - Q^2 \left(\frac{\lambda_u - 2\lambda_v}{\lambda_u} \right) \right] g_s + \dots.$$

To obtain agreement with the vertex result for this D-brane configuration, we need to set $p_1 = \frac{\lambda_v}{\lambda_u}$. These computations offer strong evidence of the equivalence between the vertex computation and the localization on the moduli space of stable open unoriented maps.

5.3 Application: the BPS Structure of the Coloured Kauffman Polynomial

One of the most interesting applications of the above results is the determination of the BPS structure of the coloured Kauffman polynomial. In contrast to the results obtained for orientifolds of toric geometries above, we will not be able to give a full determination of all quantities involved for arbitrary knots, but we can still formulate some interesting structural properties of the knot polynomials similar to those explained in [29, 30, 82, 83]. We will first recall the results for the coloured HOM-FLY polynomial, and then we will state and illustrate the results for the coloured Kauffman polynomial.

5.3.1 Chern-Simons Invariants and Knot Polynomials

Let us consider Chern-Simons theory on \mathbf{S}^3 with gauge group G . The natural operators in this theory were introduced in section 4.3.2. They consist in the holonomies of the gauge connection around a knot \mathcal{K} ,

$$W_R^{\mathcal{K}}(A) = \text{P exp} \oint_{\mathcal{K}} A. \quad (5.65)$$

If we now consider a link \mathcal{L} with components \mathcal{K}_α , $\alpha = 1, \dots, L$, the correlation function

$$W_{R_1 \dots R_L}^G(\mathcal{L}) = \langle W_{R_1}^{\mathcal{K}_1} \dots W_{R_L}^{\mathcal{K}_L} \rangle \quad (5.66)$$

defines a topological invariant of the link \mathcal{L} . In this equation the bracket denotes a normalized vacuum expectation value, and we have indicated the gauge group G as a superscript. It is well known [68] that Chern-Simons produces in fact invariants of *framed* links, but in the following we will consider knots in the so-called standard framing (see [18, 74] for a review of these topics). The correlation functions (5.66) turn out to be rational functions of the variables $q^{\pm 1/2}$, $\lambda^{\pm 1/2}$. The variables q and λ are defined as in section 4.3.1.

The vacuum expectation values of Wilson loops are related to link invariants obtained from quantum groups [68]:

1) If $G = U(N)$ and $R_1 = \dots = R_L = \square$, then

$$W_{\square \dots \square}^{U(N)}(\mathcal{L}) = \lambda^{\text{lk}(\mathcal{L})} \left(\frac{\lambda^{\frac{1}{2}} - \lambda^{-\frac{1}{2}}}{q^{\frac{1}{2}} - q^{-\frac{1}{2}}} \right) P_{\mathcal{L}}(q, \lambda) \quad (5.67)$$

where $P_{\mathcal{L}}(q, \lambda)$ is the HOMFLY polynomial of \mathcal{L} [85], and $\text{lk}(\mathcal{L})$ is its linking number.

2) If $G = SO(N)$ and $R_1 = \dots = R_L = \square$, then

$$W_{\square \dots \square}^{SO(N)}(\mathcal{L}) = \lambda^{\text{lk}(\mathcal{L})} \left(1 + \frac{\lambda^{\frac{1}{2}} - \lambda^{-\frac{1}{2}}}{q^{\frac{1}{2}} - q^{-\frac{1}{2}}} \right) F_{\mathcal{L}}(q, \lambda) \quad (5.68)$$

where $F_{\mathcal{L}}(q, \lambda)$ is the Kauffman polynomial of \mathcal{L} [31].

We will call $W_{R_1 \dots R_L}^{U(N)}(\mathcal{L})$ and $W_{R_1 \dots R_L}^{SO(N)}(\mathcal{L})$ the coloured HOMFLY and Kauffman polynomials of \mathcal{L} , respectively. Note that there is a slight abuse of language here, since these Chern-Simons correlation functions are not polynomials, but rather rational functions.

5.3.2 BPS Structure: Statement and Examples

In [29], Ooguri and Vafa extended the duality of [16] between Chern-Simons theory on \mathbf{S}^3 and topological strings on the resolved conifold by incorporating the correlation functions (5.66). We will consider the case of knots, although everything we will say has a straightforward generalization to links. The results of [29] are the following: first, to any knot $\mathcal{K} \in \mathbf{S}^3$ one can associate a Lagrangian submanifold $S_{\mathcal{K}}$ in the resolved conifold. Moreover, the generating functional of knot invariants

$$Z_{U(N)}(V) = \sum_R W_R^{U(N)}(\mathcal{K}) \text{Tr}_R V \quad (5.69)$$

where V is a $U(M)$ matrix, is the partition function for open topological strings propagating on the resolved conifold and with Dirichlet boundary conditions associated to $S_{\mathcal{K}}$ (after some appropriate analytic continuation). Equivalently, we consider M branes wrapping $S_{\mathcal{K}}$, where M is the rank of V , and compute the partition function of topological string theory in this D-brane background. Since open string amplitudes have the BPS structure explained in (5.3) and (5.4), this leads to structure results for the knot invariants $W_R^{U(N)}(\mathcal{K})$ (which play the rôle of Z_R). This is explained in detail in [30, 82, 83].

The large N duality of [16] can be generalized by considering an orientifold of the two geometries involved in the geometric transition, namely the resolved and the deformed conifold [20], which was described in detail in section 4.2. The string field theory for the resulting open strings is Chern-Simons theory with gauge group $SO(N)$ or $Sp(N)$, depending on the choice of orientifold action on the gauge group. The orientifold action on the resolved conifold is given by (4.12). It then follows from the results of [29] and the orientifold action considered in [20] that the Chern-Simons generating functional

$$Z_{SO/Sp}(V) = \sum_R W_R^{SO/Sp}(\mathcal{K}) \text{Tr}_R V, \quad (5.70)$$

where V is again a $U(M)$ matrix, is the total partition function for open strings propagating on the orientifold of the resolved conifold with M branes wrapping $S_{\mathcal{K}}$. In particular, the logarithm of (5.70) will have the structure explained in (5.14), where the oriented contribution is obtained by considering a covering geometry with both $S_{\mathcal{K}}$ and its image under the involution (4.12), $I(S_{\mathcal{K}})$. We can then translate the structure results presented in section 5.1 into structure results for the coloured Kauffman polynomial.

The main problem in making this translation precise is that, given an arbitrary knot \mathcal{K} , we lack a precise prescription to compute the contribution of the covering amplitude. The covering amplitude $\mathcal{C}_{R_1 R_2}$ is defined as the oriented amplitude in the covering geometry in the presence of two sets of branes wrapping $S_{\mathcal{K}}$ and $I(S_{\mathcal{K}})$, with representations R_1, R_2 , respectively. If one of the representations is trivial, we recover the oriented amplitude in the presence of $S_{\mathcal{K}}$, therefore $\mathcal{C}_R = W_R^{U(N)}(\mathcal{K})$. But in the general case it is not obvious how to determine $\mathcal{C}_{R_1 R_2}$. Although there are proposals for the geometry of the Lagrangian submanifolds $S_{\mathcal{K}}$ [30, 86], a direct Gromov–Witten computation of the corresponding open string amplitudes seems to be very difficult. One possible way of determining $\mathcal{C}_{R_1 R_2}$ would be to translate it into a pure knot-theoretic computation in the context of Chern-Simons theory, but we have not found a completely satisfactory solution to this problem yet.

Although we do not know how to compute the covering amplitude for an arbitrary knot, we can still extract the $\widehat{f}_R^{c=1}$ amplitudes from the knowledge of $W_R^{SO(N)}(\mathcal{K})$. This goes as follows. Let us define the rational functions $g_R(q, \lambda)$ through the following equation

$$\log Z_{SO}(V) = \sum_R \sum_{d \text{ odd}} \frac{1}{d} g_R(q^d, \lambda^d) \text{Tr}_R V^d, \quad (5.71)$$

and define as well

$$\widehat{g}_R(q, \lambda) = \sum_{RR'} M_{RR'}^{-1}(q) g_R(q, \lambda). \quad (5.72)$$

Clearly, since we are not subtracting the covering piece in the l.h.s. of (5.71), we cannot expect much structure for $\widehat{g}_R(q, \lambda)$. However, one has that

$$\widehat{f}_R^{c=1}(q, \lambda) = \frac{1}{2} (\widehat{g}_R(q, \lambda^{\frac{1}{2}}) - (-1)^{\ell(R)} \widehat{g}_R(q, -\lambda^{\frac{1}{2}})). \quad (5.73)$$

This follows from parity considerations. The invariants $W_R^{U(N)}(\mathcal{K})$ have powers of $\lambda^{\frac{1}{2}}$ of the form $\ell(R) + 2k$, while $W_R^{SO(N)}(\mathcal{K})$ have powers of $\lambda^{\frac{1}{2}}$ both of the form $\ell(R) + 2k$ and $\ell(R) + 2k + 1$. The first ones correspond to both oriented and $c = 2$ contributions, while the last ones correspond to $c = 1$ contributions. Also, the covering contribution $\mathcal{C}_{R_1 R_2}$ (being an oriented amplitude) contains only powers in $\lambda^{\frac{1}{2}}$ of the form $\ell(R_1) + \ell(R_2) + 2k$. It is now easy to see from the results in section 5.1.2 that $\widehat{f}_R^{c=1}$ does not involve at all the covering contributions, and can be computed solely from the $SO(N)$ invariants, precisely in the way specified by (5.73). We can then formulate the following conjecture concerning the structure of the coloured Kauffman polynomial:

Conjecture 5.1. *Let $\widehat{g}_R(q, \lambda)$ be defined in terms of the coloured Kauffman polynomial by (5.71) and (5.72). Then, we have that*

$$\frac{1}{2} (\widehat{g}_R(q, \lambda^{\frac{1}{2}}) - (-1)^{\ell(R)} \widehat{g}_R(q, -\lambda^{\frac{1}{2}})) = \sum_{g, \beta} N_{R, g, \beta}^{c=1} (q^{\frac{1}{2}} - q^{-\frac{1}{2}})^{2g} \lambda^\beta, \quad (5.74)$$

where $N_{R, g, \beta}^{c=1}$ are integer numbers. They are BPS invariants corresponding to unoriented open string amplitudes with one crosscap.

In the case of $W_{\square}^{SO(N)}(q, \lambda)$, which is the unnormalized Kauffman polynomial, we can be slightly more precise, since we know that $\mathcal{C}_{\square}(q, \lambda) = W_{\square}^{U(N)}(q, \lambda)$, which is the unnormalized HOMFLY polynomial. We then deduce that

$$W_{\square}^{SO(N)}(q, \lambda) - W_{\square}^{U(N)}(q, \lambda) = \sum_{g, \beta} N_{\square, g, \beta}^{c=1} (q^{\frac{1}{2}} - q^{-\frac{1}{2}})^{2g} \lambda^\beta + \sum_{g, \beta} N_{\square, g, \beta}^{c=2} (q^{\frac{1}{2}} - q^{-\frac{1}{2}})^{2g+1} \lambda^\beta. \quad (5.75)$$

On the other hand, it follows from integrality of the oriented amplitudes that

$$W_{\square}^{U(N)}(q, \lambda) = \sum_{g \geq 0} p_g^H(\lambda) (q^{\frac{1}{2}} - q^{-\frac{1}{2}})^{2g-1}, \quad (5.76)$$

where $p_g^H(\lambda)$ is an odd polynomial in $\lambda^{\pm \frac{1}{2}}$. Thus the following corollary follows from conjecture 5.1:

Corollary 5.2. *In the case where $R = \square$, the structure of the unnormalized Kauffman polynomial is given by*

$$W_{\square}^{SO(N)}(q, \lambda) = \sum_{b \geq 0} p_b^K(\lambda) (q^{\frac{1}{2}} - q^{-\frac{1}{2}})^{b-1}, \quad (5.77)$$

where $p_b^K(\lambda)$ is an odd (even) polynomial in $\lambda^{\pm \frac{1}{2}}$ for b even (odd). Moreover,

$$p_0^K(\lambda) = p_0^H(\lambda). \quad (5.78)$$

This structural prediction turns out to be a well-known result in the theory of the Kauffman polynomial, see for example [87], page 183. One can easily compute $N_{\square, g, \beta}^{c=1,2}$ for various knots by computing the corresponding Kauffman polynomial. For example, the results of [88] imply that

$$N_{\square, g, \beta}^{c=2} = 0 \quad (5.79)$$

for all torus knots.

Let us now turn to checks of conjecture 5.1 for different knots and higher representations. The simplest case is of course the unknot, but this case has been already checked in section 5.2 (indeed, in the case of the unknot we know even how to compute the covering amplitude for arbitrary representations). In order to test the conjecture, we have to compute the invariants $W_R^{SO(N)}(\mathcal{K})$ for arbitrary R . A class of nontrivial knots where this is feasible are torus knots. In the case of $U(N)$ invariants, this was done in [82] by using the formalism of knot operators [89] and the results of [90]. For $SO(N)$, the formalism of knot operators was used in [88] to compute invariants in the fundamental representation, but this has not been generalized to higher representations. For torus knots of the form $(2, m)$, however, one can use the results of [91] to write down a formula for the invariants in any representation of any gauge group. The formula reads as follows:

$$\mathcal{W}_R^G(\mathcal{K}_{(2,m)}) = \sum_{S \in R \otimes R} (\dim_q S) (c_S(R, R))^m \quad (5.80)$$

where

$$c_S(R_1, R_2) = \epsilon_{R_1 R_2}^S q^{\frac{C_{R_1} + C_{R_2}}{2} - \frac{C_S}{4}} \quad (5.81)$$

In this equation, C_R is the quadratic Casimir

$$C_R = \kappa_R + \ell(R)(N + a), \quad (5.82)$$

where a is given in (4.18), and $\epsilon_{R_1 R_2}^S$ is a sign which counts whether S appears symmetrically or antisymmetrically in the tensor product $R_1 \otimes R_2$. In cases where S appears with no multiplicity, there is an explicit expression for this sign given by [92]

$$\epsilon_{R_1 R_2}^S = (-1)^{\rho(\Lambda_1 + \Lambda_2 - \Lambda_S)}, \quad (5.83)$$

where $\Lambda_1, \Lambda_2, \Lambda_S$ are the highest weights of the representations R_1, R_2, S , respectively. Using (5.80) one can easily compute the invariants of the $(2, m)$ torus knots in the $SO(N)$ case, and extract g_R (hence $N_{R, g, \beta}^{c=1}$) for various representations. In all cases we have found agreement with the above conjecture. We now present some results for the BPS invariants for the simplest torus knot, the $(2, 3)$ knot or trefoil knot, for representations up to three boxes. We present the results up to two boxes in tables 5.1–5.3 (in the tables the representations R are denoted by their row lengths $(\mu_1, \dots, \mu_d(\mu))$). The results with three boxes are listed in appendix B.3, namely in tables B.7–B.9. All the invariants that are not shown in the tables are understood to be zero.

	$\beta = 1$	2	3
$g = 0$	3	-3	1
1	1	-1	0

Table 5.1: BPS invariants $N_{(1), g, \beta}^{c=1}$ for the trefoil knot.

	$\beta = 3/2$	5/2	7/2	9/2	11/2
$g = 0$	8	-39	69	-53	15
1	6	-61	146	-126	35
2	1	-37	128	-120	28
3	0	-10	56	-55	9
4	0	-1	12	-12	1
5	0	0	1	-1	0

Table 5.2: BPS invariants $N_{(2), g, \beta}^{c=1}$ for the trefoil knot.

	$\beta = 3/2$	5/2	7/2	9/2	11/2
$g = 0$	16	-69	111	-79	21
1	20	-146	307	-251	70
2	8	-128	366	-330	84
3	1	-56	230	-220	45
4	0	-12	79	-78	11
5	0	-1	14	-14	1
6	0	0	1	-1	0

Table 5.3: BPS invariants $N_{(1,1), g, \beta}^{c=1}$ for the trefoil knot.

Although we have focused in this section on the case of knots, it is straightforward to extend the conjecture above to the case of links, and extract the $c = 1$ piece from the SO Chern-Simons invariants. Framed knots can be also considered by using exactly the same rules that are used for $U(N)$ invariants [69]. In fact, these simple generalizations of our results have recently been worked out explicitly in [93], where many more checks of conjecture 5.1 have also been performed.

Chapter 6

Conclusions and Future Directions

In this thesis we explored various applications of toric geometry to string theory. We focused on two particular fields of research deeply rooted in concepts of toric geometry.

Our first theme relied on the construction of Calabi-Yau threefolds as hypersurfaces in toric variety, using Batyrev’s reflexive polytopes. One of the main applications of such an approach has been to dualities between compactifications of heterotic strings and type II string theory (or F-theory). Among other things, it was conjectured that the enhanced gauge group of the heterotic compactifications can be read off directly from a geometrical object that was called *top*.

In chapter 3 we classified mathematically all these tops. Moreover, we derived a simple prescription to assign an affine Kac-Moody algebra to each top. Some tops lead to twisted affine Kac-Moody algebras. These “twisted tops” may be used to build compactifications with reduced rank, which should be dual to CHL strings.

Although the duality between F-theory (or type II string theory) and heterotic strings has been conjectured quite a while ago, even the exact form of the conjecture is still unclear. Many concurrent proposals exist in the literature, applying to different situations and types of geometries. It is unclear if these proposals are all equivalent, and many subtle but important details have been glossed over. It would be interesting to use our results of chapter 3 to try to formulate rigorously this duality, and consequently shed light on its mathematical properties and physical implications.

Our second application concerned topological strings on orientifolds of toric Calabi-Yau threefolds. We found how to compute closed — in chapter 4 — and open — in

chapter 5 — topological string amplitudes on Calabi-Yau orientifolds, by using geometric transitions involving SO/Sp Chern-Simons theory, the topological vertex formalism and a suitable extension to include orientifolds, and localization techniques. We found the general structure of the twisted and untwisted contributions, determined the BPS structure of the corresponding amplitudes, and checked our results in various examples. This allowed us to extract BPS invariants counting higher genus curves with one and two crosscaps.

We want to remark that, although our main testing ground has been orientifolds of (noncompact) toric Calabi-Yau threefolds, with or without noncompact D-branes, the general results about the structure and integrality properties of the amplitudes should be valid in general.

This work can be extended in various ways. First of all, it would be very interesting to consider Calabi-Yau orientifolds in which the involution has fixed loci, like for example the ones considered in [21]. This would lead to topological strings on orientifolds with fixed planes. In this case, the geometric transition of [20] is no longer useful and one has to find other ways of implementing a Chern-Simons dual description. In the context of the topological vertex formalism, we should find the right prescription to deal with fixed point loci, by using perhaps the group-theoretic results of [72] for SO/Sp .

It would also be very important to clarify some issues that appeared in the orientifolds we studied here. For example, one would like to have a more detailed derivation of the multicovering formulae for amplitudes involving two crosscaps and of the choice of annulus operator we made, as well as a more rigorous justification of the localization techniques we used.

On a different note, one of the motivations behind the study of open topological string amplitudes developed in chapter 5 was to extend the results of [30, 83] on the BPS structure of the coloured HOMFLY polynomial to the coloured Kauffman polynomial of knots and links. Although our general structural results on open string amplitudes on orientifolds give a first principles answer to this problem, as it has been made clear in the analysis of the framed unknot and the Hopf link, we have not been able to determine the covering contribution for arbitrary knots. This is an important open issue that one should resolve in order to obtain a complete picture of the correspondence between enumerative geometry and knot invariants implied by large N dualities.

Furthermore, in this thesis we showed that the predictions obtained from the topological vertex and its extension in the unoriented case agree with unoriented localization computations. However, it would be very interesting to derive a more general and precise correspondence between these two approaches, following the lines of the mathematical treatment of the vertex given in [94, 95], and maybe connect the unoriented Gromov-Witten theory sketched here and in [26] with a moduli problem involving ideal sheaves, generalizing in this way the results of [96, 97].

Finally, various new points of view on topological string theory have recently been found. Among others, a derivation using integrable hierarchies has been proposed [98], and fascinating relations to the quantum foam [77, 99, 100, 101, 102] and to BPS black holes [103, 104, 105] have been discovered. These results also lead to the conjectured existence of a *topological M-theory* [106, 107, 108, 109, 110], in which topological strings on orientifolds may play a rôle [110]. It would be very interesting to investigate how topological strings on orientifolds and our extension of the topological vertex formalism relate to these various approaches.

Appendix A

Useful Formulae

A.1 Subsets of Young Tableaux

To compute the tensor product decomposition of irreducible representations of $SO(N)$ and $Sp(N)$ using Littlewood's technique as explained in (4.35), we had to use four different subsets of Young tableaux: $\{\delta\}$ and $\{\gamma\}$ for $SO(N)$, and $\{\beta\}$ and $\{\alpha\}$ for $Sp(N)$. These four sets are defined as follows [72].

$\{\delta\}$ is the set of all partitions into even parts only: $\{\square, \square\square, \square\square, \dots\}$.

$\{\beta\}$ is the set of all partitions such that there are an even number of parts of any given magnitude: $\{\square, \square\square, \begin{smallmatrix} \square \\ \square \end{smallmatrix}, \dots\}$.

To define the two remaining sets we have to use the Frobenius notation [71, 72]. In this notation, a Young tableau is described by an array of pair of numbers. The number of pairs is equal to the number of boxes in the leading diagonal of the tableau; the upper number of the pair is the number of boxes to the right and the lower number is the number of boxes below. For example, the Young tableau $\begin{smallmatrix} \square & \square \\ \square & \end{smallmatrix}$ is described in the Frobenius notation by $\begin{pmatrix} 2 & 1 \\ 2 & 0 \end{pmatrix}$.

Using this notation we can define the two remaining sets. Consider Young tableaux defined in the Frobenius notation by

$$\begin{pmatrix} a_1 & a_2 & a_3 & a_4 & \dots \\ b_1 & b_2 & b_3 & b_4 & \dots \end{pmatrix}. \quad (\text{A.1})$$

$\{\gamma\}$ is the set of Young tableaux such that $a_i = b_i + 1 \ \forall \ i$: $\{\square, \begin{smallmatrix} \square & \square \\ \square & \end{smallmatrix}, \begin{smallmatrix} \square & \square & \square \\ \square & \square & \end{smallmatrix}, \dots\}$.

$\{\alpha\}$ is the set of Young tableaux such that $a_i + 1 = b_i \ \forall \ i: \{\emptyset, \begin{smallmatrix} \square \\ \square \end{smallmatrix}, \begin{smallmatrix} \square & \square \\ \square \end{smallmatrix}, \dots\}$.

Note that $\{\beta\}$ and $\{\alpha\}$ are respectively related to $\{\delta\}$ and $\{\gamma\}$ by taking the transpose of the representations, where by transpose we mean exchanging rows and columns.

A.2 The Topological Vertex, Chern-Simons Invariants and Schur Functions

In this appendix we will list some useful identities of Schur functions and their relations to the unknot and Hopf link invariants. For a more detailed discussion of Schur functions see for example [76, 111]. Applications of these results to topological string computations can be found in [77, 78, 112, 113].

Let R be a partition associated to a Young tableau. Let $\ell(R)$ be the number of boxes of the Young tableau and $l_i(R)$ be the number of boxes in the i -th row. We define the quantity

$$W_R(q) = s_R(q^\rho) \quad (\text{A.2})$$

where $s_R(q^\rho)$ is the Schur function with the substitution $s_R(x_i = q^{-i+1/2})$, where i runs from 1 to ∞ . $W_R(q)$ is the leading order of the $U(N)$ quantum dimension $\dim_q^{U(N)} R$ (in the sense defined in [22]). Also, using Weyl's formula, we can write a general formula for quantum dimensions of a group G :

$$\dim_q^G R = \prod_{\alpha \in \Delta_+} \frac{[(\Lambda_R + \rho, \alpha)]}{[(\rho, \alpha)]}, \quad (\text{A.3})$$

where Λ_R is the highest weight of the representation R , ρ is the Weyl vector, and the product is over the positive roots of G . We also defined the following q -number:

$$[x] = q^{x/2} - q^{-x/2}. \quad (\text{A.4})$$

Another important object is

$$W_{R_1 R_2}(q) = s_{R_1}(q^\rho) s_{R_2}(q^{\ell(R_1)+\rho}), \quad (\text{A.5})$$

where $s_{R_2}(q^{\ell(R_2)+\rho}) = s_{R_2}(x_i = q^{l_i(R_2)-i+1/2})$. This is the leading part (again in the sense of [22]) of the Hopf link invariant $\mathcal{W}_{R_1 R_2}^{U(N)}$.

The topological vertex formula derived in [17] reads

$$C_{R_1 R_2 R_3} = q^{\frac{1}{2}(\kappa_{R_2} + \kappa_{R_3})} \sum_{Q_1, Q_2, R} N_{Q_1 R}^{R_1} N_{Q_2 R}^{R_2} \frac{W_{R_2 Q_1}^{R_2} W_{R_2 Q_2}^{R_2}}{W_{R_2}}, \quad (\text{A.6})$$

where κ_R is defined by $\kappa_R = \sum_i l_i(R)(l_i(R) - 2i + 1)$. Using (A.2) and (A.5) we can express the topological vertex in terms of Schur functions (this was first done in [77])

$$C_{R_1 R_2 R_3} = q^{\frac{1}{2}(\kappa_{R_2} + \kappa_{R_3})} s_{R_2^t}(q^\rho) \sum_Q s_{R_1/Q}(q^{\ell(R_2^t) + \rho}) s_{R_3^t/Q}(q^{\ell(R_2) + \rho}), \quad (\text{A.7})$$

where we have used skew Schur functions defined as

$$s_{R/R_1}(x) = \sum_Q N_{R_1 Q}^R s_Q(x). \quad (\text{A.8})$$

Schur functions satisfy some useful identities. First, we have

$$s_{R^t}(q) = q^{-\kappa_R/2} s_R(q) = (-1)^{\ell(R)} s_R(q), \quad (\text{A.9})$$

and similarly

$$s_{R/R_1}(q) = (-1)^{\ell(R) - \ell(R_1)} s_{R^t/R_1^t}(q). \quad (\text{A.10})$$

The two following formulae are also important:

$$\begin{aligned} \sum_R s_{R/R_1}(x) s_{R/R_2}(y) &= \prod_{i,j \geq 1} (1 - x_i y_j)^{-1} \sum_Q s_{R_2/Q}(x) s_{R_1/Q}(y), \\ \sum_R s_{R/R_1}(x) s_{R^t/R_2}(y) &= \prod_{i,j \geq 1} (1 + x_i y_j) \sum_Q s_{R_2^t/Q}(x) s_{R_1^t/Q^t}(y). \end{aligned} \quad (\text{A.11})$$

The following result was proved in [78]. Let us define the ‘‘relative’’ hook length

$$h_{R_1 R_2}(i, j) = l_i(R_1) + l_j(R_2) - i - j + 1, \quad (\text{A.12})$$

and the following functions

$$\begin{aligned} f_R(q) &= \frac{q}{(q-1)} \sum_{i \geq 1} (q^{l_i(R) - i} - q^{-i}), \\ \tilde{f}_{R_1 R_2}(q) &= \frac{(q-1)^2}{q} f_{R_1}(q) f_{R_2}(q) + f_{R_1}(q) + f_{R_2}(q). \end{aligned} \quad (\text{A.13})$$

Let us denote the expansion coefficients of $\tilde{f}_{R_1 R_2}(q)$ by

$$\tilde{f}_{R_1 R_2}(q) = \sum_k C_k(R_1, R_2) q^k. \quad (\text{A.14})$$

Alternatively,

$$\sum_k C_k(R_1, R_2) q^k = \frac{W_{R_1 \square} W_{R_2 \square}}{W_{R_1} W_{R_2}} - W_{\square}^2. \quad (\text{A.15})$$

Then it was proved that

$$\prod_{i,j \geq 1} (1 - Qq^{h_{R_1 R_2}(i,j)}) = \prod_{k=1}^{\infty} (1 - Qq^k)^k \prod_k (1 - Qq^k)^{C_k(R_1, R_2)}. \quad (\text{A.16})$$

Let us now present a useful result proved by Littlewood [72, 111]:

$$\sum_{R=R^T} s_R(x) (-1)^{\frac{1}{2}(\ell(R) \mp r(R))} = \prod_{i=1}^{\infty} (1 \pm x_i) \prod_{1 \leq i < j < \infty} (1 - x_i x_j), \quad (\text{A.17})$$

where $r(R)$ is the rank of R . The final formula that we will need reads as follows [112]

$$\prod_{i,j} (1 - Qx_i y_j) = \exp \left[- \sum_{n=1}^{\infty} \frac{Q^n}{n} \sum_{i,j} x_i^n y_j^n \right], \quad (\text{A.18})$$

from which we can deduce the identities

$$\begin{aligned} \prod_i (1 \mp Q^{1/2} q^{i-1/2}) &= \exp \left[\sum_{n=1}^{\infty} \frac{(\pm 1)^n Q^{n/2}}{n(q^{n/2} - q^{-n/2})} \right], \\ \prod_{i,j} (1 - Qq^{i+j-1}) &= \exp \left[- \sum_{n=1}^{\infty} \frac{Q^n}{n(q^{n/2} - q^{-n/2})^2} \right]. \end{aligned} \quad (\text{A.19})$$

Appendix B

Various Results

B.1 Full Classification of Tops

The following tables provide the complete list of possible tops \diamond , in terms of their duals \diamond^* . The first column of each table identifies the polygon F_0^* to which \diamond^* projects according to the numbering in figure 3.5. The following columns give $z_k := z_{\min}(b_k)$, where b_0 is the origin of F_0^* and the other b_k are the lattice points at the boundary, starting at the ‘12 o’clock position’ and proceeding clockwise. The parameter i takes values in $\{0, 1, \dots\}$. For the elements of the A -series (last row for each choice of F_0^*) the z_k are assumed to satisfy the inequalities determined by (3.3).

The last column indicates the affine Kac-Moody algebra to which \diamond corresponds, with the superscript ⁽¹⁾ suppressed for the untwisted cases. The case $i = 0$ can be special in the sense that the corresponding Dynkin diagram does not belong to the general family (this occurs when edges that are distinct for $i > 0$ merge when $i = 0$), or that \diamond is the same for some other family. In either of these cases we also display the $i = 0$ algebra, with superscripts a or b for repeated non-trivial cases.

Any two duals of tops in our tables are different, with the following exceptions. The trivial top (case 0) may occur more than once as the $i = 0$ case of a C_i series; C_0 always means the trivial case and its repetitions are not separately indicated. If a non-trivial top occurs more than once as an $i = 0$ case, it gets a superscript a or b which is the same for each occurrence. For the A -cases, we have not eliminated the equivalences coming from automorphisms of F_0^* .

F_0^*	z_0	z_1	z_2	z_3	z_4	z_5	AKMA
1	$-1/3$	-1	-1	1	$-$	$-$	E_6
	-1	-1	-1	-1	$-$	$-$	C_0
	-1	-1	-1	z_3	$-$	$-$	A_{3z_3+2}
2	$-1/2$	-1	-1	0	i	$-$	D_{2i+4}
	-1	-1	-1	-1	$i-1$	$-$	C_i
	-1	-1	-1	z_3	z_4	$-$	$A_{2z_3+2z_4+3}$
3	$-1/3$	-1	-1	1	1	$-$	E_6
	$-1/2$	-1	-1	0	$i+1$	$-$	D_{2i+5}
	-1	-1	-1	-1	$i-1$	$-$	C_i
	-1	-1	-1	z_3	z_4	$-$	$A_{z_3+2z_4+2}$
4	$-1/4$	-1	-1	$1/2$	2	$-$	E_7
	$-1/2$	-1	-1	0	$i+1$	$-$	D_{2i+4}/B_3
	-1	-1	-1	-1	$i-1$	$-$	C_i
	-1	-1	-1	z_3	z_4	$-$	A_{2z_4+1}
5	$-1/3$	-1	-1	1	1	-1	E_6
	$-1/2$	-1	-1	0	i	i	B_{2i+4}
	$-1/2$	-1	-1	0	$i+1$	i	B_{2i+5}
	-1	-1	-1	-1	$i-1$	$i-1$	C_i
	-1	-1	-1	z_3	z_4	z_5	$A_{2z_3+z_4+z_5+3}$
6	$-1/4$	-1	-1	$1/2$	2	2	E_7
	$-1/3$	-1	-1	$1/2$	2	1	E_6
	$-1/3$	-1	-1	1	3	1	E_6
	$-1/2$	-1	-1	0	$i+1$	$i+1$	D_{2i+4}/B_3
	$-1/2$	-1	-1	0	$i+2$	$i+1$	D_{2i+5}
	-1	-1	-1	-1	$i-1$	$i-1$	C_i
	-1	-1	-1	z_3	z_4	z_5	$A_{z_4+z_5+1}$

Table B.1: Duals \diamond^* of tops with F_0^* one of the polygons $1, \dots, 6$ of figure 3.5.

F_0^*	z_0	z_1	z_2	z_3	z_4	z_5	z_6	AKMA
7	-1/3	-1	-1	1	1	1	-1	E_6
	-1/2	-1	-1	0	0	i	i	D_{2i+4}
	-1/2	-1	-1	0	0	$i+1$	i	D_{2i+5}
	-1	-1	-1	-1	-1	$i-1$	$i-1$	C_i
	-1	-1	-1	z_3	z_4	z_5	z_6	$A_{z_3+z_4+z_5+z_6+3}$
8	-1/4	-1	-1	1/2	2	3/2	1	E_7
	-1/4	-1	-1	1/2	2	2	2	E_7
	-1/3	-1	-1	1/2	2	1	1	E_6
	-1/3	-1	-1	1	3	1	1	E_6
	-1/2	-1	-1	0	$i+1$	$i+1/2$	i	D_{2i+4}/B_3^a
	-1/2	-1	-1	0	$i+2$	$i+1$	i	D_{2i+4}/D_4^a
	-1/2	-1	-1	0	$i+1$	$i+1$	$i+1$	B_{2i+4}/B_3
	-1/2	-1	-1	i	$2i+2$	$i+1$	0	B_{2i+4}/D_4^a
	-1/2	-1	-1	0	$i+2$	$i+1$	$i+1$	B_{2i+5}
	-1/2	-1	-1	$i+1$	$2i+3$	$i+1$	0	B_{2i+5}
	-1/2	-1	-1	$i/2$	$i+1$	$(i+1)/2$	0	B_{i+3}/B_3^a
	-1	-1	-1	-1	$i-1$	$i-1$	$i-1$	C_i
	-1	-1	-1	$i-1$	$2i-1$	$i-1$	-1	C_i
-1	-1	-1	z_3	z_4	z_5	z_6	$A_{z_4+z_6+1}$	
9	-1/4	2	-1	-1	-1	1/2	2	E_7
	-1/3	-1	-1	1	1	1/2	0	E_6
	-1/3	-1	-1	1	1	1	1	E_6
	-1/2	-1	-1	0	$i+1$	i	i	D_{2i+4}/D_4^a
	-1/2	-1	-1	i	$i+1$	0	0	D_{2i+4}/D_4^a
	-1/2	-1	-1	$i+1$	$i+1$	0	-1	D_{2i+4}/B_3
	-1/2	-1	-1	0	$i+1$	$i+1/2$	i	D_{2i+5}
	-1/2	-1	-1	0	$i+1$	$i+1$	$i+1$	D_{2i+5}
	-1/2	-1	-1	$i+1$	$i+1$	0	0	D_{2i+5}
	-1	-1	-1	-1	$i-1$	$i-1$	$i-1$	C_i
	-1	-1	-1	$i-1$	$i-1$	-1	-1	C_i
	-1	-1	-1	z_3	z_4	z_5	z_6	$A_{z_3+z_4+z_6+2}$
10	-1/6	-1	-1	2/3	7/3	4	3/2	E_8
	-1/4	-1	-1	1/2	2	4	3/2	E_7
	-1/4	-1	-1	1/2	2	5	2	E_7
	-1/3	-1	-1	1/3	5/3	3	1	F_4
	-1/3	-1	-1	1/2	2	4	1	E_6
	-1/3	-1	-1	1	3	5	1	E_6
	-1/2	-1	-1	0	$i+1$	$2i+3$	$i+1$	D_{2i+4}/B_3
	-1/2	-1	-1	0	$i+2$	$2i+4$	$i+1$	D_{2i+5}
	-1/2	-1	-1	0	$i/2+1$	$i+2$	$(i+1)/2$	B_{i+3}/G_2
	-1	-1	-1	-1	$i-1$	$2i-1$	$i-1$	C_i
	-1	-1	-1	z_3	z_4	z_5	z_6	A_{z_5}

Table B.2: Duals \diamond^* of tops with F_0^* one of the polygons 7, 8, 9, 10 of figure 3.5.

F_0^*	z_0	z_1	z_2	z_3	z_4	z_5	z_6	z_7	AKMA
11	-1/6	-1	-1	-1	2/3	7/3	4	3/2	E_8
	-1/4	-1	-1	-1	1/2	2	4	3/2	E_7
	-1/4	-1	-1	-1	1/2	2	5	2	E_7
	-1/4	-1	-1	0	2/3	4/3	2	1/2	E_7
	-1/4	-1	-1	1	1	3/2	2	1/2	E_7
	-1/4	-1	-1	2	2	2	2	1/2	E_7
	-1/3	-1	-1	-1	1/3	5/3	3	1	F_4
	-1/3	-1	1	1	1/2	0	0	-1	E_6
	-1/3	-1	1	1	1	1	1	-1	E_6
	-1/3	-1	-1	0	1/2	1	2	1/2	E_6
	-1/3	-1	-1	1	1	1	2	1/2	E_6
	-1/3	-1	-1	0	1/2	1	3	1	E_6
	-1/3	-1	-1	1	1	1	3	1	E_6
	-1/2	-1	-1	0	0	$i+1$	$2i+2$	i	D_{2i+4}/D_4^a
	-1/2	-1	-1	-1	0	$i+1$	$2i+3$	$i+1$	D_{2i+4}/B_3
	-1/2	-1	-1	i	i	$i+1/2$	$i+1$	0	D_{2i+4}/B_3^a
	-1/2	-1	-1	i	i	$i+1$	$i+2$	0	D_{2i+4}/D_4^a
	-1/2	-1	-1	$i+1$	$i+1$	$i+1$	$i+1$	0	D_{2i+4}/B_3
	-1/2	-1	-1	0	0	$i+1$	$2i+3$	$i+1$	D_{2i+5}
	-1/2	-1	-1	-1	0	$i+2$	$2i+4$	$i+1$	D_{2i+5}
	-1/2	-1	-1	i	$i+1/2$	$i+1$	$i+2$	0	D_{2i+5}
	-1/2	-1	-1	i	$i+1$	$i+2$	$i+3$	0	D_{2i+5}
	-1/2	-1	-1	$i+1$	$i+1$	$i+1$	$i+2$	0	D_{2i+5}
	-1/2	-1	-1	0	0	$(i+1)/2$	$i+1$	$i/2$	B_{i+3}/B_3^a
	-1/2	-1	-1	-1	0	$i/2+1$	$i+2$	$(i+1)/2$	B_{i+3}/G_2
	-1	-1	-1	$i-1$	$i-1$	$i-1$	$i-1$	-1	C_i
-1	-1	-1	-1	-1	$i-1$	$2i-1$	$i-1$	C_i	
-1	-1	-1	z_3	z_4	z_5	z_6	z_7	$A_{z_3+z_6+1}$	
12	-1/4	-3/2	-2	-1	2	2	1/2	-1	E_7
	-1/4	-1	-1	-1	2	2	1/2	-1	E_7
	-1/3	-3/2	-2	-1	1	2	1/2	-1	E_6
	-1/3	-3/2	-2	-1	1	3	1	-1	E_6
	-1/3	-1	-1	-1	1	3	1	-1	E_6
	-1/3	-1	-1	-1	1	1	1/2	0	E_6
	-1/3	-1	-1	-1	1	1	1	1	E_6
	-1/2	-1	-1	0	0	i	$i-1/2$	$i-1$	D_{2i+4}/B_3^a
	-1/2	-1	-1	0	0	i	i	i	D_{2i+4}/D_4^a
	-1/2	-1	-1	0	0	$i+1$	i	$i-1$	D_{2i+4}/B_3
	-1/2	-1	-1	-1	0	$i+1$	i	i	D_{2i+4}/D_4
	-1/2	i	-1	-1	0	0	i	$2i+1$	D_{2i+4}/D_4^a
	-1/2	-1	-1	0	0	$i+1$	i	i	D_{2i+5}
	-1/2	-1	-1	-1	0	$i+1$	$i+1/2$	i	D_{2i+5}
	-1/2	-1	-1	-1	0	$i+1$	$i+1$	$i+1$	D_{2i+5}
	-1/2	-1	-1	-1	0	$i+2$	$i+1$	i	D_{2i+5}
	-1/2	i	-1	-1	0	0	$i+1$	$2i+2$	D_{2i+5}
	-1/2	$(i-1)/2$	-1	-1	0	0	$i/2$	i	B_{i+3}/B_3^a
	-1	-1	-1	-1	-1	$i-1$	$i-1$	$i-1$	C_i
	-1	$i-1$	-1	-1	-1	-1	$i-1$	$2i-1$	C_i
-1	-1	-1	z_3	z_4	z_5	z_6	z_7	$A_{z_3+z_4+z_5+z_7+3}$	

Table B.3: Duals \diamond^* of tops with F_0^* one of the polygons 11, 12 of figure 3.5.

F_0^*	z_0	z_1	z_2	z_3	z_4	z_5	z_6	z_7	z_8	AKMA
13	-1/6	3/2	-1	-3/2	-2	-1	2/3	7/3	4	E_8
	-1/6	3/2	-1	-1	-1	-1	2/3	7/3	4	E_8
	-1/4	1/2	2	-1	-4	-13/4	-5/2	-7/4	-1	$E_6^{(2)}$
	-1/4	3/2	-1	-3/2	-2	-1	1/2	2	4	E_7
	-1/4	3/2	-1	-1	-1	-1	1/2	2	4	E_7
	-1/4	2	-1	-1	-1	-1	1/2	2	5	E_7
	-1/4	1/2	2	-1	-3	-3	-7/3	-5/3	-1	E_7
	-1/4	1/2	2	-1	-3	-5/2	-2	-3/2	-1	E_7
	-1/4	1/2	2	-1	-2	-2	-2	-3/2	-1	E_7
	-1/4	1/2	2	-1	-1	-1	-1	-1	-1	E_7
	-1/3	1/2	-1	-1	-1	-1/3	1/3	1	2	F_4
	-1/3	1	-1	-1	-1	-1/3	1/3	1	3	F_4
	-1/3	1/2	-1	-1	0	0	1/2	1	2	E_6
	-1/3	1/2	-1	-1	1	1	1	1	2	E_6
	-1/3	1	-1	-1	0	0	1/2	1	3	E_6
	-1/3	1	-1	-1	1	1	1	1	3	E_6
	-1/2	i	-1	-1	0	0	0	$i+1$	$2i+2$	D_{2i+4}/D_4^a
	-1/2	$i+1$	-1	-1	-1	-1	0	$i+1$	$2i+3$	D_{2i+4}/B_3
	-1/2	-1	-1	0	$i+1$	$i+1/2$	i	$i-1/2$	$i-1$	$D_{2i+4}/D_3^{(2)a}$
	-1/2	-1	-1	0	$i+1$	$i+1$	$i+1$	$i+1$	$i+1$	D_{2i+4}/B_3
	-1/2	-1	-1	0	$i+2$	$i+1$	i	i	i	D_{2i+4}/D_4^a
	-1/2	-1	-1	0	$i+1$	$i+1/2$	i	i	i	D_{2i+4}/B_3^a
	-1/2	$i+1$	-1	-1	0	0	0	$i+1$	$2i+3$	D_{2i+5}
	-1/2	-1	-1	0	$i+2$	$i+1$	$i+1/2$	i	i	D_{2i+5}
	-1/2	-1	-1	0	$i+2$	$i+1$	$i+1$	$i+1$	$i+1$	D_{2i+5}
	-1/2	$i/2$	-1	-1	0	0	0	$(i+1)/2$	$i+1$	B_{i+3}/B_3^a
	-1/2	$(i+1)/2$	-1	-1	-1	-1	0	$i/2+1$	$i+2$	B_{i+3}/G_2
	-1/2	$i+1/2$	-1	-1	-1	-1/2	0	$i+1$	$2i+2$	$D_{2i+4}^{(2)}$
	-1/2	i	-1	-1	-1	-1/2	0	$i+1/2$	$2i+1$	$D_{2i+3}^{(2)}/D_3^{(2)a}$
	-1/2	$i-1/2$	-1	-1/2	0	0	0	i	$2i$	$D_{2i+3}^{(2)}/A_2^{(2)}$
	-1	$i-1$	-1	-1	-1	-1	-1	$i-1$	$2i-1$	C_i
	-1	-1	-1	-1	$i-1$	$i-1$	$i-1$	$i-1$	$i-1$	C_i
	-1	-1	-1	z_3	z_4	z_5	z_6	z_7	z_8	$A_{z_4+z_8+1}$

Table B.4: Duals \diamond^* of tops with F_0^* being polygon 13 of figure 3.5.

F_0^*	z_0	z_1	z_2	z_3	z_4	z_5	z_6	z_7	z_8	AKMA
14	-1/6	-1	-2	-3/2	-1	2/3	7/3	4	3/2	E_8
	-1/6	-1	-1	-1	-1	2/3	7/3	4	3/2	E_8
	-1/4	2	2	1/2	-1	-5/3	-7/3	-3	-1	E_7
	-1/4	2	2	1/2	-1	-3/2	-2	-2	-1	E_7
	-1/4	2	2	1/2	-1	-1	-1	-1	-1	E_7
	-1/4	-1	-2	-3/2	-1	1/2	2	4	3/2	E_7
	-1/4	-1	-2	-3/2	-1	1/2	2	5	2	E_7
	-1/4	-1	-1	-1	-1	1/2	2	4	3/2	E_7
	-1/4	-1	-1	-1	-1	1/2	2	5	2	E_7
	-1/3	-1	0	1/2	1	1/3	-1/3	-1	-1	F_4
	-1/3	-1	1	1	1	1/3	-1/3	-1	-1	F_4
	-1/3	-1	0	1/2	1	1/2	0	0	-1	E_6
	-1/3	-1	0	1/2	1	1	1	1	-1	E_6
	-1/3	-1	1	1	1	1/2	0	0	-1	E_6
	-1/3	-1	1	1	1	1	1	1	-1	E_6
	-1/3	-1	-1	-1	0	1/2	1	2	1/2	E_6
	-1/3	-1	-1	-1	1	1	1	2	1/2	E_6
	-1/3	-1	-1	-1	0	1/2	1	3	1	E_6
	-1/3	-1	-1	-1	1	1	1	3	1	E_6
	-1/2	-1	-1	-1	i	i	$i+1/2$	$i+1$	0	D_{2i+4}/B_3^a
	-1/2	-1	-1	-1	i	i	$i+1$	$i+2$	0	D_{2i+4}/D_4^a
	-1/2	-1	-1	-1	$i+1$	$i+1$	$i+1$	$i+1$	0	D_{2i+4}/B_3
	-1/2	-1	-1	-1/2	0	0	i	$2i+1$	i	D_{2i+4}/B_3^b
	-1/2	-1	-1	0	1	0	i	$2i+1$	i	D_{2i+4}
	-1/2	-1	-1	-1	0	0	$i+1$	$2i+2$	i	D_{2i+4}/D_4^a
	-1/2	-1	-1	-1	-1	0	$i+1$	$2i+3$	$i+1$	D_{2i+4}/B_3
	-1/2	-1	-1	-1	i	$i+1/2$	$i+1$	$i+2$	0	D_{2i+5}
	-1/2	-1	-1	-1	i	$i+1$	$i+2$	$i+3$	0	D_{2i+5}
	-1/2	-1	-1	-1	$i+1$	$i+1$	$i+1$	$i+2$	0	D_{2i+5}
	-1/2	-1	-1	-1/2	0	0	$i+1$	$2i+2$	i	D_{2i+5}
	-1/2	-1	-1	0	1	0	$i+1$	$2i+2$	i	D_{2i+5}
	-1/2	-1	-1	-1	0	0	$i+1$	$2i+3$	$i+1$	D_{2i+5}
	-1/2	-1	-1	-1	-1	0	$i+2$	$2i+4$	$i+1$	D_{2i+5}
	-1/2	-1	-1	-1/2	0	0	$i/2$	i	$(i-1)/2$	B_{i+3}/G_2
	-1/2	-1	-1	0	1	0	$i/2$	i	$(i-1)/2$	B_{i+3}/B_3^b
	-1/2	-1	-1	-1	0	0	$(i+1)/2$	$i+1$	$i/2$	B_{i+3}/B_3^a
	-1/2	-1	-1	-1	-1	0	$i/2+1$	$i+2$	$(i+1)/2$	B_{i+3}/G_2
	-1	-1	-1	-1	-1	-1	$i-1$	$2i-1$	$i-1$	C_i
	-1	-1	-1	-1	$i-1$	$i-1$	$i-1$	$i-1$	-1	C_i
	-1	-1	-1	z_3	z_4	z_5	z_6	z_7	z_8	$A_{z_4+z_7+1}$

Table B.5: Duals \diamond^* of tops with F_0^* being polygon 14 of figure 3.5.

F_0^*	z_0	z_1	z_2	z_3	z_4	z_5	z_6	z_7	z_8	z_9	AKMA
15	-1/4	-1	1	3/2	2	1/2	-1	-3/2	-2	-	E_7
	-1/4	-1	1	3/2	2	1/2	-1	-1	-1	-	E_7
	-1/4	-1	2	2	2	1/2	-1	-1	-1	-	E_7
	-1/3	-1	-1	-1	0	1/2	1	1/2	0	-	E_6
	-1/3	-1	-1	-1	0	1/2	1	1	1	-	E_6
	-1/3	-1	-1	-1	1	1	1	1	1	-	E_6
	-1/2	-1	-1	-1/2	0	0	i	$i-1/2$	$i-1$	-	$D_{2i+4}/D_3^{(2)a}$
	-1/2	-1	-1	-1/2	0	0	i	i	i	-	D_{2i+4}/B_3^a
	-1/2	-1	-1	0	1	0	i	i	i	-	D_{2i+4}/D_4^a
	-1/2	-1	-1	0	1	0	$i+1$	i	$i-1$	-	D_{2i+4}/B_3
	-1/2	-1	-1	-1	0	0	$i+1$	i	i	-	D_{2i+4}
	-1/2	i	-1	-1	0	0	0	i	$2i+1$	-	D_{2i+4}/D_4^a
	-1/2	-1	-1	-1/2	0	0	$i+1$	i	i	-	D_{2i+5}
	-1/2	-1	-1	0	1	0	$i+1$	i	i	-	D_{2i+5}
	-1/2	i	-1	-1	0	0	0	$i+1$	$2i+2$	-	D_{2i+5}
	-1/2	$(i-1)/2$	-1	-1	0	0	0	$i/2$	i	-	B_{i+3}/B_3^a
	-1/2	$(i-1)/2$	-1	-1	-1	-1/2	0	$i/2$	i	-	$D_{i+3}^{(2)}/D_3^{(2)a}$
	-1	-1	-1	-1	-1	-1	$i-1$	$i-1$	$i-1$	-	C_i
	-1	$i-1$	-1	-1	-1	-1	-1	$i-1$	$2i-1$	-	C_i
	-1	-1	-1	-1	z_3	z_4	z_5	z_6	z_7	z_8	-
16	-1/6	-1	-3	-2	-3/2	-1	2/3	7/3	4	3/2	E_8
	-1/6	-1	-3	-7/3	-5/3	-1	2/3	7/3	4	3/2	E_8
	-1/6	-1	-1	-1	-1	-1	2/3	7/3	4	3/2	E_8
	-1/4	-1	-3	-7/3	-5/3	-1	1/2	2	4	3/2	E_7
	-1/4	-1	-3	-7/3	-5/3	-1	1/2	2	5	2	E_7
	-1/4	-1	-2	-2	-3/2	-1	1/2	2	4	3/2	E_7
	-1/4	-1	-2	-2	-3/2	-1	1/2	2	5	2	E_7
	-1/4	-1	-1	-1	-1	-1	1/2	2	4	3/2	E_7
	-1/4	-1	-1	-1	-1	-1	1/2	2	5	2	E_7
	-1/3	-1	-1	-1/3	1/3	1	1/3	-1/3	-1	-1	$D_4^{(3)}$
	-1/3	-1	-1	-1/3	1/3	1	1/2	0	0	-1	F_4
	-1/3	-1	-1	-1/3	1/3	1	1	1	1	-1	F_4
	-1/3	-1	0	0	1/2	1	1/2	0	0	-1	E_6
	-1/3	-1	0	0	1/2	1	1	1	1	-1	E_6
	-1/3	-1	1	1	1	1	1	1	1	-1	E_6
	-1/3	-1	-2	-3/2	-1	0	1/2	1	2	1/2	E_6
	-1/3	-1	-2	-3/2	-1	1	1	1	2	1/2	E_6
	-1/3	-1	-2	-3/2	-1	1	1	1	3	1	E_6
	-1/3	-1	-1	-1	-1	1	1	1	3	1	E_6
	-1/2	-1	-1	-1/2	0	1	0	i	$2i$	$i-1$	D_{2i+4}/B_3^a
	-1/2	-1	-1	0	1	2	0	i	$2i$	$i-1$	D_{2i+4}/B_3
	-1/2	-1	-1	-1	0	1	0	i	$2i+1$	i	D_{2i+4}
	-1/2	-1	-1	-1/2	0	1	0	i	$2i+1$	i	D_{2i+5}
	-1/2	-1	-1	0	1	2	0	i	$2i+1$	i	D_{2i+5}
	-1/2	-1	-1	-1	0	1	0	$i+1$	$2i+2$	i	D_{2i+5}
	-1/2	-1	-1	-1/2	0	1	0	$(i-1)/2$	$i-1$	$i/2-1$	B_{i+3}/G_2
	-1/2	-1	-1	0	1	2	0	$(i-1)/2$	$i-1$	$i/2-1$	B_{i+3}/G_2
	-1/2	-1	-1	-1	0	1	0	$i/2$	i	$(i-1)/2$	B_{i+3}/B_3^a
	-1	-1	-1	-1	-1	-1	-1	$i-1$	$2i-1$	$i-1$	C_i
	-1	-1	-1	-1	z_3	z_4	z_5	z_6	z_7	z_8	z_9

Table B.6: Duals \diamond^* of tops with F_0^* one of the polygons 15, 16 of figure 3.5.

B.2 Full Results for the Closed Topological String Amplitudes

Here we present the results for the full generating functionals given by (4.60). The \pm sign corresponds to Sp and SO , respectively. Of course, the oriented contribution for $Q = 0$ agrees with previous results for the local del Pezzo dP_3 with one Kähler parameter sent to infinity [22, 114], and if we set $q_{1,2} = 0$ we recover the results presented in tables 4.1–4.24 (taking into account the $1/2$ factor in the definition of the $c = 0$ generating functional).

We computed the results up to degree 5 in e^{-t} , but we will present only the results up to degree 3 as the higher degree results are rather cumbersome. Note that $\mathcal{F}_0^{0,2}$, $\mathcal{F}_1^{0,2}$, $\mathcal{F}_2^{0,2}$ and $\mathcal{F}_3^{1,2}$ are 0 (but not $\mathcal{F}_3^{0,2}$), and therefore we omit them.

$$\begin{aligned}
\mathcal{F}_0^{0,0} &= q_1 + q_2 + \frac{1}{2}Q, \\
\mathcal{F}_0^{0,1} &= \pm[Q^{1/2}], \\
\mathcal{F}_1^{0,0} &= 3 - 2(q_1 + q_2 + Q) + (q_1q_2 + q_2Q + q_1Q), \\
\mathcal{F}_1^{0,1} &= \pm[-2Q^{1/2} + (q_1Q^{1/2} + q_2Q^{1/2})], \\
\mathcal{F}_2^{0,0} &= -6 + 5(q_1 + q_2) + 7Q - 4q_1q_2 - 6(q_1Q + q_2Q) + 4q_1q_2Q + \frac{1}{2}(q_1^2Q + q_2^2Q) \\
&\quad - Q^2 + (q_1Q^2 + q_2Q^2) - q_1q_2Q^2, \\
\mathcal{F}_2^{0,1} &= \pm[5Q^{1/2} - 4(q_1Q^{1/2} + q_2Q^{1/2}) + 3q_1q_2Q^{1/2} - 3Q^{3/2} \\
&\quad + 2(q_1Q^{3/2} + q_2Q^{3/2}) - q_1q_2Q^{3/2}], \\
\mathcal{F}_3^{0,0} &= 27 - 32(q_1 + q_2) - 42Q + 35q_1q_2 + 48(q_1Q + q_2Q) - 50q_1q_2Q + 7(q_1^2 + q_2^2) \\
&\quad + 15Q^2 - 6(q_1^2q_2 + q_1q_2^2) - 10(q_1^2Q + q_2^2Q) - 16(q_1Q^2 + q_2Q^2) \\
&\quad + 8(q_1^2q_2Q + q_1q_2^2Q) + 3(q_1^2Q^2 + q_2^2Q^2) - 2(q_1^2q_2Q^2 + q_1q_2^2Q^2) + 15q_1q_2Q^2, \\
\mathcal{F}_3^{0,1} &= \pm[-32Q^{1/2} + 35(q_1Q^{1/2} + q_2Q^{1/2}) - 36q_1q_2Q^{1/2} - 6(q_1^2Q^{1/2} + q_2^2Q^{1/2}) \\
&\quad + (q_1^2q_2Q^{1/2} + q_1q_2^2Q^{1/2}) + 30Q^{3/2} - 30(q_1Q^{3/2} + q_2Q^{3/2}) \\
&\quad + 4(q_1^2Q^{3/2} + q_2^2Q^{3/2}) + 28q_1q_2Q^{3/2} - 3(q_1^2q_2Q^{3/2} + q_1q_2^2Q^{3/2}) - 4Q^{5/2} \\
&\quad + 3(q_1Q^{5/2} + q_2Q^{5/2}) - 2q_1q_2Q^{5/2}], \\
\mathcal{F}_3^{0,2} &= Q^2 - (q_1Q^2 + q_2Q^2) + q_1q_2Q^2, \\
\mathcal{F}_3^{1,0} &= 10 - 9(q_1 + q_2 + Q) + 8(q_1q_2 + q_1Q + q_2Q) - 7q_1q_2Q, \\
\mathcal{F}_3^{1,1} &= \pm[-9Q^{1/2} + 8(q_1Q^{1/2} + q_2Q^{1/2}) - 7q_1q_2Q^{1/2} + 7Q^{3/2} \\
&\quad - 6(q_1Q^{3/2} + q_2Q^{3/2}) + 5q_1q_2Q^{3/2}].
\end{aligned}$$

B.3 BPS Invariants for the Trefoil Knot

In this appendix, we list the BPS invariants $N_{R,g,\beta}^{c=1}$ for the trefoil knot, for representations R with three boxes.

	$\beta = 2$	3	4	5	6	7	8	9
$g = 0$	18	-270	1185	-2380	2430	-1188	175	30
1	21	-753	4924	-12209	13203	-4856	-1300	970
2	8	-1007	10374	-31348	31419	4028	-22155	8681
3	1	-793	13920	-50383	30636	84956	-117415	39078
4	0	-378	12688	-54222	-24584	305272	-343318	104542
5	0	-106	8006	-40151	-118255	609701	-639896	180701
6	0	-16	3486	-20657	-178503	797521	-813994	212163
7	0	-1	1024	-7353	-161931	728309	-734484	174436
8	0	0	193	-1773	-98947	478948	-480509	102088
9	0	0	21	-276	-42205	229955	-230209	42714
10	0	0	1	-25	-12624	80705	-80729	12672
11	0	0	0	-1	-2599	20474	-20475	2601
12	0	0	0	0	-351	3654	-3654	351
13	0	0	0	0	-28	435	-435	28
14	0	0	0	0	-1	31	-31	1
15	0	0	0	0	0	1	-1	0

Table B.7: BPS invariants $N_{(3),g,\beta}^{c=1}$ for the trefoil knot.

	$\beta = 2$	3	4	5	6	7	8	9
$g = 0$	99	-1125	4359	-8096	7828	-3699	563	72
1	201	-4194	22748	-51475	53807	-21649	-2204	2766
2	164	-7702	60811	-165827	171590	-19997	-68978	29939
3	66	-8701	104757	-338906	282625	264688	-468878	164349
4	13	-6395	125047	-472907	124226	1398430	-1710505	542091
5	1	-3092	106648	-466523	-477321	3645201	-3976290	1171376
6	0	-971	65795	-331606	-1232410	6113672	-6363573	1749093
7	0	-190	29358	-171307	-1590490	7192295	-7328205	1868539
8	0	-21	9358	-64261	-1351903	6186865	-6240225	1460187
9	0	-1	2072	-17298	-815116	3979137	-3994110	845316
10	0	0	302	-3252	-358192	1934294	-1937220	364068
11	0	0	26	-405	-115397	712126	-712504	116154
12	0	0	1	-30	-26996	197286	-197315	27054
13	0	0	0	-1	-4465	40454	-40455	4467
14	0	0	0	0	-495	5952	-5952	495
15	0	0	0	0	-33	594	-594	33
16	0	0	0	0	-1	36	-36	1
17	0	0	0	0	0	1	-1	0

Table B.8: BPS invariants $N_{(2,1),g,\beta}^{c=1}$ for the trefoil knot.

	$\beta = 2$	3	4	5	6	7	8	9
$g = 0$	108	-1044	3705	-6484	6000	-2754	427	42
1	306	-4818	23074	-48785	49436	-20669	-448	1904
2	366	-11012	73663	-186538	193691	-44683	-49616	24129
3	230	-15636	151596	-453623	421630	161750	-421269	155322
4	79	-14720	216949	-756616	429479	1359478	-1836601	601952
5	14	-9381	223615	-898781	-235791	4434624	-5047078	1532778
6	1	-4047	168943	-777340	-1531480	8961515	-9525899	2708307
7	0	-1160	94128	-495542	-2661004	12577678	-12957296	3443196
8	0	-211	38523	-233794	-2843448	12900213	-13087921	3226638
9	0	-22	11409	-81283	-2124814	9936047	-10004126	2262789
10	0	-1	2373	-20525	-1160684	5832726	-5850601	1196712
11	0	0	328	-3656	-470990	2625946	-2629249	477621
12	0	0	27	-435	-142042	905758	-906165	142857
13	0	0	1	-31	-31433	237305	-237335	31493
14	0	0	0	-1	-4959	46375	-46376	4961
15	0	0	0	0	-528	6545	-6545	528
16	0	0	0	0	-34	630	-630	34
17	0	0	0	0	-1	37	-37	1
18	0	0	0	0	0	1	-1	0

Table B.9: BPS invariants $N_{(1,1,1),g,\beta}^{c=1}$ for the trefoil knot.

Bibliography

- [1] W. Fulton, *Introduction to Toric Varieties*. Annals of Mathematics Studies. Princeton University Press, 1993. 157 p.
- [2] D. A. Cox, “The Homogeneous Coordinate Ring of a Toric Variety, Revised Version,” [alg-geom/9210008](#).
- [3] V. Batyrev, “Dual Polyhedra and Mirror Symmetry for Calabi-Yau Hypersurfaces,” *J. Alg. Geom.* **3** (1994) 493, [alg-geom/9310003](#).
- [4] P. Candelas and A. Font, “Duality between the webs of heterotic and type II vacua,” *Nucl. Phys.* **B511** (1998) 295–325, [hep-th/9603170](#).
- [5] E. Perevalov and H. Skarke, “Enhanced gauge symmetry in type II and F-theory compactifications: Dynkin diagrams from polyhedra,” *Nucl. Phys.* **B505** (1997) 679–700, [hep-th/9704129](#).
- [6] P. Berglund and P. Mayr, “Heterotic string/F-theory duality from mirror symmetry,” *Adv. Theor. Math. Phys.* **2** (1999) 1307–1372, [hep-th/9811217](#).
- [7] P. Candelas, E. Perevalov, and G. Rajesh, “Comments on A, B, C chains of heterotic and type II vacua,” *Nucl. Phys.* **B502** (1997) 594–612, [hep-th/9703148](#).
- [8] P. Candelas, E. Perevalov, and G. Rajesh, “F-theory duals of non-perturbative heterotic $E(8) \times E(8)$ vacua in six dimensions,” *Nucl. Phys.* **B502** (1997) 613–628, [hep-th/9606133](#).
- [9] P. Candelas, E. Perevalov, and G. Rajesh, “Toric geometry and enhanced gauge symmetry of F- theory/heterotic vacua,” *Nucl. Phys.* **B507** (1997) 445–474, [hep-th/9704097](#).
- [10] P. Candelas, E. Perevalov, and G. Rajesh, “Matter from toric geometry,” *Nucl. Phys.* **B519** (1998) 225–238, [hep-th/9707049](#).

- [11] P. Candelas and H. Skarke, “F-theory, $SO(32)$ and toric geometry,” *Phys. Lett.* **B413** (1997) 63–69, [hep-th/9706226](#).
- [12] Y. Hu, C.-H. Liu, and S.-T. Yau, “Toric morphisms and fibrations of toric Calabi-Yau hypersurfaces,” *Adv. Theor. Math. Phys.* **6** (2003) 457–505, [math.ag/0010082](#).
- [13] M. Kreuzer and H. Skarke, “Calabi-Yau 4-folds and toric fibrations,” *J. Geom. Phys.* **26** (1998) 272–290, [hep-th/9701175](#).
- [14] S. Chaudhuri, G. Hockney, and J. D. Lykken, “Maximally supersymmetric string theories in $D < 10$,” *Phys. Rev. Lett.* **75** (1995) 2264–2267, [hep-th/9505054](#).
- [15] V. Bouchard and H. Skarke, “Affine Kac-Moody algebras, CHL strings and the classification of tops,” *Adv. Theor. Math. Phys.* **7** (2003) 205–232, [hep-th/0303218](#).
- [16] R. Gopakumar and C. Vafa, “On the gauge theory/geometry correspondence,” *Adv. Theor. Math. Phys.* **3** (1999) 1415–1443, [hep-th/9811131](#).
- [17] M. Aganagic, A. Klemm, M. Mariño, and C. Vafa, “The topological vertex,” *Commun. Math. Phys.* **254** (2005) 425–478, [hep-th/0305132](#).
- [18] M. Mariño, “Chern-Simons theory and topological strings,” [hep-th/0406005](#).
- [19] A. Neitzke and C. Vafa, “Topological strings and their physical applications,” [hep-th/0410178](#).
- [20] S. Sinha and C. Vafa, “SO and Sp Chern-Simons at large N,” [hep-th/0012136](#).
- [21] B. Acharya, M. Aganagic, K. Hori, and C. Vafa, “Orientifolds, mirror symmetry and superpotentials,” [hep-th/0202208](#).
- [22] M. Aganagic, M. Mariño, and C. Vafa, “All loop topological string amplitudes from Chern-Simons theory,” *Commun. Math. Phys.* **247** (2004) 467–512, [hep-th/0206164](#).
- [23] M. Aganagic and C. Vafa, “G(2) manifolds, mirror symmetry and geometric engineering,” [hep-th/0110171](#).

- [24] D.-E. Diaconescu, B. Florea, and A. Grassi, “Geometric transitions and open string instantons,” *Adv. Theor. Math. Phys.* **6** (2003) 619–642, [hep-th/0205234](#).
- [25] D.-E. Diaconescu, B. Florea, and A. Grassi, “Geometric transitions, del Pezzo surfaces and open string instantons,” *Adv. Theor. Math. Phys.* **6** (2003) 643–702, [hep-th/0206163](#).
- [26] D.-E. Diaconescu, B. Florea, and A. Misra, “Orientifolds, unoriented instantons and localization,” *JHEP* **07** (2003) 041, [hep-th/0305021](#).
- [27] V. Bouchard, B. Florea, and M. Mariño, “Counting higher genus curves with crosscaps in Calabi-Yau orientifolds,” *JHEP* **12** (2004) 035, [hep-th/0405083](#).
- [28] R. Gopakumar and C. Vafa, “M-theory and topological strings. II,” [hep-th/9812127](#).
- [29] H. Ooguri and C. Vafa, “Knot invariants and topological strings,” *Nucl. Phys.* **B577** (2000) 419–438, [hep-th/9912123](#).
- [30] J. M. F. Labastida, M. Mariño, and C. Vafa, “Knots, links and branes at large N,” *JHEP* **11** (2000) 007, [hep-th/0010102](#).
- [31] L. H. Kauffman, “An Invariant of Regular Isotopy,” *Trans. Am. Math. Soc.* **318** (1990) 417.
- [32] V. Bouchard, B. Florea, and M. Mariño, “Topological open string amplitudes on orientifolds,” *JHEP* **02** (2005) 002, [hep-th/0411227](#).
- [33] K. Hori, S. Katz, A. Klemm, R. Pandharipande, R. Thomas, C. Vafa, R. Vakil, and E. Zaslow, *Mirror Symmetry*, vol. 1 of *Clay Mathematics Monographs*. American Mathematical Society, 2003. 929 p.
- [34] B. R. Greene, “String theory on Calabi-Yau manifolds,” [hep-th/9702155](#).
- [35] P. Griffiths and J. Harris, *Principles of Algebraic Geometry*. John Wiley & Sons, 1978. 813 p.
- [36] H. Skarke, “String dualities and toric geometry: An introduction,” [hep-th/9806059](#).
- [37] E. Calabi, “The space of Kähler metrics,” in *Proceedings of the International Congress of Mathematicians, Amsterdam, 1954, vol. 2*, pp. 206–207. North-Holland, Amsterdam, 1956.

- [38] E. Calabi, “On Kähler manifolds with vanishing canonical class,” in *Algebraic geometry and topology, a symposium in honour of S. Lefschetz*, pp. 78–89. Princeton University Press, Princeton, 1957.
- [39] S.-T. Yau, “On Calabi’s conjecture and some new results in algebraic geometry,” *Proceedings of the National Academy of Sciences of the U.S.A.* **74** (1977) 1798–1799.
- [40] S.-T. Yau, “On the Ricci curvature of a compact Kähler manifold and the complex Monge-Ampère equations. I.,” *Communications on pure and applied mathematics* **31** (1978) 339–411.
- [41] V. Bouchard, “Lectures on complex geometry, Calabi-Yau manifolds and toric geometry,” in *Proceedings of the First Modave School in Mathematical Physics*. 2005.
- [42] D. D. Joyce, *Compact Manifolds with Special Holonomy*. Oxford Mathematical Monographs. Oxford University Press, 2000. 436 p.
- [43] M. Rossi, “Geometric Transitions,” [math.AG/0412514](#).
- [44] T. Hübsch, *Calabi-Yau Manifolds: A Bestiary for Physicists*. World Scientific, 1992. 374 p.
- [45] K. Kodaira, “On Compact Analytic Surfaces II,” *Ann. Maths.* **77** (1963) 563.
- [46] W. Barth, C. Peters, and A. van de Ven, *Compact Complex Surfaces*. Springer, 1984.
- [47] P. Goddard and D. Olive, “Kac-Moody and Virasoro Algebras in Relation to Quantum Physics,” *Int. Journ. Mod. Phys. A* **1** (1986), no. 2, 303.
- [48] V. Batyrev, *Higher-dimensional toric varieties with ample anticanonical class*. PhD thesis, Moscow State University, 1985. (Russian).
- [49] R. J. Koelman, *The number of moduli of families of curves on toric varieties*. PhD thesis, Katholieke Universiteit Nijmegen, 1990.
- [50] M. Kreuzer and H. Skarke, “On the Classification of Reflexive Polyhedra,” *Commun. Math. Phys.* **185** (1997) 495–508, [hep-th/9512204](#).
- [51] M. Kreuzer and H. Skarke, “Reflexive polyhedra, weights and toric Calabi-Yau fibrations,” *Rev. Math. Phys.* **14** (2002) 343–374, [math.ag/0001106](#).

- [52] H. Skarke, “Weight systems for toric Calabi-Yau varieties and reflexivity of Newton polyhedra,” *Mod. Phys. Lett.* **A11** (1996) 1637–1652, [alg-geom/9603007](#).
- [53] M. Kreuzer and H. Skarke, “Classification of Reflexive Polyhedra in Three Dimensions,” *Adv. Theor. Math. Phys.* **2** (1998) 847–864, [hep-th/9805190](#).
- [54] M. Kreuzer and H. Skarke, “Complete classification of reflexive polyhedra in four dimensions,” *Adv. Theor. Math. Phys.* **4** (2002) 1209–1230, [hep-th/0002240](#).
- [55] M. Bershadsky *et al.*, “Geometric singularities and enhanced gauge symmetries,” *Nucl. Phys.* **B481** (1996) 215–252, [hep-th/9605200](#).
- [56] P. S. Aspinwall and M. Gross, “The SO(32) Heterotic String on a K3 Surface,” *Phys. Lett.* **B387** (1996) 735–742, [hep-th/9605131](#).
- [57] S. Chaudhuri and J. Polchinski, “Moduli space of CHL strings,” *Phys. Rev.* **D52** (1995) 7168–7173, [hep-th/9506048](#).
- [58] J. H. Schwarz and A. Sen, “Type IIA dual of the six-dimensional CHL compactification,” *Phys. Lett.* **B357** (1995) 323–328, [hep-th/9507027](#).
- [59] M. Bershadsky, T. Pantev, and V. Sadov, “F-theory with quantized fluxes,” *Adv. Theor. Math. Phys.* **3** (1999) 727–773, [hep-th/9805056](#).
- [60] J. Park, “Orientifold and F-theory duals of CHL strings,” *Phys. Lett.* **B418** (1998) 91–97, [hep-th/9611119](#).
- [61] P. Berglund, A. Klemm, P. Mayr, and S. Theisen, “On type IIB vacua with varying coupling constant,” *Nucl. Phys.* **B558** (1999) 178–204, [hep-th/9805189](#).
- [62] W. Lerche, C. Schweigert, R. Minasian, and S. Theisen, “A note on the geometry of CHL heterotic strings,” *Phys. Lett.* **B424** (1998) 53–59, [hep-th/9711104](#).
- [63] S. Chaudhuri and D. A. Lowe, “Type IIA heterotic duals with maximal supersymmetry,” *Nucl. Phys.* **B459** (1996) 113–124, [hep-th/9508144](#).
- [64] S. Kachru, A. Klemm, and Y. Oz, “Calabi-Yau duals for CHL strings,” *Nucl. Phys.* **B521** (1998) 58–70, [hep-th/9712035](#).

- [65] M. Bershadsky, S. Cecotti, H. Ooguri, and C. Vafa, “Kodaira-Spencer theory of gravity and exact results for quantum string amplitudes,” *Commun. Math. Phys.* **165** (1994) 311–428, [hep-th/9309140](#).
- [66] I. Antoniadis, E. Gava, K. S. Narain, and T. R. Taylor, “Topological amplitudes in string theory,” *Nucl. Phys.* **B413** (1994) 162–184, [hep-th/9307158](#).
- [67] I. Brunner and K. Hori, “Orientifolds and mirror symmetry,” *JHEP* **11** (2004) 005, [hep-th/0303135](#).
- [68] E. Witten, “Quantum field theory and the Jones polynomial,” *Commun. Math. Phys.* **121** (1989) 351.
- [69] M. Mariño and C. Vafa, “Framed knots at large N,” [hep-th/0108064](#).
- [70] P. Cvitanovic, *Group Theory*. <http://www.cns.gatech.edu/predrag>.
- [71] S. Ramgoolam, “Comment on two-dimensional $O(N)$ and $Sp(N)$ Yang-Mills theories as string theories,” *Nucl. Phys.* **B418** (1994) 30–44, [hep-th/9307085](#).
- [72] D. E. Littlewood, *The Theory of Group Characters and Matrix Representations of Groups*. The Clarendon Press, Oxford, 1940.
- [73] M. Aganagic, A. Klemm, and C. Vafa, “Disk instantons, mirror symmetry and the duality web,” *Z. Naturforsch.* **A57** (2002) 1–28, [hep-th/0105045](#).
- [74] E. Guadagnini, “The Universal link polynomial,” *Int. J. Mod. Phys.* **A7** (1992) 877–946.
- [75] R. C. King, “Modification Rules and Products of Irreducible Representations of the Unitary, Orthogonal, and Symplectic Groups,” *J. Math. Phys.* **12** (1971) 1588.
- [76] W. Fulton and J. Harris, *Representation Theory: A First Course*. Springer-Verlag, 1997.
- [77] A. Okounkov, N. Reshetikhin, and C. Vafa, “Quantum Calabi-Yau and classical crystals,” [hep-th/0309208](#).
- [78] T. Eguchi and H. Kanno, “Topological strings and Nekrasov’s formulas,” *JHEP* **12** (2003) 006, [hep-th/0310235](#).

- [79] E. Witten, “Chern-Simons gauge theory as a string theory,” *Prog. Math.* **133** (1995) 637–678, [hep-th/9207094](#).
- [80] T. Graber and R. Pandharipande, “Localization of Virtual Classes,” *Invent. Math.* **135** (1999) 487, [math.AG/9708001](#).
- [81] M. Kontsevich, “Enumeration of rational curves via Torus actions,” [hep-th/9405035](#).
- [82] J. M. F. Labastida and M. Mariño, “Polynomial invariants for torus knots and topological strings,” *Commun. Math. Phys.* **217** (2001) 423–449, [hep-th/0004196](#).
- [83] J. M. F. Labastida and M. Mariño, “A new point of view in the theory of knot and link invariants,” [math.qa/0104180](#).
- [84] A. Iqbal and A.-K. Kashani-Poor, “Instanton counting and Chern-Simons theory,” *Adv. Theor. Math. Phys.* **7** (2004) 457–497, [hep-th/0212279](#).
- [85] P. Freyd *et al.*, “A new polynomial invariant of knots and links,” *Bull. Am. Math. Soc.* **12** (1985) 239–246.
- [86] C. H. Taubes, “Lagrangians for the Gopakumar-Vafa conjecture,” *Adv. Theor. Math. Phys.* **5** (2001) 139–163, [math.dg/0201219](#).
- [87] W. B. R. Lickorish, *An Introduction to Knot Theory*. Springer-Verlag, 1998.
- [88] J. M. F. Labastida and E. Perez, “A Relation between the Kauffman and the HOMFLY polynomials for torus knots,” [q-alg/9507031](#).
- [89] J. M. F. Labastida, P. M. Llatas, and A. V. Ramallo, “Knot operators in Chern-Simons gauge theory,” *Nucl. Phys.* **B348** (1991) 651–692.
- [90] J. M. F. Labastida and M. Mariño, “The HOMFLY polynomial for torus links from Chern-Simons gauge theory,” *Int. J. Mod. Phys.* **A10** (1995) 1045–1089, [hep-th/9402093](#).
- [91] P. Rama Devi, T. R. Govindarajan, and R. K. Kaul, “Three-dimensional Chern-Simons theory as a theory of knots and links. 3. Compact semisimple group,” *Nucl. Phys.* **B402** (1993) 548–566, [hep-th/9212110](#).
- [92] S. G. Naculich, H. A. Riggs, and H. J. Schnitzer, “Simple current symmetries, rank level duality, and linear skein relations for Chern-Simons graphs,” *Nucl. Phys.* **B394** (1993) 445–508, [hep-th/9205082](#).

- [93] P. Borhade and P. Ramadevi, “SO(N) reformulated link invariants from topological strings,” [hep-th/0505008](#).
- [94] D.-E. Diaconescu and B. Florea, “Localization and gluing of topological amplitudes,” [hep-th/0309143](#).
- [95] J. Li, C.-C. M. Liu, K. Liu, and J. Zhou, “A Mathematical Theory of the Topological Vertex,” [math.ag/0408426](#).
- [96] D. Maulik, N. Nekrasov, A. Okounkov, and R. Pandharipande, “Gromov-Witten Theory and Donaldson-Thomas theory. I,” [math.AG/0312059](#).
- [97] D. Maulik, N. Nekrasov, A. Okounkov, and R. Pandharipande, “Gromov-Witten Theory and Donaldson-Thomas theory. II,” [math.AG/0406092](#).
- [98] M. Aganagic, R. Dijkgraaf, A. Klemm, M. Mariño, and C. Vafa, “Topological strings and integrable hierarchies,” [hep-th/0312085](#).
- [99] A. Iqbal, N. Nekrasov, A. Okounkov, and C. Vafa, “Quantum foam and topological strings,” [hep-th/0312022](#).
- [100] N. Saulina and C. Vafa, “D-branes as defects in the Calabi-Yau crystal,” [hep-th/0404246](#).
- [101] T. Okuda, “Derivation of Calabi-Yau crystals from Chern-Simons gauge theory,” *JHEP* **03** (2005) 047, [hep-th/0409270](#).
- [102] N. Halmagyi, A. Sinkovics, and P. Sulkowski, “Knot invariants and Calabi-Yau crystals,” [hep-th/0506230](#).
- [103] H. Ooguri, A. Strominger, and C. Vafa, “Black hole attractors and the topological string,” *Phys. Rev.* **D70** (2004) 106007, [hep-th/0405146](#).
- [104] M. Aganagic, H. Ooguri, N. Saulina, and C. Vafa, “Black holes, q-deformed 2d Yang-Mills, and non-perturbative topological strings,” *Nucl. Phys.* **B715** (2005) 304–348, [hep-th/0411280](#).
- [105] C. Vafa, “Two dimensional Yang-Mills, black holes and topological strings,” [hep-th/0406058](#).
- [106] N. Nekrasov, “A la recherche de la m-theorie perdue. Z theory: Chasing m/f theory,” [hep-th/0412021](#).

-
- [107] R. Dijkgraaf, S. Gukov, A. Neitzke, and C. Vafa, “Topological M-theory as unification of form theories of gravity,” [hep-th/0411073](#).
- [108] V. Pestun and E. Witten, “The Hitchin functionals and the topological B-model at one loop,” [hep-th/0503083](#).
- [109] L. Smolin, “A quantization of topological M theory,” [hep-th/0503140](#).
- [110] J. de Boer, A. Naqvi, and A. Shomer, “The Topological G2 String,” [hep-th/0506211](#).
- [111] I. G. Macdonald, *Symmetric Functions and Hall Polynomials*. Oxford Mathematical Monographs. Oxford Science Publications, 1995. (second edition).
- [112] T. J. Hollowood, A. Iqbal, and C. Vafa, “Matrix models, geometric engineering and elliptic genera,” [hep-th/0310272](#).
- [113] A. Iqbal and A.-K. Kashani-Poor, “The vertex on a strip,” [hep-th/0410174](#).
- [114] T. M. Chiang, A. Klemm, S. T. Yau, and E. Zaslow, “Local mirror symmetry: Calculations and interpretations,” *Adv. Theor. Math. Phys.* **3** (1999) 495–565, [hep-th/9903053](#).